AN ABSTRACT OF THE THESIS OF

Brandon R. Brown for the degree of Doctor of Philosophy in Physics presented on May 8, 1997. Title: Neutron Irradiation and dc Transport in YBaCuO Single Crystals: A Study of Vortex Depinning.

Abstract approved: _____

Janet Tate

Four-terminal dc *V-I* characteristics of the high-temperature superconducting copper-oxides are usually analyzed within the framework of a second-order vortex glass-to-liquid phase transition. Such an analysis depends on universal critical parameters, but a definitive universality class has not emerged in the literature. The nature of vortex depinning in the mixed state of disordered $YBa_2Cu_3O_7$ (YBCO) continues to be a subject of controversy. This work presents dc *V-I* traces on heavily-twinned YBCO crystals for a variety of applied magnetic fields and precisely stabilized temperatures. To study the effect of disorder, data are collected before and after fast-neutron irradiation. The data show a systematic dependence on the disorder in the vortex array due to pinning. Specifically, the logarithmic derivative, n, of data at the depinning temperature depends on an estimate of the Larkin-Ovchinnikov pinning length for the YBCO crystals and for data selected from the literature. The YBCO crystal data can be collapsed with critical scaling, but they do not yield universal exponents. A less familiar analysis is used to map critical current distributions which show sensitivity to temperature, field, and pinning-site density. Given that critical parameters of the glass-to-liquid phase transitions depend on n, and given the results of a simulation based on thermal depinning, this thesis concludes that dc *V-I* data do not provide satisfactory evidence of a glass-liquid phase transition. Overall, the data are most adequately described by dislocation-mediated thermal depinning, or percolation.

Neutron Irradiation and dc Transport in YBaCuO Single Crystals: A Study of Vortex Depinning

by

Brandon R. Brown

A THESIS

submitted to

Oregon State University

in partial fulfillment of
the requirements for the
degree of

Doctor of Philosophy

Presented May 8, 1997
Commencement June 1997

Doctor of Philosophy thesis of Brandon R. Brown presented on May 8, 1997

APPROVED:

Major Professor, representing Physics

Chair of Department of Physics

Redacted for privacy

Dean of Graduate School

I understand that my thesis will become part of the permanent collection of Oregon State University libraries. My signature below authorizes release of my thesis to any reader upon request.

Redacted for privacy

Brandon R. Brown, Author

ACKNOWLEDGMENT

This work exists due in no small part to the kindly wisdom of Max Apple and his interest in science.

I thank Kristin for so agreeably enduring my long hours and vortex obsessions.

I have leaned on the unfailing support of my parents, who always had the right words, not to mention the occasional plane fare and Texan hospitality.

I appreciate and wish to distinguish the exemplary guidance, the scientific instincts, and the perfectly-timed suggestions of my advisor, Janet Tate. She has given me valuable advice on a wide variety of topics.

I thank Jeanette Roberts for patiently teaching me the ropes in the lab, for the opportunity to hop onboard her project as a co-author, and for her friendship. I thank Goran "G-man" Karapetrov for his advice, criticism, humor, and weird news stories from afar. I thank Dennis "D-Train" Tom for his assistance, his many experimental/computerese lessons, and his zany music. I thank Irene Dumkow for her cheerful and cooperative lab camaraderie. I thank Eric Moret for his assistance on crystal #3 and his insistence that I relax once a month or so.

I wish to note the cheerful and obviously crucial assistance of Bill Warnes, who was always willing to discuss the data with me.

I greatly appreciate Phil Siemens' encouragement in my pursuit of a non-traditional scientific career.

I thank Allen Wasserman for his superb instruction, his sense of humor, and the numerous odd-hour chats.

I must certainly thank Rich and Kris Daniels for their willingness to adopt me into their wonderful family.

I am grateful to Ehud Havazelet and Marjorie Sandor for making my graduate education a well-rounded experience and for their friendship. I must especially thank Tracy Daugherty, who was the first person to greet me in Oregon and has done so very much for me as a friend and teacher.

I thank Boyd Veal for providing the YBCO single crystals and providing helpful comments about the Au inclusions. The collaboration with John Farmer of the University of Missouri has been a pleasure. Arthur Sleight of Oregon State University's Chemistry Department has been very cooperative in letting me use his gas-flow ovens; I received generous assistance from his post-docs Jiangou Hou and John Evans. I would also like to thank Randy Lundquist and Peter Langer for help with digitization. I thank John Gardner for extending his RUA to cover my irradiated single crystal.

The list of those who provided helpful comments, E-mails, mini-lectures, or simply held forth to further enlighten me is long but very important: Charles Dewhurst, Richard Doyle, Mark Friesen, John Gardner, Henri Jansen, Roger Koch, Hugo Safar, Enrico Silva, Don Walser, and N.-C. Yeh. (Please, gentle reader, do not hold any of these fine people responsible for what follows).

TABLE OF CONTENTS

TABLE OF CONTENTS (CONTINUED)

LIST OF FIGURES

LIST OF FIGURES (CONTINUED)

LIST OF FIGURES (CONTINUED)

LIST OF FIGURES (CONTINUED)

LIST OF TABLES

LIST OF APPENDIX FIGURES

Neutron Irradiation and dc Transport in YBaCuO Single Crystals: A Study of Vortex Depinning

CHAPTER 1

INTRODUCTION

Applied magnetic fields limit the current-carrying capacity of high-temperature superconductors since these materials admit magnetic flux in quantized units known as vortices. In an applied current, motion of unpinned vortices gives rise to dissipation and hence resistivity. The experimental study of collective vortex behavior in the high-temperature superconductor $YBa_2Cu_3O_7$ has focused primarily on a separation of the magnetic-field versus temperature plane into distinct regions or phases -- vortex solids, vortex liquids, and vortex glasses to name a few. Four terminal voltage-current characteristics for a wide variety of $YBa_2Cu_3O_7$ samples, both thin films and single crystals, show a strong qualitative similarity as they move from truly superconducting behavior for finite currents at lower temperatures to dissipative behavior for all applied currents at slightly higher temperatures. To examine the nature of this transition, we have collected voltage-current characteristics for $YBa_2Cu_3O_7$ single crystals for a variety of applied fields before and after fast-neutron irradiation. We find that the models of a second-order phase transition from a pinned glassy state to a liquid-like state (i.e. the vortex and Bose glass models) fail to consistently describe the data. Instead, the data are more satisfactorily interpreted in the context of pinning force distributions which are sensitive to temperature, field, and the dislocation density of the vortex lattice. In addition we find that, by analyzing the data near the depinning temperature, measurements for a variety of copper-oxide superconductors can be understood within the same analytical framework.

1.1 Superconductivity

1.1.1 *Conventional Superconductivity*

Since its discovery in 1911, the phenomenon of superconductivity has sat firmly between an academic curiosity and a technological breakthrough. The phase space that this phenomenon inhabits is somewhat prohibitive for many potential applications. Before 1986, superconducting materials exhibited their signature infinite conductivity only below temperatures of, at best, 23 K. As a superconductor is warmed through its transition temperature T_C, it abruptly assumes the properties of a normal metal. Into the 1980's, superconductivity risked becoming predominantly an academic curiosity with the exception of a few exotic applications: high-field magnets, superconducting quantum interference devices, and ambitious attempts to construct computers which incorporated superconducting materials.

Meissner and Ochsenfeld discovered in 1933 that superconductors expel magnetic flux independent of whether the magnetic field is applied before or after cooling the system below T_C (Meissner and Ochsenfeld, 1933). This is referred to as the Meissner effect and it is a signature of superconductivity. The London penetration depth, λ, describes the length scale on which a magnetic field infiltrates the superconducting material from its boundaries. The London brothers rendered it quantitatively as

$$\lambda^2 = \frac{m}{\mu_0 n_s e^2} \tag{1.1}$$

where e and m are, respectively, the charge and mass of the electron and n_s represents the number density of superconducting electrons (Tinkham, 1975). The penetration depth represents the

first of an array of length scales that will make up an important focus of this work.

The first major theoretical work describing superconductivity was presented in 1950 by V. L. Ginzburg and L. D. Landau (Ginzburg and Landau, 1950). Ginzburg-Landau (GL) theory, as it has come to be called, treats superconductivity in a rather phenomenological way and is impressive in its ability to describe the macroscopic phenomenon. It assumes a pseudo-wavefunction, ψ, as an order parameter for superconducting electrons in a superconducting material. In this way, the density of states, n_s, can be accessed simply by

$$n_s = |\psi(x)|^2. \tag{1.2}$$

The use of a superconducting wavefunction with both magnitude and phase was shown in time to be quite appropriate to the superconducting state. Ginzburg-Landau theory starts from the order parameter assumption and proceeds with a Schrödinger-type wave equation approach, seeking solutions for the pseudo-wavefunction.

The theory also introduced a coherence length that represents the characteristic scale over which ψ is allowed to vary without a great energetic cost. The coherence length can be written

$$\xi(T) = \frac{h}{\mu_0 e\sqrt{2} H_c(T) \lambda_{eff}(T)}, \tag{1.3}$$

where λ_{eff} is an effective penetration depth that has now been given temperature dependence, and $H_c(T)$ is the critical field which separates the superconducting state from the normal state. The coherence length diverges as T approaches the transition T_c from below. Since λ also diverges in this limit, the GL parameter $\kappa = \lambda/\xi$ provides a very useful dimensionless parameter for classifying

superconductors. A typical elemental superconductor has $\xi \approx 300$ nm, $\lambda \approx 50$ nm, and κ much less than unity (Tinkham, 1975).

In 1957, Bardeen, Cooper and Schrieffer introduced the first comprehensive microscopic theory (BCS theory) for superconductivity (Bardeen *et al.*, 1957). They described a pairing mechanism of a weak, phonon-mediated, attractive interaction between electrons. The so-called Cooper pairs were composed of electrons with opposite momenta and spin. The theory explained experimental data of the time with convincing accuracy (Glover and Tinkham, 1957).

Also in 1957, Abrikosov introduced the concept of two distinct classes, type-I and type-II, of superconductors. What separates type-I from type-II is a term of the system's Hamiltonian which describes the interface of superconducting and non-superconducting regions. In type-I materials $\kappa < 1/\sqrt{2}$, this term is positive and such boundaries are not advantageous to superconductivity. However, in type-II materials $\kappa > 1/\sqrt{2}$, the interface term is negative, and the system benefits from normal-superconducting boundaries. This results in what Abrikosov called a "mixed state" where the superconducting region is threaded by penetrating quantized flux tubes (cylindrically symmetric in the case of an isotropic material), each containing a flux of $\phi_0 = h/2e = 2.07 \times 10^{-15}$ Tm^2. The mixed state exists between the upper critical field H_{c2}, which is analogous to H_c in type-I superconductivity, and the lower critical field H_{c1}, below which a Meissner phase is found with no flux penetration. Flux quantization follows directly from the fact that the GL order parameter ψ has a complex component and maintains its phase over macroscopic distances; it is analogous to the quantization of angular momentum in the atom. This thesis studies the behavior of the flux tubes, commonly called vortices.

1.1.2 *High-Temperature Superconductivity*

A renaissance of superconductivity research began in late 1986 when Bednorz and Müller found that $La_{2-x}Ba_xCuO_4$ exhibited superconductivity up to 35 K (Bednorz and Müller, 1986). In a flurry of activity, condensed-matter scientists soon discovered that other copper-oxide materials could superconduct at even higher temperatures. In 1987, the research teams of Paul Chu and Maw-Kwen Wu simultaneously unveiled $YBa_2Cu_3O_7$ (YBCO), with a transition temperature of 92 K, well above the boiling point of liquid nitrogen (Chu, 1996). In addition to the class of copper-oxides, of which YBCO is one of many, high-temperature (high-T_c) superconductors include bismuthate and fullerene families that will not be treated here (Chu, 1996). The copper-oxides are often described as perovskites, which have a cubic crystal symmetry and an ABO_3 stoichiometry, but technically the copper-oxides deviate from this classification in that they have orthorhombic symmetry (Holton *et al.*, 1996).

While generally more exotic than low-T_c superconductors, the high-T_c superconductors are also less hardy. Compared to low-T_c materials, they have lower functional critical currents in an applied magnetic field and less structural integrity.

All high-T_c superconductors are type-II superconductors. They exhibit larger penetration depths and much smaller coherence lengths (e.g. $\lambda \approx 150$ nm, $\xi \approx 1$ nm in the *ab* plane for YBCO at $T = 0$), resulting in $\kappa > 100$ (Mao *et al.*, 1995; Dolan *et al.*, 1989; Welp *et al.*, 1989). They display a mixed state between H_{c1} and H_{c2} as predicted by Abrikosov, and while the H_{c2} values for these materials can be quite high (e.g. 10 T for YBCO at 77 K; Kwok, 1992), the H_{c1} values are typically very low (e.g. 35 mT at 80 K; Govorkov, 1994). This makes the study of the mixed state of paramount importance to an understanding of the copper-oxide superconductors.

Another factor which distinguishes copper-oxide superconductors from their low-T_c cousins is their electrical anisotropy (see section 3.1). While most low-T_c materials display no preference for the direction of electrical transport, the copper-oxides display a strong preference for electrical transport in the $a\,b$ crystallographic planes over that parallel to the crystallographic c axis. As a result, the defining length scales have different values for different orientations. In the case of YBCO, $\xi_{ab} \approx 5\xi_c$ and $\lambda_c \approx 5\lambda_{ab}$.

1.2 Magnetic Flux Vortices

The flux tubes, originally predicted by Abrikosov and later imaged by Essmann and Träuble (1967), are most commonly called vortices, but also flux lines, or fluxons. The term vortex is appropriate because the superconductor surrounds a tube of magnetic flux with a circulating cylindrical distribution of shielding currents (see Fig. 1.1a); the radial extent of this current distribution is given by the penetration depth λ (see Eq. 1.1). The core of the vortex, ideally a region of material in the normal, non-superconducting phase, is defined by a region of order parameter ψ suppression. The typical diameter of a vortex is given by the correlation length ξ, (see Eq. 1.3). As mentioned above, a superconductor in the mixed state quantizes flux such that each vortex contains one quantum of flux, ϕ_0. Because of this quantization and because most vortices repel one another, a simple relation exists between the magnitude of an applied magnetic field and the average spacing, a_0, of flux vortices. Assuming a square lattice of vortices, the intervortex spacing can be defined as

$$a_0 = \sqrt{\frac{\phi_0}{B}}. \tag{1.4}$$

With an applied field of 1 T, $a_0 = 45$ nm, while an applied field of 1 mT (or 10 gauss) results in $a_0 = 1.5\ \mu$m.

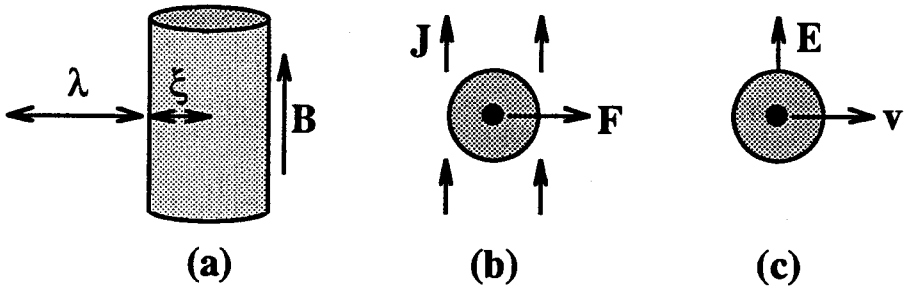

Fig. 1.1: Side view (a) and top view (b,c) of a magnetic flux vortex. The core extends to a radius ξ and shielding currents flow around the core to an extent λ. In (b) and (c), **B** is directed out of the page; applied **J** gives rise to a force density **F**, and subsequent motion (c) gives rise to an **E** component parallel to **J**. Shielding currents, not pictured, flow counter-clockwise around the core in (b) and (c).

Though favorable to the overall Hamiltonian for the mixed state of a type-II superconductor, vortices are troublesome for the transport of a bulk supercurrent. The motion of vortices leads to dissipation in the superconducting sample and electrical resistance. In an applied current, each vortex is driven by a Lorentz force per unit length (expressed in SI units)

$$\mathbf{f} = \mathbf{J} \times \phi_0 \hat{\mathbf{B}}. \tag{1.5}$$

This is depicted in Fig. 1.1b. More generally, the applied current gives a Lorentz force density

$$\mathbf{F} = \mathbf{J} \times \mathbf{B}. \tag{1.6}$$

This force tends to move vortices transverse to the applied current direction and perpendicular to the direction of the applied field (see Fig. 1.1c). Neglecting other possible forces on the vortices, they will gain a velocity **v**. The motion of flux in the presence of a current

then gives rise to an electric field which is parallel to **J** (Ullmaier, 1975)

$$\mathbf{E} = \mathbf{B} \times \mathbf{v}. \tag{1.7}$$

This electric field appears experimentally as a resistive voltage and the superconductor no longer exhibits vanishing resistivity. Note the otherwise important distinction between an applied B and the resulting H of a material is often ignored in type-II materials because the microscopic surface currents (existing to the depth λ) are much less than typical transport currents (Tinkham, 1975). The difference is most apparent for $H < H_{c1}$, the Meissner phase, where B is necessarily zero but H can be finite (see Section 1.4).

We note that the above discussion of the Lorentz force, while complete for the purposes of this work, is a bit shallow. The force on a vortex transverse to an applied current is sometimes interpreted as a Magnus force arising from the interaction of the applied current with the shielding currents; in this sense it can be loosely likened to the force on an airplane's wing (Huse *et al.*, 1992). The nature of the transverse force is still an open topic (Thouless *et al.*, 1996). Details aside, the motion of vortices causes resistance in the mixed state, and the question of whether or not vortices can be localized is a crucial one. It is also non-trivial and the subject of a great body of type-II superconductivity research.

1.3 Vortex Pinning

For an extremely clean system in the mixed state, a lone flux vortex penetrates a superconducting sample with very little perturbation. However, in anything but the most ideal sample, the superconducting order parameter is depressed in the vicinity of a defect. A nearby vortex, with its core exhibiting order parameter

suppression, finds the defect site energetically favorable. In terms of free energy, the point defect presents a local minimum; the more completely a defect disrupts superconductivity, the more strongly it can attract a vortex. A vortex caught in the local minimum of a defect is said to be "pinned", and the defect is then a pinning site or simply a pin. The attractive force that a pin exerts on a vortex is proportional to the gradient of the local potential energy, and the pinned vortex typically inhabits the edges of the defect structure.

A pinned vortex is not necessarily in a stable configuration. For nonzero temperatures, a vortex can be thermally excited away from the pin when kT is on the order of the pinning energy U_p. In low-T_c superconductors, this is germane only very close to T_c. However, for high-T_c superconductors, the mixed state can extend to 90 Kelvin or more and the thermal energies are obviously much larger. In addition to higher temperatures, several other factors increase the importance of thermal depinning in high-T_c materials. Ginzburg showed that fluctuations of the superconducting order parameter ψ are large in a temperature region $T_f \leq T \leq T_c$ where T_f denotes the temperature at which fluctuations become non-negligible (Ginzburg, 1960). Ginzburg described a constant that determines T_f according to $Gi = 1 - T_f/T_c$. For anisotropic superconductors, like the copper-oxides, the Ginzburg number (pg. 1544 of Brandt, 1995) is given by

$$Gi = \frac{1}{2}\left(\frac{2\pi\mu_o k_B T_c}{\phi_0^2}\frac{\lambda(0)^2}{\gamma\xi(0)}\right)^2 \qquad (1.8)$$

where the penetration depth λ and the coherence length ξ are both assumed to be in the ab plane. The anisotropy factor, γ, describes the preference of the material to superconduct along the ab planes instead of the c axis (see Eq. 3.1). High-T_c materials, compared to low-T_c materials, display smaller ξ values, larger λ values, higher T_c values, and lower γ values. Each of these differences serves to increase Gi and therefore lower the value of T_f with respect to the

transition temperature T_c. In the case of YBCO, $Gi \approx 10^{-2}$, whereas $Gi \approx 10^{-12}$ for most low-T_c materials (Blatter, 1994).

As described above (see Eq. 1.5), an applied current exerts a Lorentz force on a vortex. When the Lorentz force exceeds the pinning force, a vortex is swept away from the pin. Roughly speaking, a pinning site gives rise to a local potential well $U(\mathbf{r})$, and the force exerted can be described as $F_p = -\nabla U(\mathbf{r})$ (Ullmaier, 1975). This force will typically oppose translational motion of the vortex (e.g. the motion induced by an applied electric current). Simplicity ends there, however, as the possibilities for $U(\mathbf{r})$ are both numerous and complex depending on the type of defect, the influence of neighboring vortices, and the influence of a non-zero temperature.

In 1962, Anderson first proposed the idea of flux creep, in which type-II superconductivity is viewed, at best, as a metastable state at non-zero temperature. Vortices, singly or in "bundles", jump over pinning barriers at a rate related to the available thermal energy. Given pinning barriers $U(J)$ and a temperature T, the rate of activation is given by (Anderson, 1962)

$$v = v_0 e^{-U(J)/k_B T}. \tag{1.9}$$

For the mechanism of flux creep, the pinning barrier is assumed to vanish as J approaches the critical current density J_c (Anderson, 1962). Its functional form can be approximated as

$$U(J \to J_c) \approx U_c\left(1-\frac{J}{J_c}\right)^{\alpha}, \tag{1.10}$$

where U_c is the characteristic scale of the pinning energy. Anderson originally proposed a value of α=1 for the exponent. As described above, vortex motion results in dissipation and a lack of true superconductivity. In the view of flux creep then, true superconductivity is not attainable in the mixed state.

Once vortices are removed from their pinning potentials, they flow in the presence of an applied current. A flux flow voltage signal is characterized by a linear response to an applied $I > I_c$, the critical current. Kim first treated this problem with the assumption that the resulting flux flow velocity $\mathbf{v_f}$ reflected the balance of three forces represented by

$$\mathbf{F}_L = \mathbf{F}_p + \frac{B}{\phi_0}\eta \mathbf{v}_f, \tag{1.11}$$

where $\mathbf{F_L}$ is the applied Lorentz force density, $\mathbf{F_p}$ is the pinning force density, and the third term expresses an effective viscosity with $\eta(B,T)$ denoting the viscosity coefficient (Kim, 1963). According to Eq. 1.7, the resulting E parallel to the applied current is given by

$$E = \frac{\phi_0}{\eta}\left(F_L - F_p\right) = \frac{\phi_0 B}{\eta}(J - J_c), \tag{1.12}$$

which matches the experimental observations of a constant resistivity above J_c. In the model of Kim, one expects from Eq. 1.12 a flux-flow resistivity ρ_f that is directly proportional to the applied field.

After the discovery of high-T_c superconductivity, the work of Anderson and Kim was modified to account for the higher temperatures. A thermally assisted flux flow resistivity was expressed for $J < J_c$ by Kes *et al.* in 1989 as

$$\rho_{TAFF} = \rho_0 \frac{U_p}{k_B T} \cdot exp\left[-\frac{U_p}{k_B T}\right] \tag{1.13}$$

where U_p is a current-independent pinning energy and the constant ρ_0 incorporates details of the flux creep process.

Competing with the effects of pinning on an assembly of vortices are the interactions of the vortices themselves which can be non-negligible if the magnitude of the applied field is high or pinning is somewhat weak. A theory of collective pinning will be described in Chapter 2; for now, we describe two interacting vortices. Neighboring vortices experience a repulsive interaction whose energy can be approximated by

$$E_{int} = \frac{\Phi_0^2}{2\mu_0\lambda^2} K_0\left(\frac{r_{12}}{\lambda}\right), \tag{1.14}$$

where r_{12} is the distance separating the two vortices and K_0 is zero-order Hankel function (Tinkham, 1975). K_0 has the following two limiting forms for the interaction energy:

$$E_{int} \rightarrow \frac{\Phi_0^2}{2\mu_0\lambda^2}\left(\frac{\pi}{2}\frac{\lambda}{r_{12}}\right)^{1/2} e^{-r_{12}/\lambda} \qquad r_{12} \rightarrow \infty \tag{1.15a}$$

$$E_{int} \approx \frac{\Phi_0^2}{2\mu_0\lambda^2} ln\frac{\lambda}{r_{12}} \qquad \xi \ll r_{12} \ll \lambda \tag{1.15b}$$

Typically, interactions strengthen with increasing λ, and the added importance of vortex interactions follows for high-T_c materials with their relatively large λ values.

In sum, the mixed state for a current-carrying superconductor can be fundamentally described by the competition between four mechanisms: thermal excitation, pinning via defects, vortex-vortex interactions, and the Lorentz force. For high-T_c superconductors, the energy scales for these four are roughly equivalent; it is the interplay of the four that makes the physics of the mixed state in YBCO a fascinating and challenging area of study.

1.4 Brief History of a Phase Diagram

To better describe the behavior of vortices, researchers commonly divide a H versus T diagram into distinct regions. The line which separates the normal and superconducting states is the temperature dependent critical field $H_c(T)$. For type-II superconductors, the upper critical field line $H_{c2}(T)$ separates the superconducting and normal states. Below $H_{c2}(T)$, vortices are present, ideally in the form of a solid vortex lattice like that described by Abrikosov (Abrikosov, 1957). At still lower fields and temperatures, the lower critical field $H_{c1}(T)$ defines the boundary for the Meissner state, a small region which emulates type-I behavior with complete flux expulsion. (A B-T diagram is similar to an H-T diagram, except that a $B_{c1}(T)$ line coincides with the x-axis and the Meissner state is not pictured). The region between $H_{c1}(T)$ and $H_{c2}(T)$ is called the mixed state.

In 1979, the idea of subdividing the mixed state was first introduced; some postulated that the ideal vortex lattice could become unstable to thermal fluctuations and actually melt from a solid lattice to a vortex liquid (Huberman and Doniach, 1979). Thermal fluctuations are obviously even more influential for high-T_c materials, and since their discovery in 1986, the efforts to perceive, define, and map subdivisions of the mixed state in the copper-oxides have been vigorous.

For a disordered high-T_c superconductor, where pinning effects compete with thermal fluctuations, the phase diagram is believed to resemble Fig. 1.2. $H_{c2}(T)$ is depicted as a rough boundary since, in the presence of an applied field, it is not especially abrupt. The line is hazy because near $H_{c2}(T)$ large-scale fluctuations of ψ coincide with the rapid growth of ξ (to the point that vortices begin to overlap). The line which separates a pinned vortex system from a liquid-like vortex system was originally

proposed in the form of Fig. 1.2 by Fisher (Fisher, 1989). Experimentally it is often fit to the function

$$H(T) = H(0)\left(1-\frac{T}{T_c}\right)^{\beta} \tag{1.16}$$

where β falls between 1 and 2. In Section 4.5, we present a good fit to this expression for twinned YBCO crystals and find β = 1.47. Authors have alternately claimed that this line denotes a first-order solid-liquid phase transition, an line of irreversible magnetization (called the irreversibility line), a simple depinning line, a second-order phase transition of vortex matter, or some combination of these possibilities. As we show below, many efforts have claimed that there are numerous lines in close proximity further splintering the phase diagram (Worthington *et al.*, 1992; Doniach *et al.*, 1994). Also, the diagram is often modified to allow for a reentrant vortex liquid at very low fields (Blatter, 1994).

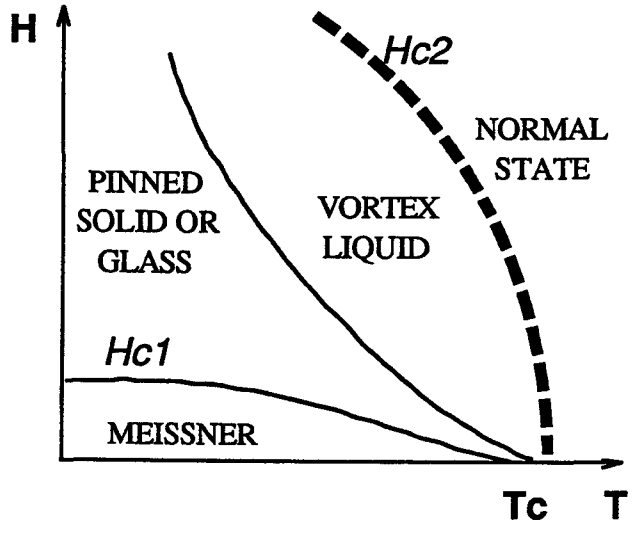

Fig. 1.2: H-T phase diagram for a disordered high-temperature superconductor.

The boundary is especially interesting in light of some predictions that a glassy phase localizes vortices to the extent that zero linear resistivity can be attained in the mixed state (Fisher *et al.*, 1991; Nelson and Vinokur, 1993). This differs notably from more conventional pictures of the mixed state where the vortex system, as a solid or a liquid, will always experience flux creep effects, and hence resistance, in a finite applied current.

Sensibly, the phase diagram differs for different materials. For instance, the greater anisotropy of Bi-based materials moves the melting line to lower fields and temperatures (refer to Eq. 1.8) than the line of YBCO (Zeldov *et al.*, 1995). In addition, the phase diagrams vary for different types of samples; thin films are believed to be too disordered to exhibit a true vortex solid-liquid transition, while pinning is much weaker in single crystals. This thesis focuses on single crystals of YBCO, but even for such a specific topic, a number of interpretations have appeared in the literature.

In 1988, a group from AT&T Bell Laboratories presented torsional oscillator measurements of YBCO single crystals that exhibited a sharp dissipation for $T < T_c$ (Gammel *et al.*, 1988). The authors claimed that the vortex matter exhibited a thermodynamic phase transition between a solid state and liquid state at a melting temperature T_m. Their interpretation was disputed by those who thought that the data could easily be interpreted by the more conventional approach of collective pinning (Brandt *et al.*, 1989); in this view, at a temperature $T < T_c$ the vortices are thermally excited away from their pinning sites and allowed to flow.

Since then, many experiments have addressed this issue. Those that specifically attempt to map a boundary in the context of Eq. 1.16 are summarized in Table 1.1 below. Included is a brief statement summarizing the interpretation of each effort. The determination of β is not a central focus of this work; as Ziese *et al.* (1994) note, the functional form of a line in the H-T or B-T plane,

given the experimental and theoretical results to date, is probably not a good criterion to prove or disprove a phase transition. We list it in this section merely as an overview which includes many of the techniques and interpretations in the literature.

Table 1.1: Summary of experiments which probe the H-T phase diagram for YBCO single crystals.

author	sample	method	β	interpret.
Gammel *et al.* (1991)	twinned	ac resistivity	4/3 or 1	vortex glass transition
Farrell *et al.* (1991)	untwinned	torsional oscillator	2	1st-order melting
Safar *et al.* (1992)	untwinned	ac resistivity	2	1st-order melting
Krusin-Elbaum *et al.* (1992)	twinned	dc magnetization	3/2	irrevers. line
Worthington *et al.* (1992)	twinned, irradiated	dc resistivity	3/2	1st-order melting
Kwok *et al.* (1992)	untwinned	dc resistivity	1.41	1st-order melting
Salamon *et al.* (1993)	twinned	specific heat	4/3	3D-XY transition
Jiang *et al.* (1993)	twinned, irradiated	dc resistivity	4/3	2nd-order melting
Gupta *et al.* (1993)	twinned	vibrating reed	3/2	thermal depinning
Jiang *et al.* (1994)	twinned, irradiated	ac resistivity	β(θ)	Bose glass transition
Krusin-Elbaum *et al.* (1994)	twinned, irradiated	ac susceptibility	β(B)	Bose glass transition
Ziese *et al.* (1994)	twinned	vibrating reed	2	thermal depinning
Welp *et al.* (1996)	untwinned	SQUID magnetometry	4/3	1st-order melting

Several efforts have attempted to derive β theoretically. Most authors agree that one should find β=2 for lattice melting (Houghton *et al*,, 1989; Feigelman and Vinokur, 1990; Glazman and Koshelev, 1991). However, Houghton *et al.* (1989) note that β could decrease for increasing field strengths, and some calculations which incorporate quantum fluctuations predict β = 3/2 (Blatter and Ivlev, 1993). Theories of a second-order phase transition predict β = 4/3 (3D-XY and vortex glass models, Fisher *et al.*, 1991). When comparing these scattered predictions to the results in table 2.1, one finds a very homogeneous muddle.

At the time of this writing, it appears that a consensus is emerging for untwinned single crystals. The measurements of Welp *et al.* (1996) have convincingly shown a sharp magnetization jump which gives direct evidence of a first-order vortex phase transition. In addition, complex resistivity measurements for untwinned YBCO have now found an abrupt collapse of the vortex lattice's shear modulus, further substantiating the claims of melting (Wu *et al.*, 1997). For twinned or irradiated crystals, however, the debate concerning vortex behavior in the mixed state continues. Whether or not a twinned crystal can strongly pin vortices and exhibit zero resistivity is still a vital question, even after ten years of study.

As shown in Table 1.1, claims for twinned crystals include second-order vortex glass-liquid phase transitions, a somewhat non-committal depiction of irreversible magnetic behavior, a residual first-order or second-order solid-liquid transition, and a simple depinning transition. Of particular note, the magnetization measurements of Krusin-Elbaum *et al.* (1992) give the most thorough attempt to divide the *H-T* diagram for YBCO crystals. The authors, in addition to mapping the line of irreversible magnetization, map somewhat ambitious boundaries separating single-vortex, small-bundle, and large-bundle regimes in the context of collective pinning theory (see Section 2.1).

The listing of β values provides a handy overview and underlines the diversity of experimental interpretations for twinned YBCO crystals. However, a discussion of the phase diagram would be incomplete without mentioning several other theoretical species and interesting experimental works which do not happen to report β. Perhaps most relevant to twinned YBCO is the Bose glass theory and it, along with its experimental supports, will be discussed in Section 2.1.

The 3D-XY model (see Table 1.1) was originally used to explain superconducting fluctuations for very low magnetic fields in the vicinity of T_c (Fisher *et al.*, 1991). Since it was not originally formulated to account for anything but the fringes of the mixed state, we do not explore the 3D-XY model in this thesis. However, at the time of this writing, a debate exists as to whether or not the model can increase its domain of relevance in the mixed state. Some claim that the model is relevant up to 8 T (Overend *et al.*, 1994), while others claim that their data cannot be fit by the model for anything but very low fields (Jeandupeux *et al.*, 1996). Other researchers claim that the extent of the model's relevance in temperature (on both sides of T_c) is quite vast (Friesen *et al.*, 1997).

The existence of a Bragg glass has been postulated for very weak disorder and low magnetic fields (Giamarchi and Le Doussal, 1995). The Bragg glass phase is characterized by very few lattice dislocations; it is nearly a perfect Abrikosov lattice, despite the presence of dilute pinning sites. With an increase in magnetic field or augmentation of pinning strength, the Bragg glass is expected to collapse to a vortex glass or pinned vortex liquid. More recently, the study of static lattices with few dislocations has led to vigorous research in the realm of *moving* lattices (Giamarchi and Le Doussal, 1996). The zoology of dynamic vortex phases now subdivides the region of Fig. 1.2 that was once simply labeled vortex liquid; we do not treat this issue here.

Finally, we must mention the interesting measurements and interpretations of Abulafia *et al.* who studied the magnetic relaxation of twinned YBCO crystals using an array of Hall probe sensors (Abulafia *et al.*, 1996). After noticing an abrupt change in the relaxation behavior at a boundary well below the traditional depinning or melting line described above, the authors propose a cross-over from *elastic* vortex response at lower fields and temperatures to *plastic* vortex response at somewhat higher fields and temperatures, both below the vortex liquid regime (for an elastic versus plastic delineation, see Chapter 2). For example, at 85 K, the vortices exhibited elastic response below 0.4 T and plastic response above 0.4 T. The region studied in this thesis is thought to be primarily *above* the proposed elastic-plastic transition line -- that is to say in the plastic regime.

In general, the results of resistivity measurements, (see Section 1.5 below), are interpreted in the language of phase transitions, while the results of vibrating reed and magnetization measurements are sometimes interpreted in the language of collective pinning (most recently Hiergiest and Hergst, 1997). The different theoretical approaches will be discussed in Chapter 2. As noted by Ziese *et al.* (1994), the different techniques necessarily appeal to different criteria to define their H-T lines and it is not clear that these different approaches should necessarily arrive at the same conclusions. Presently, many authors choose to accept the coexistence of separate boundaries in the H-T plane (e.g. Doniach *et al.*, 1994, distinguish a melting line, an irreversibility line and a depinning line in their theoretical study of disordered crystals; Abulafia *et al.*, 1996, report at least two distinct boundaries within the mixed state). The subject of vortex behavior in twinned YBCO crystals merits further study.

1.5 Transport: Indirect Study of Vortex Behavior

One common method used for studying vortex behavior is four-terminal electrical transport. This geometry is treated in Chapter 3. In essence, a current is applied to a sample and its electrical reaction, an induced E, is measured. In the superconducting state, a zero voltage would ideally be measured from the sample since it presents zero resistance. However, as mentioned above, vortices can move in an applied current, giving rise to dissipation and hence, a voltage signal. Tiny voltage signals measured under the superconducting transition temperature are generally believed to be meaningful evidence of vortex behavior. However, their interpretations are as controversial as they are plentiful. Theoretical interpretations (see Chapter 2) of four-terminal measurements range from the existence of distinct thermodynamic vortex phases to the more microscopic picture of pinning force distributions.

For superconducting thin films of YBCO, the second-order vortex phase transition picture has found experimental support in dc transport measurements. These are summarized in the Ph.D. thesis of Roberts (1995). Anomalous low-field results motivated the work included in this thesis to explore single crystals of YBCO where the systems are generally much larger (thickness on the order of 100 μm as opposed to thicknesses of 0.1 μm for films) and finite-size effects are less worrisome. Furthermore, the published dc transport data are less comprehensive for high-T_c single crystals than for thin films.

The bulk of published transport data for single crystals has presented ρ-T data formats instead of V-I formats. The V-I data for YBCO crystals (surveyed in detail in Section 3.3), though qualitatively similar to that of thin films, has not fit second-order vortex phase-transition pictures as readily (Jiang *et al.*, 1993; Worthington *et al.*, 1992). No rigorous field dependence of crystal

data has appeared in the literature. In addition, as described in Section 1.4, the physics of the mixed state in twinned and impurity-ridden YBCO crystals is still in a state of flux (no pun intended). With these points in mind, this thesis presents four-terminal dc V-I measurements for three single crystals of YBCO with unsurpassed temperature resolution, variation of applied magnetic field, and the introduction of pinning sites via fast neutron bombardment.

CHAPTER 2

THEORY

This survey of theory for vortex behavior in high-T_c materials attempts to construct a thorough backdrop for the specific task of analyzing and understanding *V-I* data for twinned YBCO crystals. It is therefore not exhaustive for the field on the whole, but it is still quite broad. Below, theories hailing from scrutiny of low-T_c materials are considered alongside theories tailored specifically for high-T_c materials, and theories less than two years old are presented with the same attention as those that have thrived in the literature for nearly three decades. In particular we examine several theories of collective vortex behavior, explore the available predictions (both theoretical and numerical) for *V-I* characteristics in the mixed state, and address the specific cases of variable pinning and field strengths.

2.1 Collective Description of Vortex Depinning

2.1.1 *Collective Pinning and Creep*

Long before the discovery of high-T_c superconductivity, a theoretical framework had been established for the effect of pinning on an assembly of vortices. Larkin and Ovchinnikov (LO) first predicted in 1973 that an Abrikosov flux lattice would be distressed by pinning and broken into smaller regimes, or bundles, which retained Abrikosov-like lattice order (Larkin and Ovchinnikov, 1973). The length-scale characterizing the remnant extent of lattice order is now called the Larkin-Ovchinnikov pinning

length, L_p. Later, LO introduced an extensive approach for describing the collective pinning of bundles by material disorder, which is now known as collective pinning theory (Larkin and Ovchinnikov, 1979).

Collective pinning assumes weak pinning, which is to say that vortex-vortex interactions are equal to or greater than the vortex-pin interactions. Pinning centers are assumed to be numerous and randomly distributed in a sample. Various values of the applied magnetic field give different vortex densities, as per Eq. 1.4 above. The variable vortex density gives rise to the different pinning regimes in the theory of LO. Low densities leave vortices to fend for themselves in a forest of pinning sites, and this is called single vortex pinning. At higher fields, vortices assemble in groups of Abrikosov-like lattice order and this is described as small bundle pinning. At still higher values of magnetic field, very large arrays of vortices act collectively and this is called large bundle pinning.

The assumption of weak pinning means that the bundles of correlated vortices may be treated as an elastic manifold. The alternative to this assumption, in the presence of very strong pinning, is vortex *plasticity*, in which pinning overcomes the elastic moduli to the extent that the vortex bundles are irreversibly deformed (LO, 1979; Blatter *et al.*, 1994; Abulafia *et al.*, 1996). For plastic vortex motion, pinning forces and Lorentz forces dominate the vortex equations of motion. In particular, the shear modulus c_{66} is no longer a relevant quantity in plastic flow. Plastic depinning results in islands of strongly pinned vortices surrounded by channels of unpinned or weakly pinned vortices which are uncorrelated with the pinned vortices and free to move. The reader is referred to the work of van der Beek and Kes (1991), who first investigated "plastic creep" in high-T_c superconductors and the recent simulations directed by F. Nori (Groth *et al.*, 1996; Reichhardt *et al.*, 1996).

Collective pinning is discussed in the context of elastic manifolds in quenched random media, of which a vortex lattice is just one possible example. The collection of flux lines is assumed to react elastically to the displacement $u(\mathbf{r})$ of a single flux line. The diagonal elements of the elastic matrix C_{ij} are given by c_{11}, the compression modulus, the tilt modulus c_{44}, and the shear modulus c_{66}. The variation and relative strengths of these moduli under a variety of temperatures, applied fields, and applied currents accounts for a wide range of possible vortex lattice behavior. Taking the line distortion u to reciprocal space, the elastic moduli can be approximated by (Brandt, 1995)

$$c_{11}(\mathbf{k}) \approx c_{44}(\mathbf{k}) \approx \frac{B^2}{\mu_0} \frac{1}{1+\lambda^2 k^2}, \tag{2.1}$$

$$c_{66}(\mathbf{k}) \approx \frac{\phi_0 B}{16\pi\mu_0\lambda^2}, \tag{2.2}$$

where λ is the London penetration depth given by Eq. 1.1 and $\mathbf{k}$ is the wave vector associated with the vortex lattice distortion (Blatter *et al.*, 1994). The most important point at this juncture is that all three are expected to strengthen with an increasing applied field.

As noted before, high-T_c materials require an added emphasis on thermally induced motion of vortices, and the consequences of this effect for collective pinning were examined by several authors in the years immediately following the discovery of high-T_c superconductivity (Feigel'man *et al.*, 1989; Natterman, 1990; Feigel'man and Vinokur, 1990). These authors sought to combine the concept of flux creep with the theoretical structure of collective pinning, and in this vein the idea of collective creep has evolved. It is most admirably and exhaustively set out by Blatter *et al.* (Blatter *et al.*, 1994).

To survey collective creep, we refer to the discussion in Section 1.3 above. With the introduction of collective effects and higher thermal energies, the explicit current dependence of the pinning energy has become more controversial. Now it is generally agreed that characteristic parameters such as α (see Eq. 1.10) will depend strongly on the character of the vortex interactions, the range of applied J, and the temperature of the system. According to Feigel'man and Vinokur (1990), thermally induced disorder in a vortex lattice becomes significant above a field-dependent temperature T^* which they estimated as

$$T^*(B) = \frac{\gamma \phi_0^{3/2}}{\mu_0 k_B \pi \kappa^2} \sqrt{B}, \tag{2.3}$$

where γ is the material anisotropy given by Eq. 3.1, μ_0 is the permeability of free space, k_B is the Boltzmann constant, and κ is the Ginzburg-Landau ratio defined in Chapter 1. Evaluating the expression above for YBCO in SI units, we can simplify it to $T^*(B)=32.84(B)^{1/2}$ for fields expressed in T with the result expressed in K. We see that, given a transition temperature circa 90 K and fields on the order of 1 T, thermal effects are relevant for a large portion of the mixed state for our experiments.

Discussions of collective creep have splintered into a large array of special cases, with different behaviors and numerical parameters predicted not only for single vortex, small bundle, and large bundle pinning, but also for different applied currents, different temperatures, and different material anisotropies. Of primary interest to collective creep is the behavior of a vortex ensemble for vanishingly small currents. The generic prediction for this case is (Blatter *et al.*, 1994; Brandt, 1995)

$$U(J \to 0) \approx U_c \left(\frac{J}{J_c} \right)^{\mu}. \tag{2.4}$$

Such a form leads to a non-ohmic V-I characteristic given by

$$V \propto exp\left[-\frac{U_c}{k_B T}\left(\frac{J_c}{J}\right)^{\mu}\right]. \tag{2.5}$$

The value of μ is then used as a signature for the different regimes of collective pinning. In particular, one expects μ = 1/7 for single-vortex pinning, 3/2 for small-bundle pinning, and 7/9 for large-bundle pinning (Blatter *et al.*, 1994). This relation has proven difficult to verify experimentally for high-T_c superconductors; in general μ is observed to be current, temperature, field, and sample dependent (see Section 4.5). As some authors have noted, the particular influence of current density on the different collective pinning regimes makes it extremely difficult to reconcile the theory with the corresponding analysis of experimental data (Hiergeist and Hergt, 1997). This is simply due to the fact that experiments which seek to test J-dependence will cover a range of J values, passing through several different regimes in a single data set.

2.1.2 *Vortex Glass*

Amid the debate as to whether or not zero linear resistivity could be realized in the mixed state of high-T_c superconductors, a group proposed a truly superconducting phase in the mixed state in the presence of robust pinning. Fisher, Fisher and Huse (FFH) named this phase the "vortex glass" (VG) and predicted a second order phase transition between a pinned glassy state of immobile vortices for $T < T_g$ and an unpinned liquid-like state of finite linear resistivity for $T > T_g$ (Fisher *et al.*, 1991). Characterizing this phase transition are the vortex-glass correlation length ξ_{VG} and a time scale τ. These quantities diverge at a glass-liquid transition temperature T_g according to

$$\xi_{VG} \propto \left|1-\frac{T}{T_g}\right|^{-\nu}, \tag{2.6a}$$

$$\tau \propto \xi_{VG}^{z}, \tag{2.6b}$$

where ν is the static and z is the dynamic critical exponent. The VG theory predicts that $1 \geq \nu \geq 2$ and $4 \geq z \geq 6$. These two exponents combine to define the critical parameter S via $S = \nu(z-1) \approx 6$; this parameter describes the linear resistivities of the vortex liquid ($T > T_g$) through

$$\rho_{lin} \propto \left|\frac{T}{T_g}-1\right|^{S}. \tag{2.7}$$

In addition, the VG theory predicts $0 \geq \mu \geq 1$ (see Eq. 2.5 above). These exponents are expected to be universal for all cases of strong pinning.

Since pinning disrupts the standard Abrikosov flux lattice, the vortex glass theory predicts an absence of long-range translational order for a vortex system. However, in the glassy state where the vortices are strongly pinned, the phase of the superconducting order parameter ψ establishes a non-trivial long-range order.

The theory predicts specific critical behavior to be manifest in a variety of measurements. Below, we focus on dc resistivity measurements (see Section 2.2.1). It is important to note that the results of four-terminal dc resistivity measurements provided the first experimental support of the vortex glass theory.

2.1.3 *Bose Glass*

A different sort of superconducting phase was proposed by Nelson and Vinokur (1992). They treated the case of a vortex system in the presence of correlated disorder; correlated disorder includes twinning boundaries, grain boundaries and columnar defects resulting from heavy-ion irradiation. Specifically, Nelson and Vinokur described pinning in the case of columnar defects. In most crystalline high-T_c samples, correlated disorder is believed to be more prevalent, or at least more relevant to vortex pinning, than are point defects. Focusing on correlated disorder presents a certain simplification in that one can consider a 2D array of line-like pinning centers instead of a 3D array of point-like pinning centers. Nelson and Vinokur mapped the physics of vortices onto the problem of localization of quantum-mechanical bosons in two dimensions, and this allowed them to borrow from the results of other investigations such as ^{4}He films on disordered substrates (Fisher *et al.*, 1989).

For the case of correlated order along the crystallographic c axis parallel to an applied magnetic field, the Bose glass model predicts a second-order phase transition between the Bose glass state, characterized by strongly pinned vortices localized to the areas of correlated disorder, and a flux liquid state as the temperature is increased from $T < T_{BG}$ to $T > T_{BG}$. The Bose glass displays true superconductivity with zero linear resistivity; in addition, the vortices possess an infinite tilt modulus, c_{44}, such that they remain strongly localized even for nonzero tilt angles of the applied field with respect to the c axis. The flux liquid exhibits finite linear resistivity and is therefore a non-superconducting state.

As set out rigorously in 1993, the Bose glass formalism begins with a analogy between vortex lines trapped by columnar pinning sites and a quantum particle in a two-dimensional cylindrical

potential (Nelson and Vinokur, 1993). The potential well for a vortex is composed of both the sharp hole of the columnar pinning site and the vortex-vortex repulsion that the vortex experiences from its nearest neighbors (see Fig. 2.1). The model assumes that a vortex spends most of its time around one defect site or another. This "tight-binding" allows the vortices to hop from one site to another, but it does not allow them to linger somewhere in between sites. The tight-binding Hamiltonian is most simply written

$$H_{TB} = -\mu \sum_j a_j^\dagger a_j + \sum_{i \neq j} t_{ij} (a_i^\dagger a_j + a_j^\dagger a_i) + V_{int} \sum_j a_j^\dagger a_j a_j^\dagger a_j, \qquad (2.8)$$

where μ is the chemical potential, t_{ij} represents the elements of a probability matrix for site-to-site vortex hopping, and V_{int} is an interaction energy for two vortices occupying the same pinning site. The $a_j\dagger$ and a_j create and destroy flux lines on a columnar pin site $\mathbf{R}_j$

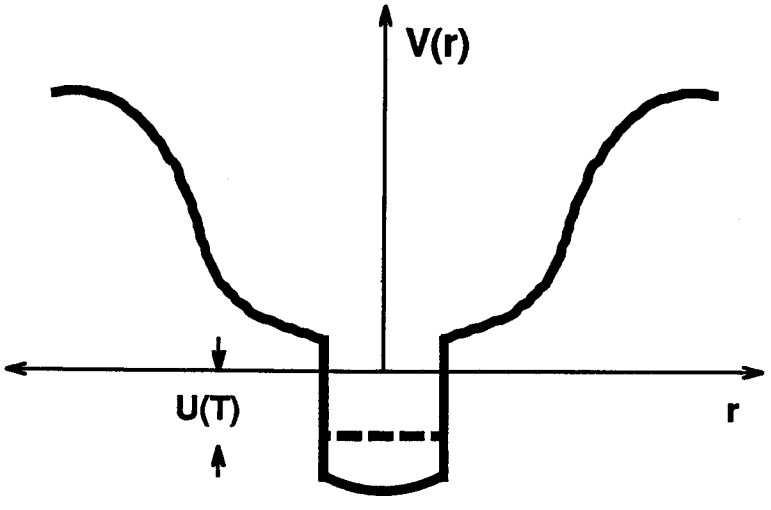

FIG. 2.1 A cross section of the potential for a vortex confined to a columnar pinning site. $U(T)$ represents a temperature-dependent barrier to flux activation. (Adapted from Fig. 12 of Nelson and Vinokur, 1993)

(positions in a plane perpendicular to the c axis). The flux line "particles" described here are bosons because subsequent versions of the Hamiltonian are symmetric under permutation, and the ground-state wavefunction of such a Hamiltonian is necessarily bosonic (Feynman, 1972). It is this elegant mapping of vortices onto bosons that gives the model its name. In most cases, V_{int} is taken to be prohibitively large, such that double-occupancy of a pinning site is neglected; instead, most of the effort focuses on determining the hopping matrix elements.

As in the vortex glass model, certain length scales are crucial to the description of the Bose glass. The most important of these is the localization length $l_\perp$ which measures the extent to which a vortex wanders from a columnar pin. Delocalization occurs when the temperature and applied field are such that the eigenfunctions of the tight-binding Hamiltonian give vortex position ranges, $\mathbf{r}_j(z)$ that overlap those of neighboring vortices. Formally, one defines this length via

$$\lim_{z\to\infty}\overline{\left\langle|\mathbf{r}_j(z)-\mathbf{r}_j(0)|^2\right\rangle}=l_\perp^2(T). \tag{2.9}$$

The localization length diverges at the transition temperature T_{BG},

$$l_\perp(T)\sim\frac{1}{(T-T_{BG})^{\nu_\perp}}, \tag{2.10}$$

where the critical exponent $\nu_\perp$ is similar to ν of the vortex glass theory. While $l_\perp$ is difficult to obtain experimentally, $\nu_\perp$ should be within an experimenter's reach. Unlike the vortex glass theory, the Bose glass theory accounts for the inherent anisotropy of the copper-oxide materials. Just as $l_\perp$ describes the localization perpendicular to the applied field and hence to the correlated disorder, a localization length parallel to the applied field (c axis) is given by

$$l_{\parallel}(T) \sim \frac{1}{(T - T_{BG})^{\nu_{\parallel}}}, \tag{2.11}$$

where the exponent $\nu_{\parallel} = 2\nu_{\perp}$ (with $\nu_{\perp}$ predicted to be $\approx$ 1). The theory also has a dynamic exponent z' (predicted to be $\approx$ 6 or 7).

The Bose glass model is based on a sample with correlated disorder, but the authors acknowledge that point disorder will be present in almost any real sample. Comparing point and correlated disorder is a non-trivial task. Proceeding with a rough comparison of pinning energies, Nelson and Vinokur estimate that, for weak point disorder, twin boundary pinning dominates the physics of vortex dynamics for any vortex excitation (in the language of the Bose glass model, a "kink") smaller than two kilometers. They therefore conclude that point defect interference is only of academic interest in a sample with correlated disorder, except in cases of more robust point defects, such as those introduced by neutron or proton irradiation (see Section 3.7).

For single crystals of YBCO, the most prevalent type of disorder is twinning. Even for crystals with impressive transport characteristics, twin boundaries have been measured via TEM to be spaced 50-100 nm apart (Drake *et al.*, 1993). This corresponds to the intervortex spacing a_o for applied fields of, respectively, 1-0.2 T; obviously the pinning by twin boundaries is critical to an analysis of vortex dynamics in YBCO crystals. In their original work, the authors of the Bose glass model give the subject of twin boundaries limited attention, stating that the problem is more complex than that presented by columnar defects. Given a parallel set of twin boundaries, a new diverging length scale and exponent are required analogous to 2.9 and 2.10 to describe the flux correlation perpendicular to the applied field but parallel to the twin planes. A different universality class for the Bose glass critical exponents should necessarily follow. Later, Marchetti and Vinokur (Marchetti

and Vinokur, 1995) developed a theoretical treatment specifically for the case of twin boundary pinning (see Section 2.3).

Though similar in many ways to the vortex glass model, the Bose glass presents important differences as well. Most notably, the Bose glass should be very sensitive to the angle, θ, between the applied field and a sample's correlated disorder. Though the strong pinning of correlated disorder is predicted to hold the vortices in a parallel orientation for small, non-zero values of θ, any considerable tilt angle will destroy the glassy state as individual vortices tunnel (assuming very low temperatures) through the disorder potential. Fig. 2.2 (Fig. 4 of Nelson & Vinokur, 1993) presents an informative theoretical phase diagram for such a system where, for small θ one assumes that $\theta \approx H_{\perp}/H_{z}$ for the components of the applied field perpendicular and parallel to the correlated disorder.

Numerous experiments have provided strong evidence for the existence of a Bose glass phase. Krusin-Elbaum *et al.* (1994) first reported Bose glass melting in twinned YBCO crystals with columnar defects created by Au ion irradiation; the authors measured the complex component of the ac susceptibility and watched it change sharply at a temperature T_{BG}. These results were further bolstered by the third-harmonic transmissivity measurements of Reed *et al.* (1995) who studied similar crystals, irradiated by Pb ions. The authors varied the angle between the applied field and the axis of the columnar defects to map the predicted cusp in $T_{BG}(\theta)$. Despite these strong pieces of evidence, we note that *V-I* measurements on YBCO crystals with columnar defects have not supported the Bose glass theory (Legris *et al.*, 1993); these efforts noted results that varied greatly with the magnitude of the applied field.

Evidence of the Bose glass in unirradiated crystal systems -- those where native twinning boundaries serve as the primary pinning sites -- has been harder to find. The strongest evidence to date comes from angle-resolved magnetization measurements

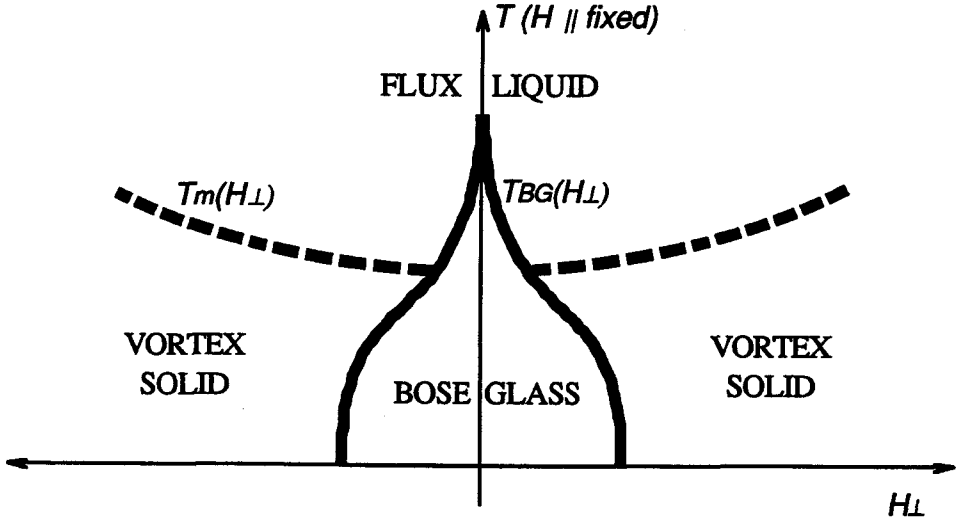

FIG. 2.2: A simplified Bose glass phase diagram for the case of a finite perpendicular field component. (Adapted from Fig. 4 of Nelson and Vinokur, 1993)

which compare detwinned YBCO crystals to crystals with only parallel families of twins (Oussena *et al.*, 1996). These measurements show a dramatic difference between the two systems and report a range of θ about $\theta = 0$ (the alignment of B with the twin boundaries) for which the vortices are "locked-in", or strongly pinned, by the twins. We note that the parallel set of twins is quite different from the twinning in the crystals studied in this thesis (see Chapter 3); ours are heavily twinned in a mosaic pattern.

Evidence for the Bose glass theory has typically been absent in data collected from thin films of YBCO (Wöltgens *et al.*, 1993). However, transport measurements taken from new very thick films of YBCO have shown a sharp cusp in $T_{BG}(\theta)$, matching Fig. 2.2, and have been reported as strong Bose glass evidence (Safar *et al.*, 1996). The thick film data of Safar *et al.* provide a landmark to which we will compare the results of this thesis; just as high-quality thick films hope to emulate single crystals, neutron-irradiated crystals hope to resemble films.

2.2 Interpretations of Voltage-Current Characteristics

2.2.1 *Second Order Transition*

In the view of a second-order vortex phase transition, increasing temperature transforms a truly superconducting phase of immobile vortices to a resistive phase of vortices exhibiting liquid-like motion in an applied current. In the superconducting phase, the vortex structure is characterized as glassy, as described by the vortex glass and the Bose glass.

In an extremely clean material, where disorder does not disrupt the natural structure of the Abrikosov vortex lattice, one expects an abrupt first-order transition between a vortex solid and a vortex liquid (e.g. the melting observed in untwinned YBCO crystals, see Section 1.4). In this case, the shapes of isothermal V-I traces change radically as the temperature moves from one side of the melting transition to the other. Such a change has been reported in the literature (Worthington *et al.*, 1992). However, since V-I traces do not measure thermodynamic quantities directly, they cannot produce direct evidence of melting like the magnetization measurements (Welp *et al.*, 1996).

For a second-order transition, one expects a more gradual change in the V-I isotherms. A trace at the transition temperature T_g should show power law dependence, $V \propto I^n$, with $n > 1$. Isotherms below T_g should show sharp non-linear behavior, exponentially turning down for low current values. Above T_g, the isotherms should show positive concavity and a constant non-zero resistance at low current values. Figure 2.3 depicts the three different types of isotherms in V-I representation, as the data is taken, and also in ρ-J representation. The data is easily analyzed in the ρ-J format, since the constant resistivity plateaus are readily apparent.

According to the vortex glass theory, ρ-J curves are subject to a scaling collapse where all isothermal traces above and below T_g fall onto universal curves F_+ and F_- respectively. In essence, the scaling ansatz proposes $\rho_{scaled}=F_{\pm}(J_{scaled})$ where the scaled quantities incorporate the diverging vortex glass correlation length, ξ_{VG}. Specifically, a dimensional argument in the original formulation predicts the scaling relation

$$\rho(J) \propto \xi_{VG}^{d-2-z} F_{\pm}\left(\frac{J\xi_{VG}^{d-1}\phi_o}{k_B T}\right). \tag{2.12}$$

where d is the dimensionality of the system (presumably 3 in all but the most anisotropic superconductors) and z is the dynamical critical exponent (Huse *et al.*, 1992). The static critical exponent ν also plays a crucial role in the scaling machinery as it describes the divergence of ξ_{VG} as T approaches T_g. We leave the topic of scaling

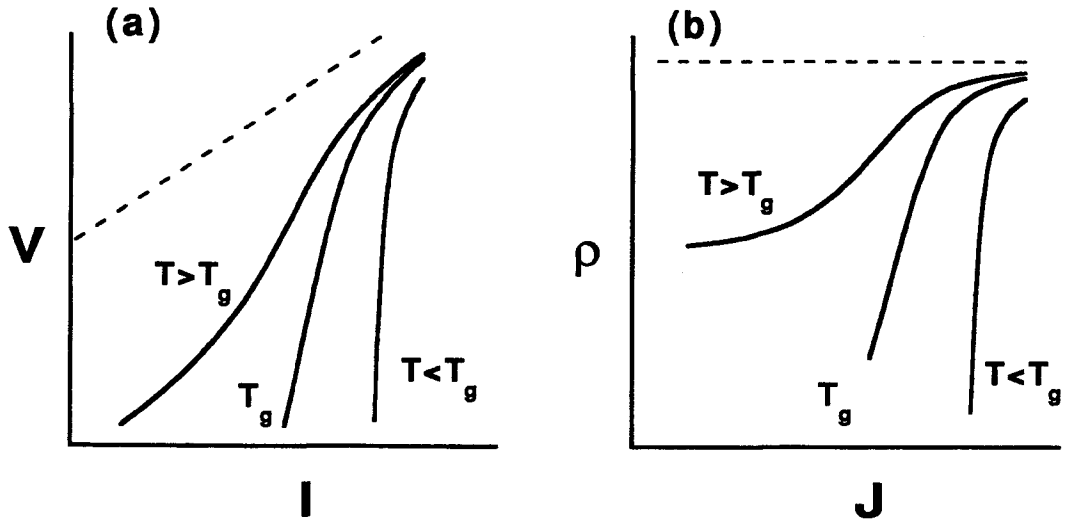

Fig. 2.3: Three regimes expected for second-order vortex phase transition in (a) V-I, and (b) ρ-J formats. Both are double-log plots. The dotted lines depict the slope of Ohmic behavior.

at this overview level, since it does not contribute to the main analytical focus of this work. The explicit forms of Eq. 2.12 for $d = 3$, along with scaled data for YBCO crystals, are given in Section 4.4.

2.2.2 *Pinning Force Distributions*

Traditionally, the dc *V-I* trace serves as a useful diagnostic tool for a superconducting sample. In the low-T_c superconductivity community, the slope of a *V-I* trace is used as a measure of sample homogeneity. Usually, the data are fit to a power-law form, $V \propto I^n$, and the magnitude of n reveals the constitution and overall homogeneity of the superconducting sample (Warnes and Larbalestier, 1986; Warnes, 1988; Jenkins *et al.*, 1991; Goodrich *et al.*, 1993). Higher n values denote more structurally homogeneous superconducting samples. It is not uncommon in low-temperature type-II materials such as NbTi or Nb_3Sn to find n values as high as 100 (Jenkins *et al.*, 1991). The value of n can be temperature and field dependent; in cases where the critical currents are limited by vortex-pin interactions, the n values of low-T_c samples have been found to decrease monotonically with increasing field strengths (Warnes and Larbalestier, 1986; Acerbi *et al.*, 1994).

In the high-T_c copper-oxides, *V-I* traces have been subjected to a different type of scrutiny. This is primarily due to the assumption that the higher thermal energies and stronger vortex-vortex interactions (expected because of larger λ values) manifest in high-T_c systems create an environment very different from that in low-T_c systems.

Greater analytical potential was given to low-T_c *V-I* traces in 1986 when Warnes and Larbalestier, using the earlier results of Baixeras and Fournet (1967), suggested that a critical current distribution could be derived from an experimental *V-I* data set.

Assuming different vortices are depinned at different magnitudes of applied current is equivalent to claiming that different pinning sites may exert different magnitudes of force on vortices. It is then reasonable to describe the voltage across a superconducting sample by

$$V(I) = A\int_0^I (I-I')f(I')dI' \tag{2.13}$$

where $f(I)$ is a normalized distribution of depinning currents and the prefactor A contains the specifics of the dissipative processes. Over all possible positive currents, $f(I)$ is normalized to unity. By simply using Leibnitz' rule for integral differentiation, one solves for $f(I)$.

$$\frac{d^2V}{dI^2} = Af(I) \tag{2.14}$$

Hence, from sufficiently clean V-I data, one can obtain approximate distribution functions. This technique is revisited and proves to be useful in the analysis of V-I data from YBCO crystals in Section 4.6.

Using three specific assumptions, this technique was further developed by Edelman and Larbalestier (Edelman and Larbalestier, 1993). The authors assume that the prefactor A can be set to the normal-state resistance R, that $f(I)$ can be described by a Gaussian distribution, and that the area under $f(I<0)$ should be reassigned to a delta function at $I = 0$ (see Appendix A for details). Starting with these assumptions and Eq. 2.13, they derive

$$V(I) = \frac{R}{2}\left[\begin{array}{l}(I-I_c)erf\left(\dfrac{I-I_c}{\sigma\sqrt{2}}\right) - I_c erf\left(\dfrac{-I_c}{\sigma\sqrt{2}}\right) + \\ I + \dfrac{\sigma\sqrt{2}}{\sqrt{\pi}}\left(e^{-\left((I-I_c)^2/2\sigma^2\right)} - e^{-\left(I_c^2/2\sigma^2\right)}\right)\end{array}\right] \tag{2.15}$$

where *erf* denotes a Gauss error-function integral, I_c is the center and σ the width of the Gaussian. Hence, using R, I_c and σ as fitting parameters, Edelman and Larbalestier are able to fit Eq. 2.15 to experimental *V-I* traces for a NbTi monofilament and a long, Ag-clad $Bi_2Sr_2Ca_2Cu_3O_{10}$ (BSCCO) tape, both for $T < T_c$ (*ibid.*). However, the experimental fits they obtain for R do not match the measured values for the normal state resistance.

It is important to recognize the natural connection between the picture of depinning current distributions and the percolative pictures of vortex depinning which are gaining momentum in the study of high-T_c materials. To the best of our knowledge, this connection has not yet appeared in the literature. Percolation theory for vortex depinning is outlined in the work of Ziese (Ziese, 1996a, 1996b), and is assumed by some of the modeling efforts that appear in Section 2.5.

2.3 Effect of Variable Disorder

To treat the effects of varying disorder on a flux lattice requires a work similar in scope to that of Blatter *et al.* (1994) or Brandt (1995). This section introduces the effects of crystalline disorder relevant to the analyses presented below, touching on the theoretical frameworks above, and treating in particular the cases of twin boundary pinning and changing disorder.

Larkin and Ovchinnikov first showed that the translational crystalline order of a flux lattice is distorted by pinning sites (Larkin and Ovchinnikov, 1973). Recall from section 2.1.1 that the authors described a length L_p that describes the spatial extent to which a vortex array maintains Abrikosov-like lattice order. This length, referred to as the Larkin-Ovchinnikov pinning length, is crucial to the analysis ahead (see Section 3.9).

For examining the effect of disorder, it is instructive to compare the vortex density to pinning site density in a sample. Conversely, one can compare a_o to an average distance between pinning sites, r_p. Note that r_p is not equivalent to L_p; while r_p is determined solely by the defect structure of the sample, L_p reflects the strength of vortex pinning and it depends on the properties of the vortex array (e.g. vortex interactions).

The case of $r_p \gg a_o$, with vortices outnumbering pinning sites, is obviously a very different physical system than $r_p \ll a_o$, where pinning sites are plentiful. For simplicity, we will treat vortices here as rigid rods so that with an applied magnetic field in the z direction, looking along the z axis we can examine the problem in two dimensions. This picture is especially germane to the cases of columnar and correlated pinning.

The vortex glass theory assumes plentiful disorder and increasing the degree of disorder will not adversely affect the vortex glass phase. However, in an absence of plentiful disorder, the vortex glass model is not applicable. The numerous point defects and grain boundaries of thin films make them the most relevant domain for the vortex glass.

The Bose glass theory is quite dependent on the relation of r_p and a_o. For $a_o > r_p$, where every vortex has a columnar pinning site, the theory predicts a strong glassy phase for $T < T_{BG}$. When $a_o = r_p$, the theory predicts a "Mott insulator" phase characterized by an infinite compression modulus c_{11} and an infinite tilt modulus c_{44}. The analogy to the Mott metal-insulator transition likens localized vortices to localized charge carriers (Jones and March, 1973). The magnetic field corresponding to the Mott insulator is designated as B_ϕ, the matching field, and it serves as a scale, or landmark, for the predictions of the theory. To increase or decrease the density of columnar pins is, in the Bose glass picture, to respectively increase or decrease B_ϕ. For $a_o < r_p$, where some vortices are unpinned, the

existence of a glass is predicted at a much lower temperature, $T' \ll T_{BG}$; the "interstitial" vortices must rely on elastic interactions with pinned neighbors to avoid activation. Predictions are submitted much more cautiously for this case since the inclusion of elastic factors brings a new set of variables to the problem.

Marchetti and Vinokur have provided the most thorough theoretical treatment of vortices pinned by a parallel set of twin planes (Marchetti and Vinokur, 1995). The authors assume a magnetic field applied parallel to the c-axis (hence parallel to the twin planes) and an applied transport current both perpendicular to the applied field and parallel to the twin planes. In this geometry, the subsequent Lorentz force on the vortices will always be perpendicular to the twin planes. This case was chosen to avoid the controversial case of vortex motion along twin planes.

In the most simple case of low temperatures and very low magnetic fields ($a_o \gg d$, the average distance between twin boundaries), the problem becomes one dimensional. For simplicity, the authors restrict their treatment to these conditions, namely $T \ll T_c$ and $a_o \gg d$. Having reduced the problem to one dimension, with the twin planes acting only as barriers to vortex activation and vortices so widely scattered that collective effects are negligible, the authors make heavy use of an analogy to variable-range hopping (VRH) of electrons in disordered semiconductors. Using the Bose glass language, VRH corresponds to a vortex "superkink" in which the vortex has nucleated an extensive flux loop, covering several twin plane separations. The other primary mechanism of vortex activation is the standard half-loop nucleation (see Fig. 2.4), which is analogous to carrier tunneling from impurity levels to the conduction band in disordered semiconductors.

Given the assumptions above, the cases of varying applied current and sample size are described in some detail, with predictions for the dependence of the resistivity on current density

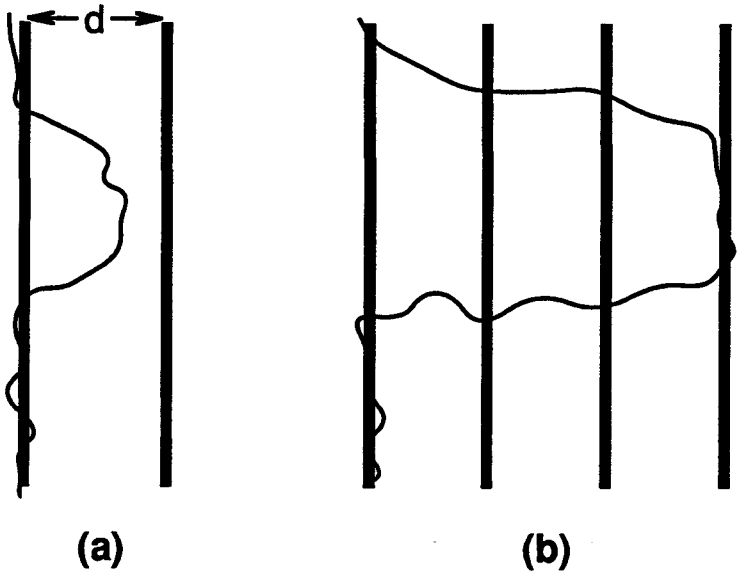

Fig. 2.4: Sketch of (a) half-loop and (b) variable-range hopping for vortices between twin-boundaries. The twin boundaries (heavy lines) are separated by a distance d and run perpendicular to the page. The applied field is parallel to the twin boundaries.

in each case. For low currents, $J \ll J_c$, vortex motion is predicted to precede via VRH with kink sizes much larger than the average twin plane spacing. The corresponding resistivity is given by

$$\rho_{VRH} \approx \rho_0 exp\left[-\left(\frac{E_k}{T}\right)\left(\frac{J_0}{J}\right)^{1/2}\right], \qquad (2.16)$$

where E_k is a characteristic energy scale, ρ_o is the flux flow resistivity, and J_o is a current density which depends greatly on the assumptions for a given case. For larger currents, $J < J_c$, the kink size is expected to shrink to a size less than d. In this case, the measured resistivity is expected to follow

$$\rho_{hl} \approx \rho_0 exp\left[-\left(\frac{E_k}{T}\right)\left(\frac{J_1}{J}\right)\right], \tag{2.17}$$

where J_1 is the current which divides the regions of VRH and half-loop excitation. Though this theoretical approach is the most complete treatment of twin boundary pinning to date, the strict assumptions set out above make its relevance to experiments near T_c very limited. In the case of the present work, even for data taken at very low fields (e.g. 3 mT for crystal #1), the temperatures are quite high, generally within 10% of T_c. In addition, the families of twin boundaries in the crystalline samples are not consistently parallel, but rather make a complicated cross-hatched, (or mosaic), pattern (see Section 3.2) such that Lorentz forces are not exclusively acting transverse to twin planes. Nevertheless, we attempt to fit our data to Eq. 2.16 and Eq. 2.17 in Section 4.6.

2.4 Effect of Variable Magnetic Field

At first glance, this appears to merely be the other side of the coin presented in Section 2.3. Instead of changing r_p, a variation of magnetic field simply changes a_o and one is left with same set of comparisons. However, the matter is much more complicated since both vortex-vortex interactions and vortex-pin interactions are strongly field-dependent.

For the process of collective creep, the strength of the applied magnetic field is crucial. Different predicted behaviors of the fluxoid manifold follow for different values of field (Blatter *et al.*, 1994). Recalling that collective creep assumes weak pinning, the case of $a_o \approx r_p$ only arises for very low fields and this results in single vortex pinning. Collective effects are negligible. Recall from Section 2.1.1 that, as the field is increased, one expects to move from single-vortex to small-bundle pinning to large-bundle pinning.

Further increases in the field lead to the charge density wave pinning regime (Blatter *et al.*, 1994); for the high-T_c copper-oxides, the charge density wave regime is only a matter of theoretical study since extremely pin-free samples are required.

The sensitivity of vortex interactions to the field strength is encapsulated in the field-dependence of the elastic moduli which generally increase with field (see Eq. 2.1 and 2.2). It should be noted that these expressions are often modified for specific cases. For a highly anisotropic material, each modulus is separated into an expression parallel to the applied field and perpendicular to the applied field. In particular, the shear modulus c_{66} is thought to drop off abruptly (in the plane perpendicular to the applied field) as B approaches B_{c2}. This collapse has now been observed experimentally (Wu *et al.*, 1997).

The vortex glass model is field-independent. Given strong pinning and a correspondingly short r_p, any applied field in the mixed state is predicted to follow the glass-to-liquid phase transition governed by the universal critical exponents ν and z. The glass transition temperature T_g is expected to decrease with field following

$$H \propto \left|T_c - T_g\right|^{2\nu_o}, \tag{2.18}$$

where T_c is the superconducting transition temperature and ν_o is expected to be about 2/3 (Eq. 2.18 is simply a restatement of Eq. 1.16; see Section 1.4). The universality is predicted to hold down to the extreme case of $r_p \ll a_o$, where even an isolated pinned vortex is predicted to undergo a glass-liquid transition (Fisher *et al.*, 1991).

As described in the previous section, the Bose glass theory uses the matching field B_ϕ as a landmark for its various predictions. For magnetic fields $B > B_\phi$, vortices outnumber sites of correlated disorder and the existence of a glass is much more fragile in the

presence of thermal excitations. For this case, theoretical refinement for the Bose glass theory has recently been proposed that make B_ϕ an even stronger dividing line than before (Radzihovsky, 1995).

Radzihovsky describes a division of vortex populations into those localized to columnar pinning sites and those left to inhabit the interstitial regions between pinning sites (*ibid.*). The vortices localized to the pinning sites form, independently, a strong Bose glass (SBG) equivalent to the Bose glass phase for $B < B_\phi$. However, the interstitial vortices, with a population defined by the fraction $(B - B_\phi)/B$, are localized only for low temperatures, when the pinned vortices "cage" them through strong vortex interactions. The combination of the pinned and interstitial vortices form a weak Bose glass (WBG) at low temperatures which gives way to an interstitial liquid with increasing temperatures and finally a total vortex liquid at even higher temperatures where both vortex populations are depinned. The corresponding phase diagram is depicted in Fig. 2.5.

Interestingly, the implications of this modification to the Bose glass theory for *V-I* measurements are substantial. For $B > B_\phi$, one now expects to find two flux flow regimes -- one for the flow of the interstitial population and one, at higher currents, for the flow of the strongly pinned population. A *V-I* curve in this regime would correspondingly show two separate regions of Ohmic behavior, one beginning at a characteristic critical current J_{cw} for the WBG and another at a higher current J_{cs} for the SBG. The first resistivity plateau is approximated by

$$\rho_{ff}^{II} = \rho_n \frac{\left(B - B_\phi\right)}{B_{c2}}, \tag{2.19}$$

where ρ_n is the normal-state resistivity and B_{c2} is the upper critical field.

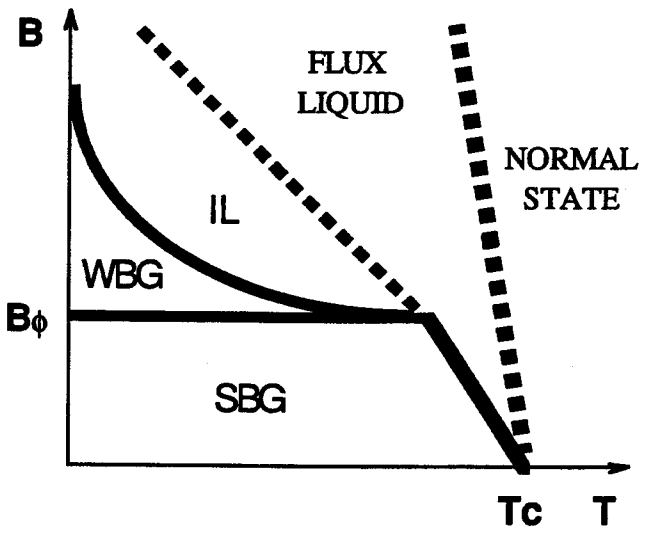

Fig. 2.5: Phase diagram for the modified Bose glass theory of Radzihovsky (1995). IL is the interstitial liquid, WBG is the weak Bose glass, SBG is the strong Bose glass, and the Mott insulator exists between WBG and SBG at the matching field B_ϕ.

2.5 Modeling Results

Though the second-derivative analysis as presented in Section 2.2 has rarely been applied to the experimental *V-I* data of copper-oxides, several theoretical and numerical efforts have used the same spirit -- namely, starting from the notion that applied currents probe a distribution of pinning strengths -- to simulate *V-I* traces for high-T_c superconductors. This section surveys the most successful and meaningful attempts to construct *V-I* isotherms from basic principles.

It is somewhat surprising how easily a power-law isotherm can be generated using nothing more than a Gaussian approximation of *f(I)* and Eq. 2.14 from above. This is shown in the work of Edelman and Larbalestier, (1993), and in Appendix A. In the remainder of this section, three of the most attractive

simulations of *V-I* data for high-T_c superconductivity are reviewed: that of Wörderweber (1992), that of Yamafuji and Kiss (1996), and that of Faleski *et al.* (1996).

In 1992, Wörderweber set out a simple model of vortex depinning in high-temperature superconductors that quantitatively simulated *V-I* traces. This approach was labeled the modified flux-line shear (FLS) model, referring in part to the flux-line shear model originally developed for the study of low-T_c materials by Kramer (1976). The FLS method assumes that some flux lines are more strongly pinned than others. With an applied field along the *c* axis of a sample and a current applied in the *ab* planes, a resistive signal arises when the more weakly pinned flux lines overcome the vortex interactions of their more strongly pinned neighbors. These depinned vortices form percolative channels of flux flow along areas of weak pinning. Once the Lorentz force of the applied current exceeds the shear force of the local flux line lattice, dissipation occurs via the channels of flow. The FLS model, as first postulated, is limited by the assumption that all channels of flow are identical.

This does not present an accurate picture of real materials, especially in the case of high-T_c samples, and Wörderweber set out to modify the FLS model to account for the natural variability of the flux motion channels. Ignoring other possible contributions, including the crucial role of thermally activated flux motion, the modification predicts an electric field of the following form.

$$E = \sum_i \left(J - J_{c,i}\right)\rho_n\left[B/B_{c2}(0)\right], \tag{2.20}$$

where the index i represents the various channels and ρ_n is the normal-state resistivity. The critical current density, $J_{c,i}$, varying from one channel to the next, accounts for a distribution of pinning strengths much like the approach of Warnes. However, instead of working from a distribution of critical currents, Wörderweber

expresses the channel currents as they depend on a distribution of upper critical fields $B_{c,i}$ within the sample via

$$J_{c,i} \approx (B_{c,i}^2 / w_i)(1/B_{c,i})(1-b_i)^2(1-0.29b_i), \qquad (2.21)$$

where w is the width of a channel, $B_{c,i}$ is the critical field of that channel and $b_i = B/B_{c,i}$. In this way, the relevant distributions of channels are expressed in terms of the applied magnetic field. The modified FLS model uses a simple Gaussian centered around $B_{c,mid}$:

$$n_i \propto \exp\left[-(B_{c,mid} - B_{c,i})^2 / 2\sigma^2\right]. \qquad (2.22)$$

The width of the distribution, σ, depends on the quality of the sample. Since thermal energies are crucial to the study of the mixed state, temperature dependence is provided for each $B_{c,i}$ by assuming that $B_c \alpha (T_c - T)$. Using Eq. 2.20 and the distribution in Eq. 2.22, the modified FLS model provides set of isofield V-I traces given a set temperature (e.g. 77 K for many early experiments).

Although the format of the data collected here for YBCO crystals makes it difficult to compare with this model (see Chapter 3; we did not collect data for scores of fields at a fixed temperature), we set forth Wörderweber's simulation because it embraces the idea of distributions of critical parameters within a superconducting sample for high-T_c materials. For our experimental critical current distributions (see Section 4.6) and subsequent data simulation (see Appendix A), the work of Wörderweber provides helpful context. In particular, Wörderweber notes that σ fits cleaner samples at smaller values than it does more disordered samples. He finds that the V-I traces simulated for smaller values of σ are much steeper than those simulated for larger values of σ. Similar results are found from our data when we assume a distribution of critical currents (see Section 4.6). Finally, we note that the FLS model is a natural stepping stone for connecting the concepts of critical current distributions and plastic vortex motion.

Yamafuji and Kiss (YK) have recently explored the depinning of vortices with the aim of explaining the various results of V-I measurements for the copper-oxides (YK, 1996). Specifically, the authors attempt to account for the variety of reported critical exponents for the supposed second-order phase transition between a pinned glassy state and the flux liquid. Not only does their percolative model calculate sets of V-I traces, but it also calculates scaling functions in the spirit of the vortex glass model.

Like Wörderweber, the authors assume a percolative mechanism of flux flow, with more weakly pinned vortices (or clumps of correlated vortices) being stripped from their positions before the more strongly pinned vortices. However, YK start with distribution functions of critical currents; this renders the theoretical superconducting sample as a network of islands, each with their own J_c, much like the picture provided by Warnes and Larbalestier (1986). The distribution function, $P(j_c)$, and the probability distribution function, $S(j_c)$, are set out simply as

$$\int_{j_c^{min}}^{j_c^{max}} P(j_c)dj_c = 1, \tag{2.23}$$

$$S(j_c) = \int_{-\infty}^{j_c} P(j_c)dj_c. \tag{2.24}$$

The electric field induced by the flow of flux follows from

$$E(J) = \rho_f S(0)J + \rho_f \int_0^J S(j_c)dj_c, \tag{2.25}$$

where ρ_f represents the flux flow resistivity for a depinned channel of vortices and $S(0)$ represents the vortex population that is unpinned with zero applied current. In this sense, $S(0)$ contains the qualification for true superconductivity. A non-zero $S(0)$ precludes zero linear resistivity, while a zero $S(0)$ denotes true superconductivity, at least for infinitesimal currents. The so-called phase transition in this model occurs as increasing temperature

moves the distribution $P(j_c)$ to lower and lower current ranges. At low temperatures, $P(j_c)$ possesses a finite minimum j_c^{min} that allows for zero linear resistance for $J < j_c^{min}$. The percolative transition occurs when, at a higher temperature T_p, $j_c^{min} = 0$. For $T > T_p$ a segment of the vortex population is always depinned and a non-zero linear resistance follows.

Instead of a Gaussian or other simple assumption for the distribution functions of high-temperature superconductivity, YK skip the $P(j_c)$ step altogether, opting instead for a probability function both phenomenological and contrived:

$$S(j_c) = 0 \quad ; j_c < j_c^{min},$$

$$= \left(j - j_c^{min}\right)^{\frac{z-1}{2}} \left[\frac{j_c^{2(1-s)}\left(j_c^s + \left(j_c^{min}\right)^s\right) + \left(j_c^{min}\right)^2}{j_c^2 + \left(j_c^{min}\right)^2} \right]^{\left(\frac{(z-1)}{2}+1-s\right)q} \quad ; j_c^{min} \le j_c < j_c^{max}. \quad (2.26)$$

Here, z corresponds to the critical exponent as it appears in the vortex glass picture, while s and q are both numerical fitting parameters. Using 2.26, YK simulate E-J curves and scale them according to the vortex glass prescription. Though the underlying mechanisms appear somewhat arbitrary, the important result of this modeling effort is that is gives ν and z values which depend directly on the flux pinning characteristics, such as j_c^{min} which represents the current at which a percolative network has formed in the sample and a finite resistivity appears macroscopically. Unfortunately, YK do not quantitatively predict how z and ν should vary. In addition, they do not speculate on the physical significance of s and q, even though these parameters also significantly affect the critical parameters.

A promising and sensible approach has recently been set forth by Faleski *et al.* (1996). Though their simulation is carried out

in the $T = 0$ limit and presently offers more qualitative than quantitative information, the lack of phenomenological compromise in the simulation is very attractive. The goal of the authors' efforts is obtaining a connection between different types of flux motion (e.g. elastic versus plastic, see Section 2.1.1) and macroscopically observable quantities (e.g. *V-I* characteristics). They note that the interpretation of *V-I* results is still highly controversial. By varying the strength of pinning in their model, Faleski *et al.* show that large-scale patches of vortex flow at weak disorder give way to a plastic response, or channel-based in the arguments above, as the strength of pinning is increased.

In a two-dimensional framework Faleski *et al.* start with equations of motion for the vortex positions $\mathbf{r}_i$ in the presence of a Lorentz force $\mathbf{F}$, (originally set out by Jensen *et al.*, 1988) given by

$$\gamma_1 \frac{d\mathbf{r}_i}{dt} = -\sum_{j \neq i}^{N_v} \nabla_i V_v(\mathbf{r}_i - \mathbf{r}_j) - \sum_{k=1}^{N_p} \nabla_i V_p(\mathbf{r}_i - \mathbf{R}_k) + \mathbf{F}, \tag{2.27}$$

where the N_p pinning centers have positions $\{\mathbf{R}_k\}$, there are N_v total vortices, and γ_1 represents the coefficient of friction for a single vortex. The potentials V_v and V_p denote, respectively, the vortex-vortex and vortex-pin interactions. Given the model's assumptions for the basic form of the repulsive V_v and the attractive V_p, the simulation solves for the drift velocity in the direction of the applied Lorentz force, which can be defined as

$$v_d(F) = \left\langle \frac{1}{N_v} \sum_{i=1}^{N_v} \mathbf{v} \cdot \hat{\mathbf{F}} \right\rangle, \tag{2.28}$$

where the brackets denote an average over disorder. By calculating v_d versus F curves, Faleski *et al.* essentially describe *V-I* curves since v_d is presumably proportional to the measured V and F to the applied I.

The model creates distributions of instantaneous velocity. Fig. 2.6 displays their main results, showing both the pinned and depinned populations. Upon studying two extreme cases -- one of very weak pinning and one of strong pinning, achieved by varying the V_p depth by a factor of five -- the authors find two very different pictures. For weak pinning, patches of correlated vortices move at a smooth distribution of velocities, but for stronger pinning the distribution clearly displays a bimodal structure of "slow" vortices and "fast" vortices. Logically, the slow lobe of the distribution corresponds to the vortices which, in plastic flow, are strongly pinned, whereas the fast lobe corresponds to the vortices flowing through the channels. Interestingly, by monitoring the time evolution of a single vortex in their simulations, Faleski *et al.* show that all vortices participate in both types of behavior. Apparently, there is a regular interchange between vortices in pinned islands and vortices in the fast-flowing channels. This has direct ramifications for voltage noise observed in high-T_c superconductors (see Appendix B).

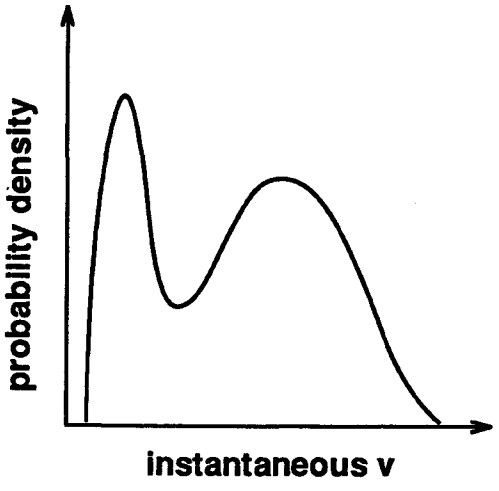

Fig. 2.6: Sketch of vortex velocity distribution for the case of strong pinning. (Faleski *et al.*, 1996). The left-most, narrow peak corresponds to strongly pinned vortices, while the right-most, broad peak corresponds to vortices which flow in channels around the pinned vortices.

Unfortunately, the predictions for the shape of experimental *V-I* characteristics are still very rough, though the authors note that non-linear *V-I* traces are more readily generated in the plastic regime than they are in the weakly-pinned elastic regime. In any case, the simulations of Faleski *et al.* are only truly relevant for very low temperatures given their assumptions. The authors promise more complete models in the near future.

CHAPTER 3

EXPERIMENT

3.1 YBaCuO Biography

Soon after Bednorz and Müller's discovery of superconductivity in $La_{2-x}Ba_xCuO_4$, the groups of Paul Chu and Maw-Kwen Wu synthesized the compound $YBa_2Cu_3O_7$ (YBCO) in 1987 (Wu *et al.*, 1987, Chu *et al.*, 1987); it was superconducting at 92 K. YBCO has a nearly perovskite crystal structure with two CuO planes per unit cell; these planes are crucial to superconductivity in the high-T_c copper-oxides (Chu, 1996).

The unit cell of $YBa_2Cu_3O_7$ is rectilinear, with the c axis measuring 11.68 Å and nearly symmetric axes a = 3.88 Å and b = 3.82 Å. This structural asymmetry between the c axis and the ab planes (also called the CuO planes) is responsible for the well-documented anisotropy in the electrical transport properties of YBCO. The anisotropy γ can be defined by

$$\gamma \equiv \left(\frac{m_{ab}}{m_c}\right)^{\frac{1}{2}} = \frac{\xi_c}{\xi_{ab}} = \frac{\lambda_{ab}}{\lambda_c} \tag{3.1}$$

where the m values denote the effective carrier masses, ξ is the superconducting coherence length, and λ is the magnetic penetration depth. Using the convention of Eq. 3.1, the anisotropy of YBCO is 0.2, but it should be noted that the anisotropy is often defined as the inverse of Eq. 3.1, such that 5 is often quoted for γ in YBCO.

3.2 Crystalline Samples

The crystals studied in this thesis were synthesized by B. W. Veal and his coworkers at Argonne National Laboratory using the self-flux method. Samples #1 and #2 were grown in an Au crucible and were consequently Au-doped at 3% for Cu. Sample #3, of significantly lower quality than the first two samples, was grown in an Al crucible. The YBCO crystals are heavily twinned in a mosaic pattern. Images from a polarized light microscope, as in Fig. 3.1, show them to be twinned to the smallest resolvable optical scale (approximately a micron); similar crystals in the literature have been shown via TEM (transmission electron microscopy) to possess twinning domains of approximately 50-100 nm in width and tens of microns in length (Drake *et al.*, 1993).

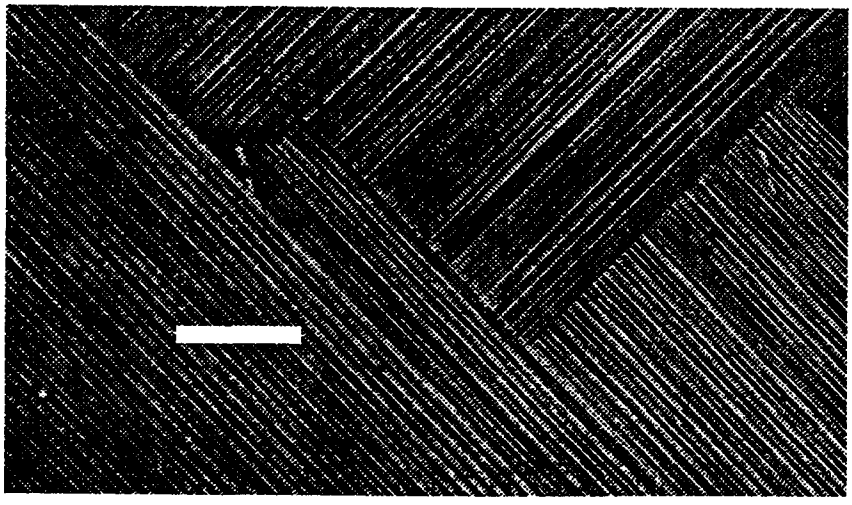

Fig. 3.1: Digitally enhanced image of the surface of an YBCO crystal seen through a polarized light microscope. This crystal, not studied, was synthesized in the same crystal batch as crystal #2. The white bar represents 20 μm in length. The *c* axis of the material is perpendicular to the page.

Each "plank" in Fig. 3.1 corresponds to one of two *a b* orientations (see Fig. 5.1). In one case, the *a* axis is aligned with the vertical boundary of the figure and the *b* axis is aligned with the horizontal boundary of the figure. In the other case, both axes are rotated ninety degrees.

The crystals' specifications are listed in Table 3.1. In addition, the ρ-T characteristics are shown in Fig. 3.2, 3.3, and 3.4 for crystals #1, #2, and #3 respectively. The normal state resistivities for crystals #1 and #2 compare nicely to other reports in the literature (Zeldov *et al.*, 1989; Palstra *et al.*, 1989).

The effect of Au impurities on the characteristics and performance of these crystals is negligible (B. W. Veal, private communication; H. Claus *et al.*, 1993). The Au impurities do not impede superconductivity and since they do not form normal islands in the superconductor, they are not expected to function as pinning sites. The transition temperatures of Au-doped YBCO crystals are comparable (if not better in some cases) than Au-free crystals, and the sensitivity of the Au-doped crystals to oxygen depletion is much less severe than that in Au-free crystals (Claus *et al.*, 1993).

Table 3.1: Sample descriptions and parameters for YBCO crystals.

YBaCuO sample	dopant	dimensions (mm^3)	T_c(K)	ΔT(K)	ρ_n ($\mu\Omega$cm)
crystal #1	Au (3%, Cu)	2x1x 0.08	90.7	0.4	40
crystal #2	Au (3%, Cu)	1x1.15x0.15	92.8	0.3	60
crystal #2 irradiated	Au (3%, Cu)	1x1.15x0.15	92.6	0.4	60
crystal #3	Al (3%, Cu)	1.1x1x0.22	83	8	580

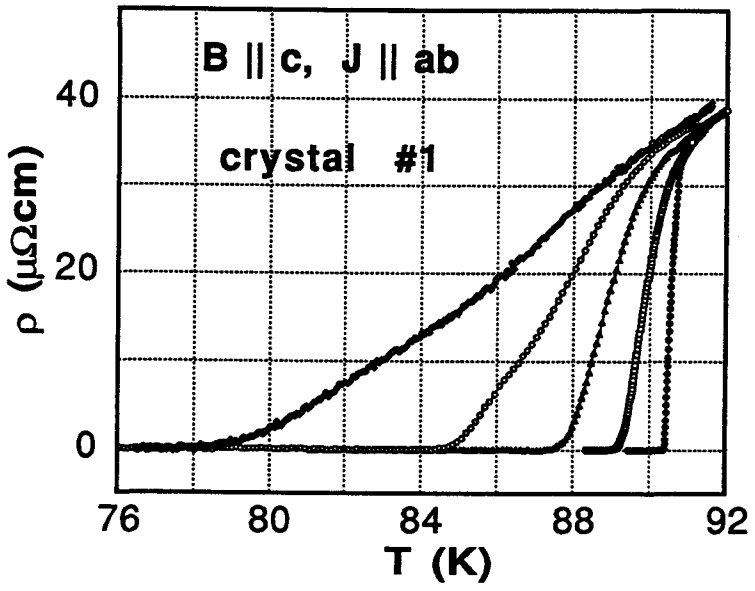

Fig. 3.2: ρ-T traces for YBCO crystal #1. From right to left, applied field values are: 0, 0.25, 0.5, 1.5, and 5 T. All data taken with 8 mA.

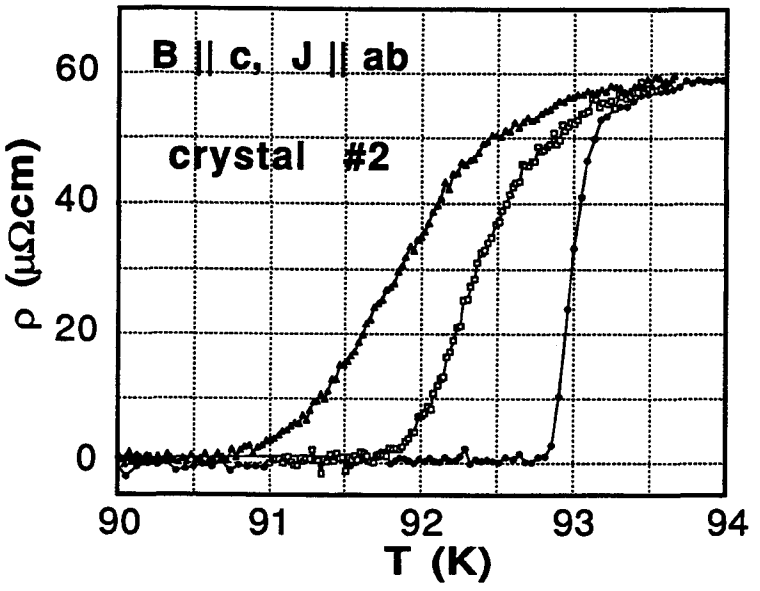

Fig. 3.3: ρ-T traces for YBCO crystal #2. From right to left, field values are: 0, 0.25, and 0.5 T. All data taken with 10 mA.

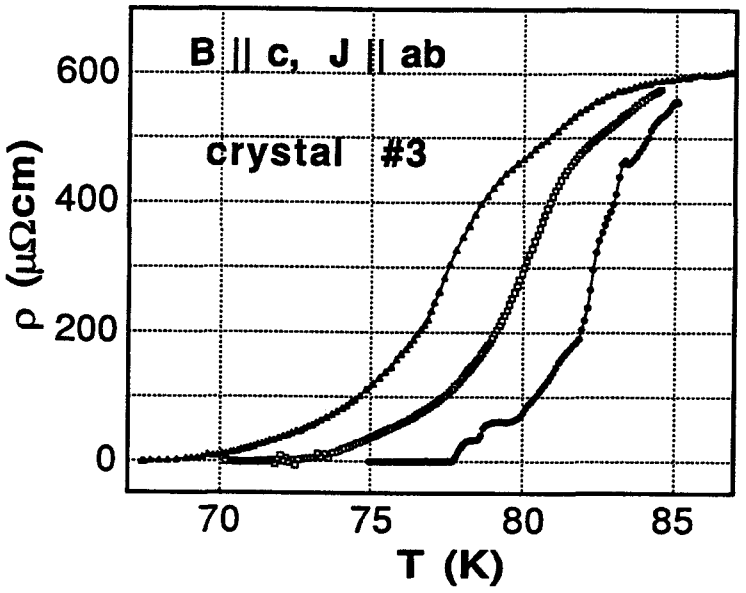

Fig. 3.4: ρ-T traces for YBCO crystal #3. From right to left, field values are: 0, 0.5, and 1.0 T. All data taken with 5 mA, except for the 0 T set which was taken with 1 mA.

3.3 Resistivity Measurements

High-T_c materials have been vigorously studied using a variety of techniques in the decade since their discovery, and, as with any research endeavor, the quantity of publications risks outstripping the quality of progress. Therefore, it is necessary to set out a litany of published resistivity measurements for YBCO crystals with the goal of providing a comprehensive context for the work presented in this thesis. We focus here exclusively on twinned and/or irradiated crystals because our samples are twinned and, in one case, irradiated, but also because the results for untwinned single crystals, as mentioned in Chapter 1, are much more thoroughly understood at the time of this writing (Crabtree *et al.*, 1996). The principal results and their implications can now be

meaningfully addressed since a theoretical framework has been established in Chapter 2.

Four-terminal dc resistivity measurements are a fundamental method of studying the electrical properties of a material. They are a particularly useful diagnostic tool for superconductors since the onset of superconductivity is dramatically apparent, as seen in Fig. 3.1 - 3.3. In addition, these measurements provide information about the behavior of flux vortices in the mixed state. In the presence of an applied magnetic field, the resistive signal below the zero-field transition temperature can be attributed to the motion of vortices (Bardeen and Stephen, 1965; Y. B. Kim *et al.*, 1965). Dissipation arising from vortex motion accounts for the broadening witnessed in the ρ-T characteristics pictured above.

Four-terminal resistivity measurements for YBCO crystals have been conducted by many authors. T. K. Worthington *et al.* published the first measurements in 1990 with a sensitivity of 200 nV. This work, conducted in fields from 0 to 9 T for a presumably twinned single crystal, showed a resistive shoulder at about 20% the normal state resistivity. Similar shoulders are now familiar for YBCO crystals (see the kink in Fig. 3.2 $T < T_c$). More twinned crystals were measured in 1991 by P. L. Gammel *et al.* and their V-I measurements, without a critical scaling analysis, were presented as qualitative evidence confirming a vortex glass phase transition. However, the V-I traces did not clearly show a $T < T_g$ regime; the authors admitted that the determination of T_g for their data was difficult at best.

The following year saw increased activity for twinned crystals. N.-C. Yeh *et al.* (1992) presented a vortex glass critical scaling analysis for ac resistivity measurements of twinned YBCO. They concluded their results were consistent with a second-order phase transition, with critical exponents $z = 3$ and $\nu = 2/3$. Later, W. K. Kwok *et al.* (1992) published copious ρ-T curves for twinned

crystals with various field orientations with respect to the twin boundaries. They concluded that a first-order solid-liquid melting transition was possible when the applied field was misaligned with the twins, but that the melting was suppressed by pinning when the field was aligned with the twins (parallel to the c axis).

A landmark paper for YBCO crystals was published in 1992 by T. K. Worthington *et al.* (Worthington *et al.*, 1992). This work presented thorough, closely spaced V-I isotherms in the region of T less than but near T_c before and after proton and Au ion irradiation. Both the pre-irradiation and post-irradiation data showed S-shaped isotherms in a ρ-J representation. Such curves are difficult to interpret in the picture of a second-order vortex phase transition since a single power-law isotherm is not present and two plateaus of linear resistivity appear. The authors claimed their data was indicative of an intermediate vortex state, the "vortex slush", between the vortex glass and the vortex liquid.

In 1993, similar measurements were published by W. Jiang *et al.* and N.-C. Yeh *et al.* for twinned YBCO crystals before and after proton irradiation. These data showed none of the S-shaped behavior of Worthington's measurements, but the current density window examined was narrower. These data were interpreted in the vortex glass framework, and critical exponents of $z = 3$ and $\nu = 0.65$ were reported.

The effect of columnar defects on the resistivity measurements of twinned YBCO crystals was described by A. Legris *et al.* in late 1993. Pb ion irradiation created homogeneous columnar defects in the crystals and the authors examined the V-I characteristics before and after irradiation. Specifically, they chose in each case a temperature which separated regions of negative curvature from positive curvature and fit this isotherm to $V \alpha I^n$. Values of n showed no sensitivity to field before irradiation ($n = 2$ for 0 to 4 T fields), but demonstrable sensitivity afterwards ($n = 3.4$

for 8 T up to $n = 8$ for 0.5 T). The authors claimed that this showed that a second-order vortex phase transition was not a relevant picture for crystals with defects. However, their data lack isotherms in the important regions of flux flow (high-J behavior) and of $T < T_p$, the temperature from which the authors derived n.

W. K. Kwok *et al.*, in 1994, published ρ-T curves for an YBCO single crystal with only two twin boundaries. They found the curves depended strongly on the angle between the applied field and the twins; in addition, they mapped the "peak effect" (a sharp critical current J_c enhancement for T just under T_c) and correlated it to their resistivity data. They concluded that the solid vortex lattice softened as it began to melt and this allowed to twin boundaries to pin the lattice more effectively, thus increasing the critical current. Despite discussing the shear moduli of the vortex lattice, their interpretation focused on vortex phase transitions.

Unusual V-I characteristics of unprecedented sensitivity were published in 1995 by Charalambous *et al.* using a novel technique on a twinned single crystal. The isotherms, of a very noisy character in the pV range, were few and far between. Qualitatively, they did not match vortex glass predictions and the authors did not present a critical scaling collapse. However, since the isotherms did appear to change slope at a temperature T_g, the authors concluded that the measurements provided evidence for a vortex glass-liquid phase transition in twinned YBCO crystals. In addition, they claimed that measurements of courser sensitivity could not be trusted to probe the vortex glass phase.

Finally, in 1996, ρ-T data were published by W. K. Kwok *et al.*, this time for an YBCO crystal containing only *parallel* twin boundaries. With a current applied perpendicular to the twins, the authors presented data for a variety of geometrical orientations, again showing a dramatic effect of the angle between the twins and the applied field. They found maximum pinning effects for a field

parallel to the twins, and defined three temperatures: $T_m < T_c$ the lattice melting temperature; $T_p < T_m$ a temperature which marks the boundary between elastic ($T < T_p$) and plastic ($T > T_p$) response of the vortex solid; and $T_i < T_p$ a temperature below which bulk pinning dominates pinning by twins (see Section 5.1).

Whereas ρ-T measurements are both thorough and plentiful in the list above, what is lacking is a thorough study of the field-dependence of V-I isotherms which clearly includes T less than the depinning temperature (or the glass transition temperature, T_g, depending on one's analytical preference). In addition, though light ion irradiation and heavy ion irradiation (resulting in columnar tracks) have been employed, no group has yet taken four-terminal measurements after using fast-neutron irradiation, which, at the moderate doses we describe below, creates point defects homogeneously without adversely affecting the superconducting properties of a sample.

On a more analytical note, one sees in the list above the strong tendency of the community to interpret resistivity measurements in the context of thermodynamic phase transitions even though these measurements can only produce indirect evidence for such behavior (Crabtree *et al.*, 1996). This persists, even as authors studying twinned crystals with other techniques (e.g. torque magnetometry and vibrating reeds) often analyze their results in the more conventional context of collective pinning. Therefore, in addition to addressing the holes in the resistivity experiments carried out to date, we hope to interpret our data in a broader context, considering both vortex phase transitions and less sexy possibilities such as thermal depinning. Finally we hope to directly address, for the first time, the qualitative similarity of ρ-J measurements in a variety of copper-oxide superconductors, including thin films, single crystals, and materials other than YBCO.

3.4 Crystal Mounting

To ease handling and decrease the possibility of damaging the crystalline samples, each single-crystal YBCO sample was attached to a small (roughly 0.1"x0.1"x0.06") piece of MgO substrate using Ag epoxy. The MgO was cut using a razor blade and a hammer; the resulting piece was cleaned with acetone in an ultrasonic bath.

Each crystal/MgO combination was attached to a sample holder before any electrical measurements were made. The sample-holders were fabricated in-house starting with Cu-coated, printed circuit (PC) board. Electrical leads were patterned onto the PC board using photolithography; the remaining Cu was later plated with Au. The reader is referred to the Ph.D. thesis of J. M. Roberts (1995) for further details. The pattern used is depicted in Fig. 3.5. After patterning, a pocket was milled in the center of the PC board to accommodate the crystal/MgO combination. The pockets were approximately 0.1"x0.1" and 0.04" deep (leaving 0.01" of thickness), but varied with the MgO slab chosen for the particular crystal. Silly putty^{TM} lined the pocket to ensure a tight reliable coupling between the MgO and the milled pocket of the PC board. In addition, two threaded holes were made in the PC board to accommodate screws which provided further security for keeping the MgO in place.

When the investigation of voltage fluctuations in an applied field became important (see Appendix B), an optimized sample holder was made to test for systematic noise. Fig. B.4 depicts the new holder and the relative noise level for the two holders.

3.5 Electrical Contacts

The quality of electrical contact to a sample is of the greatest importance to four-terminal measurements since contact resistance

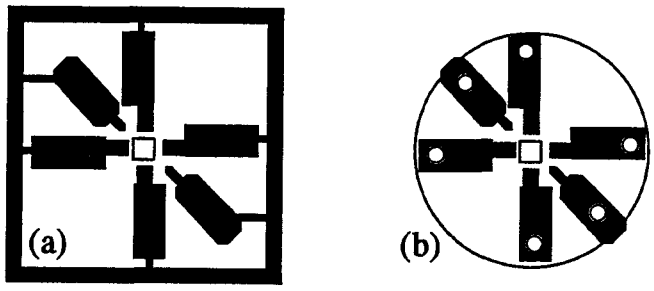

Fig. 3.5: Sample holder (shown to scale) for YBCO crystal (a) during patterning, machining and Au-plating, and (b) in its finished form. Square shows sample pocket in each case and white circles in (b) depict holes which accommodated Au pins for electrical connections.

will contribute to the noise level of the voltage measurements and in this way limit the overall sensitivity. Furthermore, resistance from the current contacts gives rise to heating and temperature instability during data collection. Making reliable electrical contact to the crystals was complicated by many factors. The slick ceramic surfaces of the crystals did not readily bond to metallic paints, epoxies or solders. The tiny size of the crystals required both manual dexterity and the use of a microscope. The brittle nature of the crystals required minimal sample handling.

Many recipes exist for such contacts; it is left to the preferences of the researcher, the equipment available to that researcher, and perhaps even her or his spiritual leanings to select a method. In this work, one method worked especially well, and given a little patience, durable contacts which measured approximately 100 mΩ each were achieved.

All crystal handling was conducted in gloves that had been washed and dried. To position the crystal in a way that rendered as many sides accessible as possible, a tiny ball of silly putty^{TM} was stuck to the end of a sewing needle. This ball was then used to carefully snare the crystal. The eyed end of the needle was fixed in

a rectangle of Styrofoam which was, in turn, weighted by a quarter to provide stability. YBCO single crystals stuck readily to the silly putty^{TM}, and in the absence of excess heat it was a simple matter to remove the crystalline samples completely from the putty. Brightly colored putty was ideal (fluorescent orange and pink) since any putty residue remaining on the dark crystal was visible or, in the case of the irradiated sample, any crystalline fragment was easily seen against the colorful putty background.

With the crystal situated on the putty and focused under a microscope of 150x magnification, a sharpened wooden shaft (fashioned from a Q-tip^{TM}) was used to take a raisin-sized bit of Dupont 5504N Ag epoxy from its container. The epoxy was placed on a clear glass slide and given fifteen minutes to thaw (the epoxy is stored in a freezer). While the epoxy thawed, drops of acetone were occasionally added and stirred in, leaving the epoxy soupy but not runny -- ideal for painting.

A 10–μm diameter Au wire was then grasped gently with soft tweezers. This thin type of wire makes for a challenging paint-brush because it can be difficult to see outside the field of view of the microscope, but it is capable of making very thin contact lines on a crystal. After dipping the wire gently in epoxy, two opposite ends of the crystal, (typically the two ends of smallest overall area and certainly ends that were perpendicular to the *c*-axis of the crystal), were painted with epoxy. These faces constitute the current contacts and they were thoroughly coated in epoxy to encourage homogeneous current flow throughout the crystal. On the top surface of the crystal, thin straight lines were painted parallel to the two coated faces of the crystal (see Fig. 3.6). If the crystal was large enough, more than two lines were painted to provide multiple options for the voltage contacts. Many practice runs were carried out before an YBCO crystal was painted. In addition to doggedly avoiding the ingestion of caffeine, painting many practice lines on a slide is strongly recommended for the novice.

After letting the epoxy patches dry in air for at least twelve hours, the crystal was placed in an oven under continuous O_2 flow. The contact pads were sintered by baking at 360 C° for at least 150 minutes. Optimum contacts were achieved for 190 minutes of baking. A slowly ramped warming and cooling (no more than 3.5 C°/min.) strategy is recommended before and after the baking.

Wires were connected to the sintered pads by dipping them in silver epoxy which was prepared in the same fashion as described above. Gold wires of 50 μm diameter were connected to the large pads on the ends of the crystal, while gold wires of 10 μm diameter were used for the voltage contacts on the top face of the crystal. See Fig. 3.6 for a diagram of a contacted crystalline sample. After twelve hours of drying under air, the crystal was again baked under flowing O_2 gas. The contacts were annealed at 160 C° for at least 150 minutes. Extra baking time in an O_2 flow did not appear to hurt the contacts or the crystal properties.

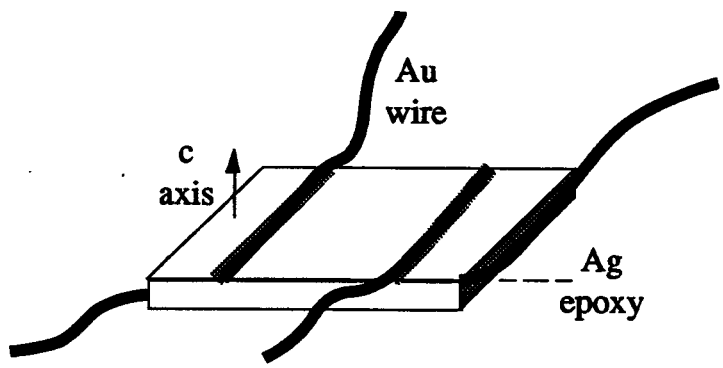

Fig. 3.6: Electrical contact configuration for an YBCO crystal. Wires on opposing ends correspond to applied current contacts and wires on top crystal face correspond to voltage measurement contacts.

3.6 Data Accumulation Procedure

ρ-J data were collected with the YBCO crystal placed in a variable temperature insert inside a liquid-He dewar. Temperatures were stabilized to within 10 mK for a given data set with the aid of a LakeShore DRC-91CA temperature controller and careful manual management of the rate of liquid He flow from the He reservoir to the variable temperature insert. Even for minor adjustments of temperature between data sets, twenty or more minutes were allowed to elapse to minimize both the temperature gradient between the crystal and the He flow valve and the gradient between the crystal and the nearby Pt thermometer. In contrast to the film experiments of Roberts (Roberts, 1995), an observable and sometimes stable temperature gradient manifest itself between the crystal and the Pt thermometer. This gradient was found during ρ-T measurements for sample characterization, and is attributed to the necessarily modest thermal contact (a tiny blob of Ag epoxy) between the crystal and the MgO substrate.

A magnetic field, generated by a 9-T NbTi magnet, was applied parallel to the c axis of the crystal. Most data sets were taken for a field-cooled (FC) crystal. However, data collected for a zero-field-cooled (ZFC) crystal were indistinguishable from the field-cooled data. Though one expects greater instability for the ZFC data as flux makes its way into the crystal, the lack of an observed difference here is probably due to the relatively high temperatures at which the experiments were run (Ziese *et al.*, 1994). Ziese *et al.* (1994) carefully mapped the effect of FC versus ZFC in crystals and films using a vibrating reed technique; they found that, for $B \parallel c$, FC and ZFC YBCO crystals exhibited identical flux behavior for $T > 79$ K ($T_c = 90.5$ in this case). All ρ-J measurements for crystals #1 and #2 were taken above 79 K. When changing field magnitude between data sets, careful attention was given to avoiding trapped flux. Generally, sets of data were taken in order of increasing field strength, and when the field was decreased, the crystal was taken

well above its transition temperature and field-cooled at the new lower field value before any new data were collected.

All E-J data were collected at stabilized temperatures and are referred to as isotherms. An isotherm itself consisted of a sweep of current values, starting at currents so low as to see no resistive signal and ending at the detection of sample heating via contact resistance. Typically, all isotherms were taken with logarithmically increasing current; however, the data were sometimes taken with decreasing current and no hysteresis was observed for any of the crystals (see Fig. 3.7). After a given isotherm had been collected, a slightly higher temperature was targeted and, after twenty to thirty minutes of T stabilization, another isotherm could be collected in the same manner. For most fields, isotherm spacing was 0.08 - 0.10 K, but for the lowest fields spacings dipped as low as 0.03 K.

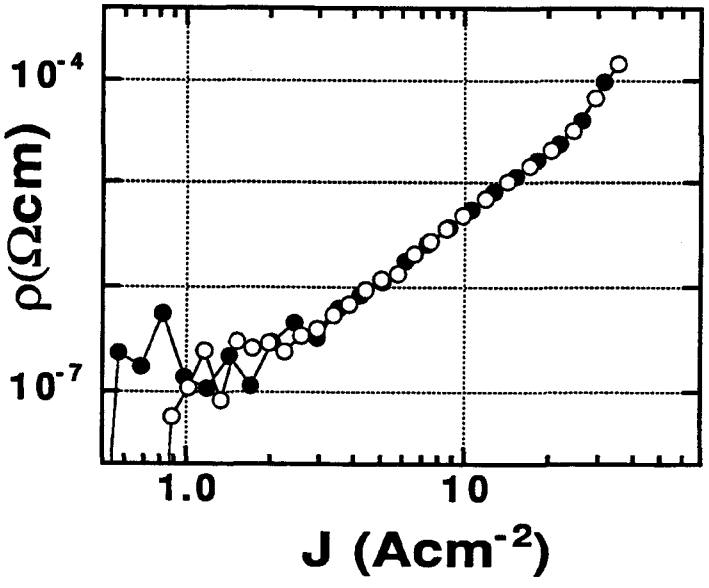

Fig. 3.7: ρ-J data exhibiting no hysteresis. Data taken for YBCO crystal #3 in 0.25 T || c with increasing J for 74.001±.002 K (filled circles) and with decreasing J for 74.004±.003 K (open circles).

3.7 Neutron Irradiation of YBaCuO Crystals

To create point defects in crystal #2, fast neutron bombardment ($E > 0.1$ MeV) was employed. The irradiations took place at the Missouri University Research Reactor (MURR), lasting three hours each. Fast neutrons are known to produce a homogeneous distribution of point defects in YBCO crystals at a rate of approximately 1 defect per cubic meter for a flux of 2 neutrons per square meter (Sauerzopf *et al.*, 1995). The average diameter of the damage sites, as measured by TEM, is 2.5 nm (Frischherz *et al.*, 1994). The added defects enhance the critical current of the crystal by strengthening the bulk pinning force exerted by the defects on the vortices. In fact, for modest neutron dosage (less than 8×10^{21} n/m^2) and an applied field oriented parallel to the crystal's c axis, the critical current in the ab planes can be accurately approximated by $J_c \propto \Phi_n^{1/2}$ where Φ_n represents the total neutron flux. The enhancement is only observed up to certain fluences (approximately 1×10^{22} n/m^2); critical currents fall again as copious defect levels render a crystal incapable of superconductivity. The first irradiation of crystal #2 lasted three hours and yielded a net flux of 1.5×10^{21} n/m^2. The second irradiation raised this total to 3×10^{21} n/m^2.

Neutron irradiation also affects the transition temperature of YBCO. A decrease in T_c of about 2 K for every 10^{22} n/m^2 is expected (Sauerzopf *et al.*, 1995). However, for low levels of neutron flux, annealing the crystal in O_2 can partially restore pre-irradiation T_c values. For this experiment, the T_c of crystal #2 decreased by approximately 0.3 K after the 1.5×10^{21} n/m^2 irradiation and subsequent annealing schedule. Fig. 3.8 shows ρ-T traces collected from crystal #2 after the first irradiation. The transitions are still quite sharp and the broaden with field in a manner very similar to the pre-irradiation data. However, an anomalous hump appears in the normal state, just above T_c in the ambient-field data set. This feature is weakly current-dependent and appears in the flux-flow

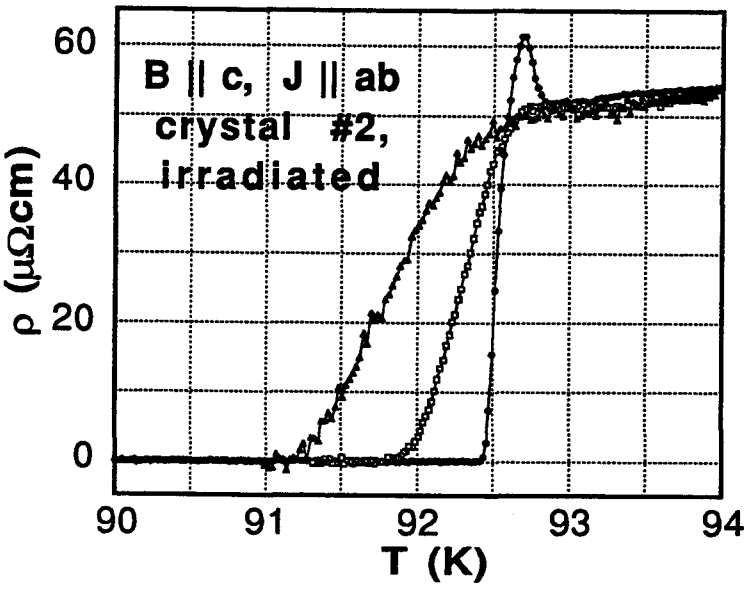

Fig 3.8: ρ-T traces for YBCO crystal #2 after irradiation. From right to left, fields values are: 0, 0.25, and 0.5 T. All data taken with 8mA.

V-I data depicted in Fig. 3.17 and 3.18. The feature is absent for applied fields greater than 0.25 T. This feature has been seen in the literature for single crystals of $L_{2-x}Ce_xCuO_4$ (L = Pr, Nd, Sm) and $Bi_2Sr_2CaCu_2O_8$ (Crusellas *et al.*, 1992; Briceño *et al.*, 1991). It has been attributed to T_c inhomogeneity in superconducting samples and is thought to reflect the intrinsic granularity of copper-oxide single crystals (Crusellas *et al.*, 1992). Specifically, the inhomogeneity in T_c arises from variations in oxygen content from one region to another. An applied field suppresses the effect since it essentially homogenizes T_c across the entire sample. For most applied fields and $T < T_c$, the feature is absent and is not problematic for the V-I data we collect.

Though the irradiations themselves were relatively simple, the subsequent experiments were complicated by several factors. The most obvious by-product of the irradiation was the resulting

radioactivity of the crystal. The crystal gained an activity -- primarily beta -- of 50 μCi but decayed within a matter of weeks to a long-term 1 μCi after the first irradiation, and a long-term 2 μCi after the second. The primary radioactive isotopes resulting from the neutron irradiation were Ag110 and Au198. Table 3.2 lists the detectable activated isotopes of Au-doped YBCO crystals containing residual Ag from electrical contacts.

The residual radioactivity complicated the electrical contact procedure. To limit dosage, we were required to limit the time used in making contacts, increase the average distance maintained between fingers and the crystal, and use a clear perspex shield to protect the body and head of the researcher. Since Ag was one of the most susceptible isotopes to neutron activation, removing the old electrical contacts before an irradiation was critical. This extra handling of the crystal, especially removing the hardened epoxy and pulling off the Au wires, risked complete sample destruction.

Another factor that complicated the resistivity measurements was the decrease of structural integrity resulting from the irradiation damage. The crystal's integrity was so compromised

Table 3.2: Radioactive isotopes and their activity levels following 6 hours of neutron irradiation at MURR.

isotope	activity (μCi)	half-life (days)	primary decay	energies (keV)
Cu-64	7890	0.05	E.C.; β+	511, 1346
Au-198	2010	2.71	β-	412
Y-90	254	2.67	β-	1761
Ag-110m	8	250	β-	658, 885, 938
Ba-131	1.3	11.8	E.C.	216, 373, 496

after the *second* irradiation that it shed large flakes under the slightest physical pressure and it disintegrated entirely before any four-terminal measurements could be collected. Assuming a 2.5 nm diameter for each damage site introduced by fast-neutron impact and using the approximations of Sauerzopf *et al.* (1995), one finds an average damage site volume of approximately 8 nm^3 (1.5 x 10^{11} damage sites in all) after the two irradiations. When comparing the resulting total volume of damaged crystal to the crystal volume, one finds a volume fraction of 1 : 8 x 10^5. Though it is reasonable to conclude that this would be difficult to observe optically, the surface and edges of crystal #2 were easily seen to be degraded under an optical microscope (x300 magnification).

Two factors could contribute to the discrepancy between the calculated volume fraction and the obvious structural damage introduced by the fast-neutron irradiations. For one, the crystalline samples are doped with Au, and Au is known to stress its nearest neighbor bonds after neutron irradiation (private communication, J. Farmer). The affected Au substitutions stress the surrounding crystal lattice and result in damaged regions much larger than the initial 2.5 nm site. Another possibility, undocumented as far as we know, is that the resulting beta-activity continues to damage a crystal. The energies of the beta decays (0.5-1 MeV) are quite comparable to the 1 MeV range which is usually employed in electron-irradiation experiments (Fendrich *et al.*, 1995). Though the total beta dosage estimate of crystal #2 after several months of decay is only 1 x 10^{20} m^{-2} which is at least 1,000 times less than that of Fendrich *et al.*'s experiments, it should be noted that the beta-irradiations of those experiments were conducted at 30 K (*ibid.*). According to Caton *et al.* (1990) electron irradiation at elevated temperatures (i.e. room temperature) can result in catastrophic damage in the form of large amorphous regions of material which subsequently tend to grow even larger if left in a room-temperature environment.

3.8 Data

In the following figures we present ρ-J isotherms for the three YBCO crystals in various applied fields. For crystal #2, we show data taken both before and after fast-neutron irradiation. Each set includes highly non-linear isotherms at high J and, as the temperatures increase from one isotherm to the next, more linear isotherms indicating dissipative, non-superconducting behavior for all J. The plots can be read starting with the lowest T parallel to the right border and ending with the highest T parallel to the top border. The standard deviation of T is generally less than 5 mK for an isotherm. Some data have been omitted for the high J and high T regions in each plot. This is for the sake of clarity since data show very little temperature dependence in some regions and it becomes difficult to distinguish the individual data sets. The current-dependent resolution of the resistivity simply reflects a constant voltage resolution. Since they affect the sensitivity of the experiment, voltage fluctuations were studied in detail (see Appendix B).

We start with crystal #1 for six different applied fields (see Fig. 3.9-3.14). Higher fields give larger temperature windows of scrutiny than lower fields. This is consistent with the field-induced resistive broadening shown in Fig. 3.2-3.4. The data for 3 mT (Fig. 3.9) show very abrupt behavior. The two broken isotherms correspond to 90.315±.002 K on the right and 90.494±.003 K above. The shape of the data changes dramatically within 180 mK. It is possible that 3 mT is below H_{c1} and that the data in Fig. 3.9 probe the Meissner phase. The most recent estimates for YBCO crystals give $H_{c1} \approx 35$ mT at 80 K (Govorkov *et al.*, 1994), and there is strong evidence that H_{c1} falls under 1 mT for $T > 90$ K (Koncykowski *et al.*, 1991). All data for fields of 30 mT (Fig. 3.10) and higher are confidently classified as mixed state data.

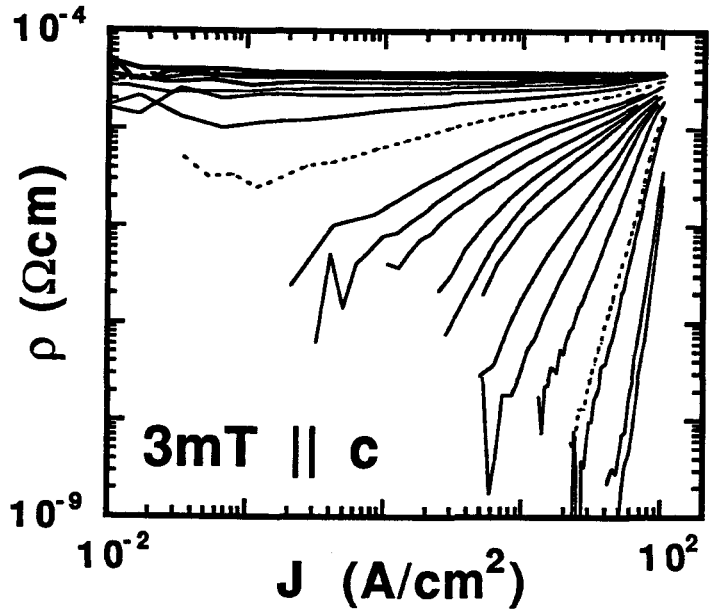

Fig. 3.9: ρ-J data for crystal #1 in 3 mT. Temperatures range from 90.20 to 90.90 K with an average spacing of 30 mK.

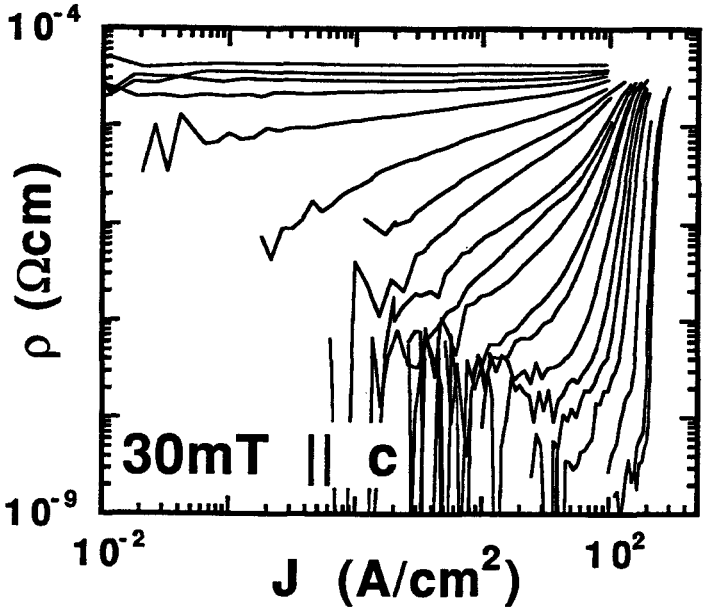

Fig. 3.10: ρ-J data for crystal #1 in 30 mT. Temperatures range from 89.35 to 91.49 K with an average spacing of 50 mK.

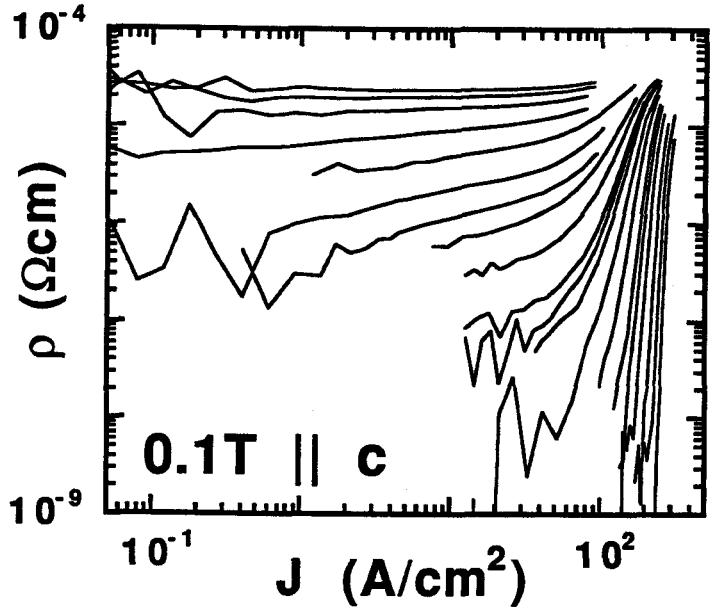

Fig. 3.11: ρ-J data for crystal #1 in 0.1 T. Temperatures range from 88.77 to 90.32 K with an average spacing of 80 mK.

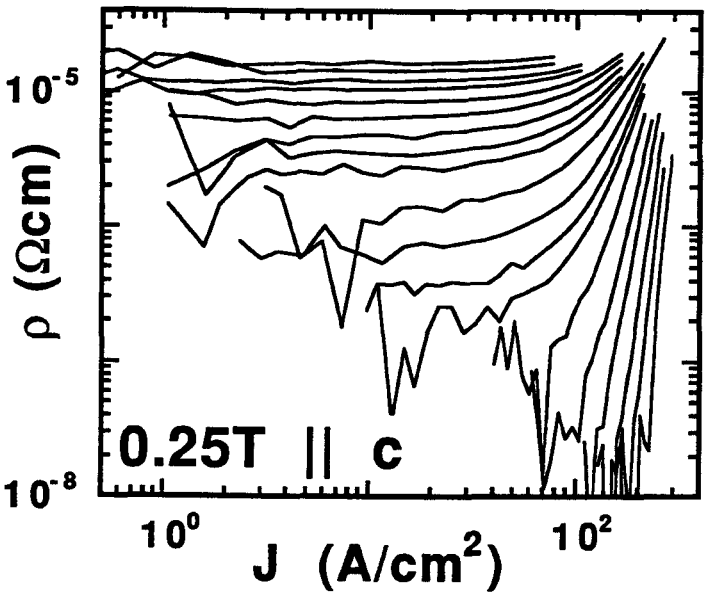

Fig. 3.12: ρ-J data for crystal #1 in 0.25 T. Temperatures range from 88.37 to 89.81 K with an average spacing of 75 mK.

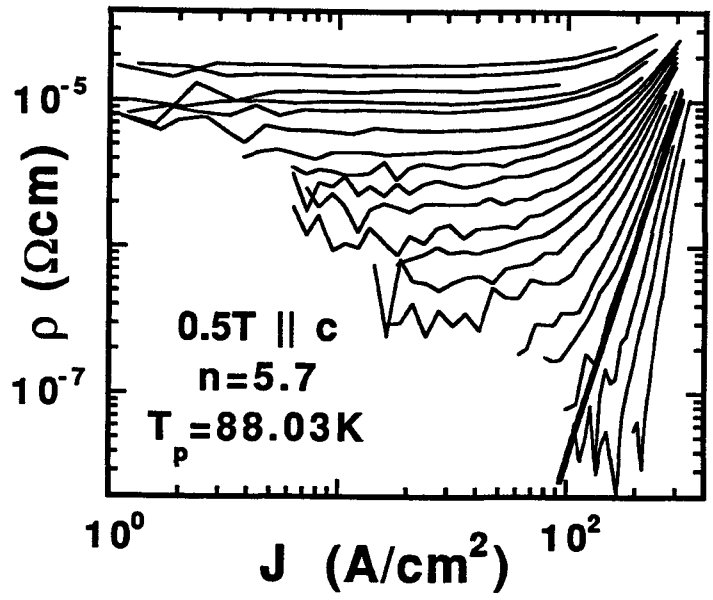

Fig. 3.13: ρ-J data for crystal #1 in 0.5 T. Temperatures range from 87.57 to 89.44 K with an average spacing of 100 mK.

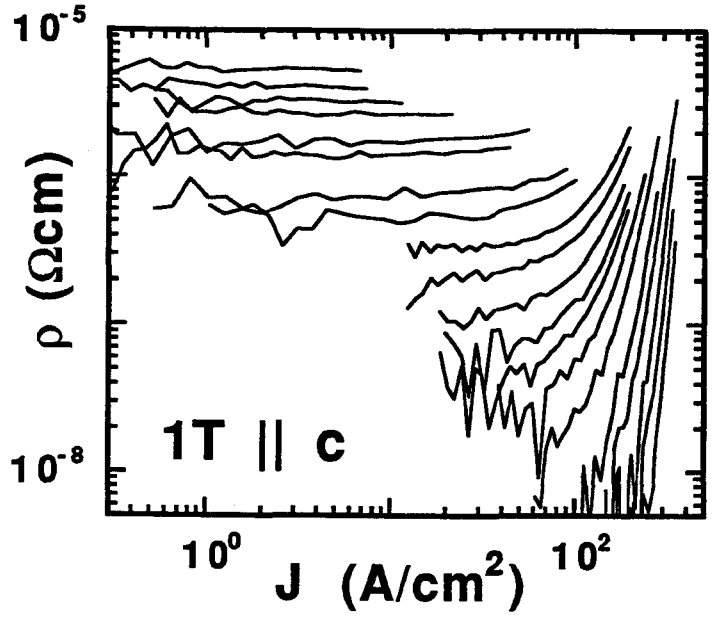

Fig. 3.14: ρ-J data for crystal #1 in 1.0 T. Temperatures range from 85.45 to 87.75 K with an average spacing of 100 mK.

The heavy line and the parameters shown in Fig. 3.13 are related to the analytical method described in Section 3.9. In addition, we point out that the data for 1 T presented in Fig. 3.14 appear less thorough than the other sets because of the experimental difficulty involved. For all crystals, the depinning region occurs at higher J for higher fields. The J needed to probe the region of interest for 1T required applied currents of up to 0.25 A. This led to contact heating, and many isotherms were cut short to avoid contact or sample damage. Unfortunately, in the case of Fig. 3.14 (and to a much lesser extent Fig. 3.12 and 3.13), this impeded the mapping of the flux flow region where the isotherms bend over towards a constant resistivity at high J.

Next we show five plots for crystal #2. Data taken before fast-neutron irradiation are displayed in Fig. 3.15 and 3.16. Note that the J needed to probe the depinning region are somewhat lower for crystal #2 than for crystal #1. This points to weaker pinning in crystal #2. Again, the heavy lines and the parameters listed are explained below in Section 3.9.

Fig. 3.17, 3.18, and 3.19 depict data for crystal #2 in three different applied fields after fast-neutron irradiation. Note that, on average, the post-irradiation data inhabit a higher J region than the pre-irradiation data; this denotes stronger vortex pinning. Some odd behavior is observed in the post-irradiation ρ-J data in the flux-flow regime. The dashed lines in Fig. 3.17 and 3.18 correspond to an estimate for the onset of flux flow (see section 3.9 for details). After this onset, isotherms are observed to cross paths, which is highly unusual and essentially impossible to account for with a description of vortex behavior. This effect is another manifestation of the temperature-dependent resistive hump that is discussed in Section 3.7.

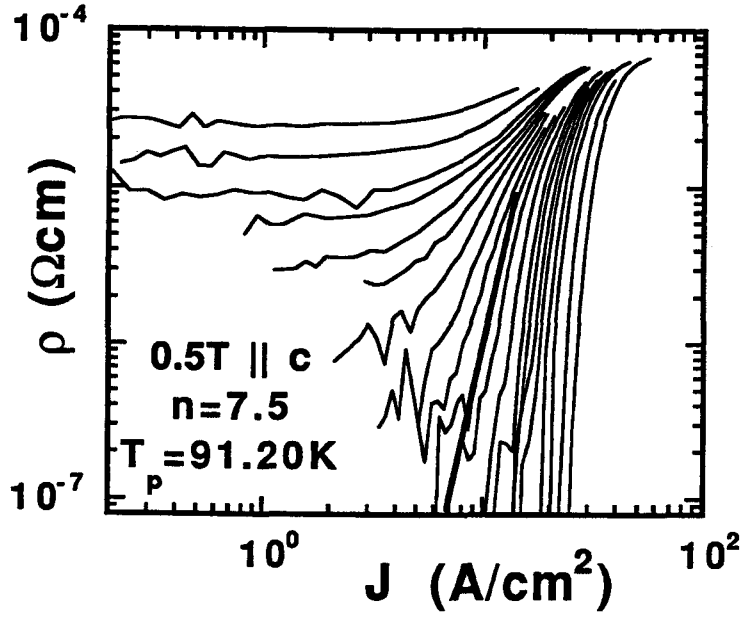

Fig. 3.15: ρ-J data for crystal #2 in 0.5 T. Temperatures range from 89.50 to 92.00 K with an average spacing of 100 mK.

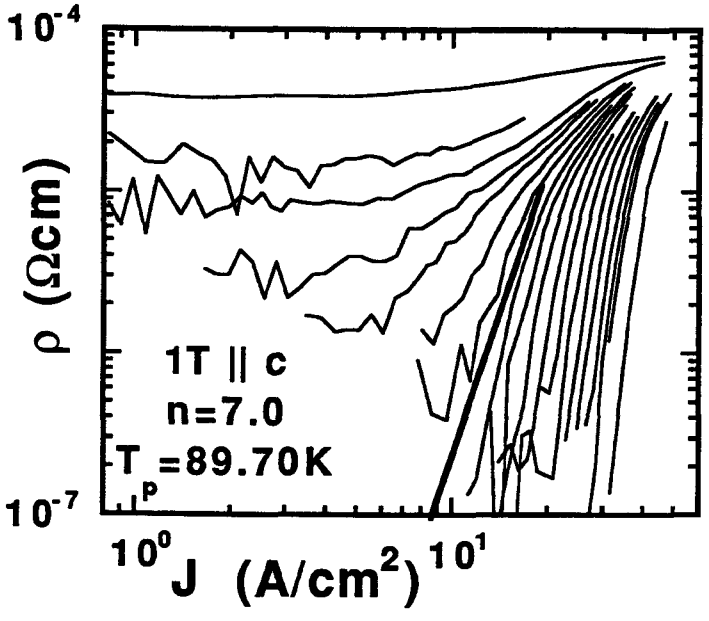

Fig. 3.16: ρ-J data for crystal #2 in 1.0 T. Temperatures range from 86.56 to 91.41 K with an average spacing of 150 mK.

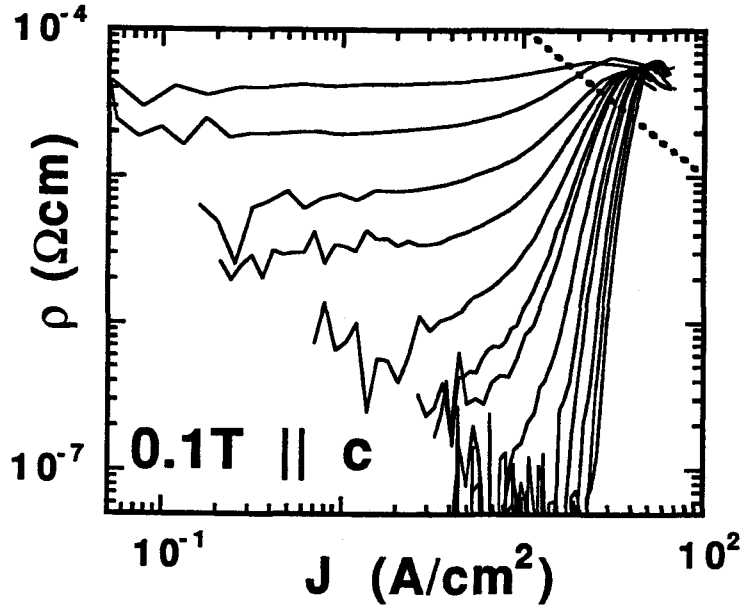

Fig. 3.17: ρ-J data for crystal #2, irradiated, in 0.1 T. Temperatures range from 91.98 to 92.69 with an average spacing of 50 mK.

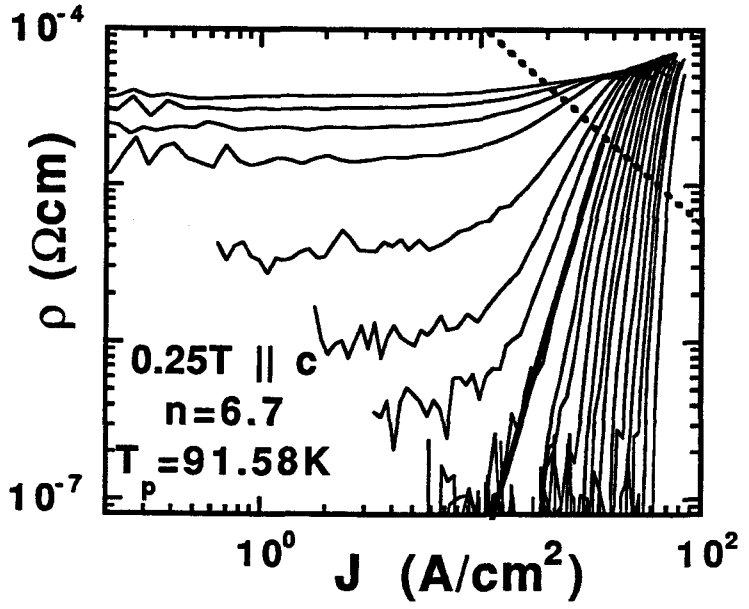

Fig. 3.18: ρ-J data for crystal #2, irradiated, in 0.25 T. Temperatures range from 90.12 to 92.39 K with an average spacing of 100 mK.

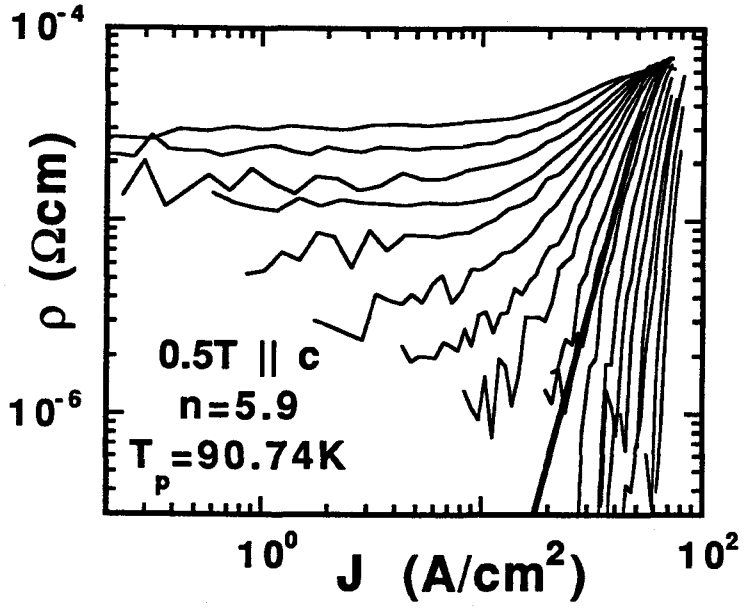

Fig. 3.19: ρ-J data for crystal #2, irradiated, in 0.5 T. Temperatures range from 89.31 to 91.81 K with an average spacing of 100 mK.

A critical scaling analysis, proposed by theories of a glass-liquid vortex phase transition, has been applied to much of the data (see Section 4.4). Scaling collapses for Fig. 3.13 - 3.16, 3.18 and 3.19 are shown below in Fig. 4.5 - 4.10.

Data for crystal #3 are shown in Fig. 3.20 over a 6.5 K range of temperatures. The shoulder of the data at high J is atypical for the single crystals and is similar to data from superconducting multilayers. The atypical ρ-J measurements and the broad zero-field resistive transition (see Fig. 3.4) lead us to believe that crystal #3 is much more inhomogeneous than the other crystals and much less accessible for an analysis of vortex depinning.

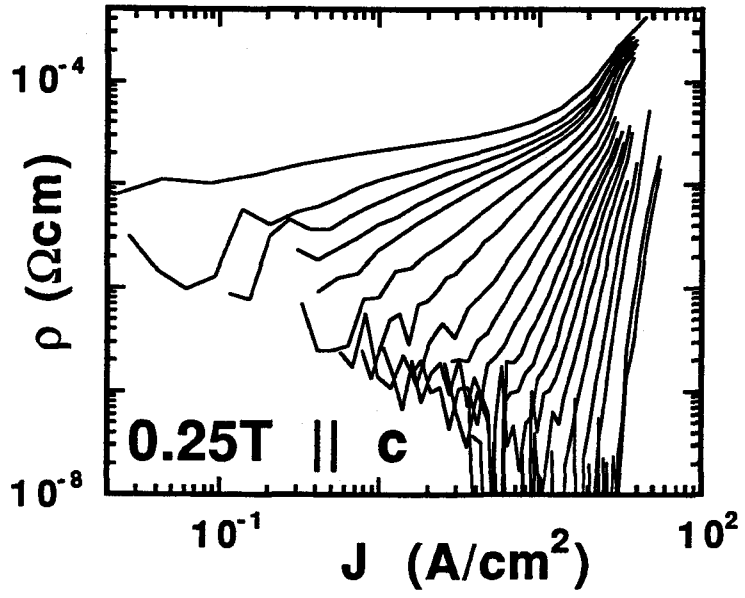

Fig. 3.20: ρ-J data for crystal #3 in 0.25 T. Temperatures range from 69.49 to 76.01 K with an average spacing of 300 mK.

3.9 Analytical Focus: Extracting n and L_p

Each set of data above, except those noted at higher fields, displays a change in the isotherms' behavior with changing temperature. At lower temperatures, for the resolution of this experiment, the crystals show a vanishing resistivity for non-zero applied current densities. These isotherms are closely bunched even with changes of 0.5 K or more in temperature, and they show negative concavity. At higher temperatures, they show positive concavity and a finite linear resistivity -- the signature of vortices in a liquid-like state. We focus on the isotherms in the region between the two very different sorts of behavior, the so-called transition between the two. The temperature separating these behaviors is labeled T_p, the depinning temperature. In addition to it functioning as a boundary between two distinct regions, this temperature is defined by a power-law dependence of E (and hence

ρ) on J. We examine the power-law slope (the logarithmic derivative) of the isotherm chosen to be nearest T_p. The logarithmic derivative, n, is extracted from the T_p isotherm via the relation

$$E \propto J^n. \tag{3.2}$$

T_p was consistently chosen by fitting the five to eight isotherms closest to the transition region to a power-law and selecting the one that gave the best fit. When more than one isotherm gave an excellent fit, T_p was designated as the isotherm which more clearly separated the closely bunched isotherms from those quickly spreading out into the regime of finite linear resistivity. For the data plotted in Section 3.8, one should note that the logarithmic derivative for ρ versus J is equivalent to n -1.

The logarithmic derivative at T_p is particularly interesting because it is described by theoretical models for vortex phase transitions high-T_c materials (see Section 2.2.1), and it is also the subject of extensive scrutiny in low-T_c materials (see Section 2.2.2). For the vortex glass and Bose glass theories, the n value at T_g or T_{BG} gives, respectively, the critical exponent z or z'. The values are directly related via

$$n = \frac{z+1}{2} = \frac{z'+1}{3}. \tag{3.3}$$

For low-T_c superconductors, n is often used as a quality index with higher n values denoting more homogeneous materials (Jenkins *et al.*, 1991; W. H. Warnes, private communication).

For the low-field data depicted in Fig. 3.9-3.12, a T_p could not reliably be determined since the transition between the pinned and depinned behavior occurred in such a tiny temperature window. Though a quick change in behavior would seem to help one define T_p, the subsequent extraction of n is prone to great uncertainty since, as the crucial temperature window shrinks (or the critical

regime in the picture of a second-order phase transition), the likelihood of having taken an isotherm of data close enough to T_p becomes negligible.

For each data set from which one could confidently extract an n value, we also calculated an estimate for the Larkin-Ovchinnikov pinning length, L_p, described in Section 2.3 above. The calculation used an estimate first employed in thin films of YBCO and since used by other researchers for V-I measurements (Dekker *et al.*, 1992). For an isotherm T_p, one can estimate the Larkin-Ovchinnikov length as

$$L_p = \left(\frac{kT_p}{\gamma \phi_o J_d} \right)^{\frac{1}{2}}, \tag{3.4}$$

where γ is the material anisotropy (see Eq. 3.1), ϕ_o is the flux quantum, and J_d is the deviation current, the current density at which the isotherm deviates from power-law behavior. J_d is considered the signature of flux flow and one can see in all the complete data sets of Section 3.8 that isotherms tend to flatten out for high current densities. Conventional wisdom interprets this flattening as a sign that most, if not all, vortices have been depinned, such that the system approaches an Ohmic response to the applied current. We note that, contrary to this point of view, the observed flux-flow resistivity in our experiments generally matches the estimated normal state resistivity (extrapolated linearly with descreasing temperature).

The estimate in Eq. 3.4 provides values for the effects of pinning on a vortex lattice that agree with others in the literature. For thin films, the estimate gives approximately 10-50 nm at high fields and 100-400 nm for lower fields. For the twinned crystals of this work, the estimate gives values in the range of 1-5 μm; though this matches other results for YBCO crystals (Charalambous *et al.*, 1995), we note that 1 μm covers many twin-boundary spacings.

CHAPTER 4

RESULTS

The *V-I* data of YBCO crystals show a systematic variation of the shapes of the isotherms with the characteristic scale of vortex lattice disorder. This variation holds before and after fast-neutron irradiation. It also extends to the dc *V-I* data published by other researchers, including data from thin films of YBCO, thin films of $Nd_{2-x}Ce_xCuO_{4-\delta}$ (NCCO), and tapes of $Bi_2Sr_2Ca_2Cu_3O_{10}$ (BSCCO). We attempt to interpret the data within the context of critical scaling, variable-range hopping, half-loop excitation, and collective creep. An interpretation which relates *V-I* data to pinning force distributions is used for the first time in the study of YBCO crystals. The technique shows great promise and can be linked to simulations in the literature. The analysis shows that thermal depinning describes the dc *V-I* data in these materials as well as or better than the mechanism of a second-order phase transition.

4.1 Disorder Dependence

For each crystalline sample and applied magnetic field that reliably yielded values of n and L_p at the depinning temperature T_p, the results appear in Fig. 4.1. Not only do the data from crystal #1 and crystal #2 differ, but the effect of neutron irradiation is both obvious and consistent with the sample-to-sample trend. Multiple points for a given symbol denote different applied magnetic fields, with higher fields for a given sample resulting in lower values of both n and L_p. The variation of n with applied field has also been observed in YBCO crystals with columnar pins (Legris *et al.*, 1993) and polycrystalline YBCO (Babic *et al.*, 1990).

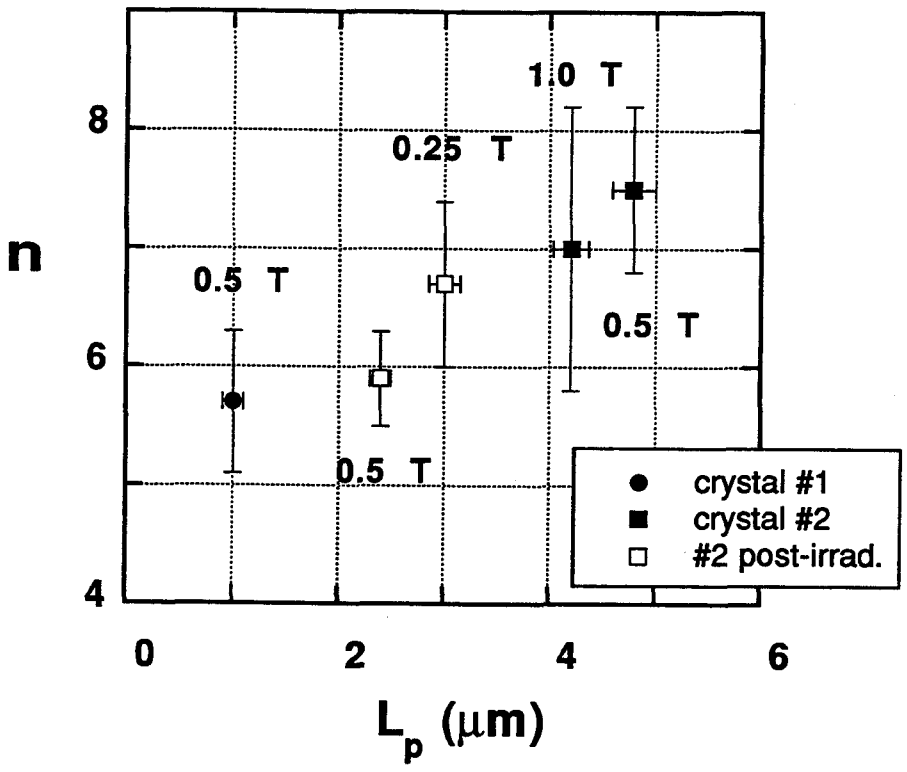

Fig. 4.1: Logarithmic derivative, n, of E-J traces at T_p versus L_p for YBCO crystals. Field strength || c noted for each point.

Though one may initially wish to interpret L_p as the separation between defects and, hence, a direct measure of sample purity, we see that L_p is field-dependent. L_p is derived from macroscopic evidence of vortex behavior, and it is, in these measurements, best interpreted as a measure of pinning-site spacing as perceived by the ensemble of flux vortices. The correlation between the pinning density of a crystal and the logarithmic derivative of its T_p isotherm, in addition to the striking inclusion of other results from the literature (see Section 4.2) constitutes the primary contribution of this work.

4.2 Extension to Film Data and Literature

Before crystal #2 was subjected to neutron irradiation, the n versus L_p picture was found to provide a coherent interpretation of other V-I data for high-T_c materials in the literature. Most notably, the copious data for YBCO and NCCO thin films in the work of Roberts (1995) were reanalyzed and the n values showed a strong dependence on L_p. Furthermore, other V-I measurements were incorporated. Though many sets of such data exist for the high-T_c copper-oxides, not all of these data were suitable for accurate derivations of n and/or L_p. Reasons for exclusion include: the data did not include in the flux flow regime (high J) that help one determine J_d; the isotherms had spacing of more than 1 K or displayed overly course J resolution, such that a reliable n value could not be obtained; the data were simply too noisy to give reliable values of J_d and/or n. Even with these criteria, the incorporation of data from the literature is not exhaustive. As a general rule, the most oft-quoted or unique measurements were included. A summary of the incorporated works, including the numbers extracted from a reanalysis of those works, appears in Table 4.1.

In addition to the data of Roberts, the measurements from two other sources are included for YBCO films (Koch *et al.*, 1989; Lang *et al.*, 1996). The work of Koch *et al.* included easily analyzed data sets for 4 T and 0.5 T applied fields. The overlap with the data of Roberts is apparent, but it is noteworthy since Koch *et al.* excluded the analysis of their 0.5 T data and their results are most often quoted as solid proof for the vortex glass theory. The data of Lang *et al.* (1996) are unique in that the authors study films of mediocre quality (T_c = 88 K at ambient field) in fields up to 8 T. Note that, in Fig. 4.2, the data of Lang *et al.* account for the lowest values of n and L_p. The BSCCO tape data of Li and coworkers are the most comprehensive and detailed set for that material to date (Li *et*

al., 1994). The T_p values and J_d values were easily derived from that data, but the uncertainty in L_p is augmented due to the debatable value of γ for the Bi compounds -- estimates range from γ=1/50 to 1/100 (Wahl *et al.*, 1994). As with YBCO and NCCO, the higher estimates were uniformly chosen.

Table 4.1: Summary of data extracted from the literature and incorporated into the n-L_p analysis.

author	material	B||c (T)	T_p(K)	J_d(A/m^2)	γ
Koch *et al.*,	YBCO film	0.5	87.2	1.5x10^8	0.2
1989		4	77.5	5.0x10^8	
Lang *et al.*,	YBCO film	1	81	3.0x10^9	0.2
1996		2	79	5.0x10^9	
		4	77	9.0x10^9	
		8	72	1.2x10^{10}	
Roberts, 1995	YBCO film	0.015	85.4	3.0x10^8	0.2
		0.1	84.8	5.0x10^8	
		2.5	79.9	1.0x10^9	
		5	74.3	1.0x10^9	
Roberts, 1995	NCCO film	0.005	18.1	1.5x10^7	0.05
		0.03	17.8	2.2x10^7	
		0.05	17.7	3.0x10^7	
		0.1	17.1	5.0x10^7	
		0.5	12.7	1.5x10^8	
		1	9.6	3.0x10^8	
Jiang *et al.*, 1993	YBCO crystal	1	87.5	1.8x10^6	0.2
Li *et al.*, 1994	BSCCO tape	1	60	5.0x10^7	0.02

The YBCO crystal data of Jiang *et al.* (1993) is incorporated as a landmark work for this system. Interestingly, the reanalysis gives results that are at odds with the published analysis. For the transitional temperature -- T_g in their analysis -- they did not choose the isotherm of best power-law fit, but instead chose a T_g that gave them universal values of z and ν, the critical exponents of the vortex glass theory. They chose this T_g even though the E-J isotherm in question is overtly non-power-law in character and displays a non-zero linear resistivity at low currents. At any rate, the values that appear in Table 4.1 for the work of Jiang *et al.* are the results of our reanalysis, as opposed to the values for Lang *et al.*, Koch *et al.*, and Li *et al.*, where our choices are in agreement for T_p and n.

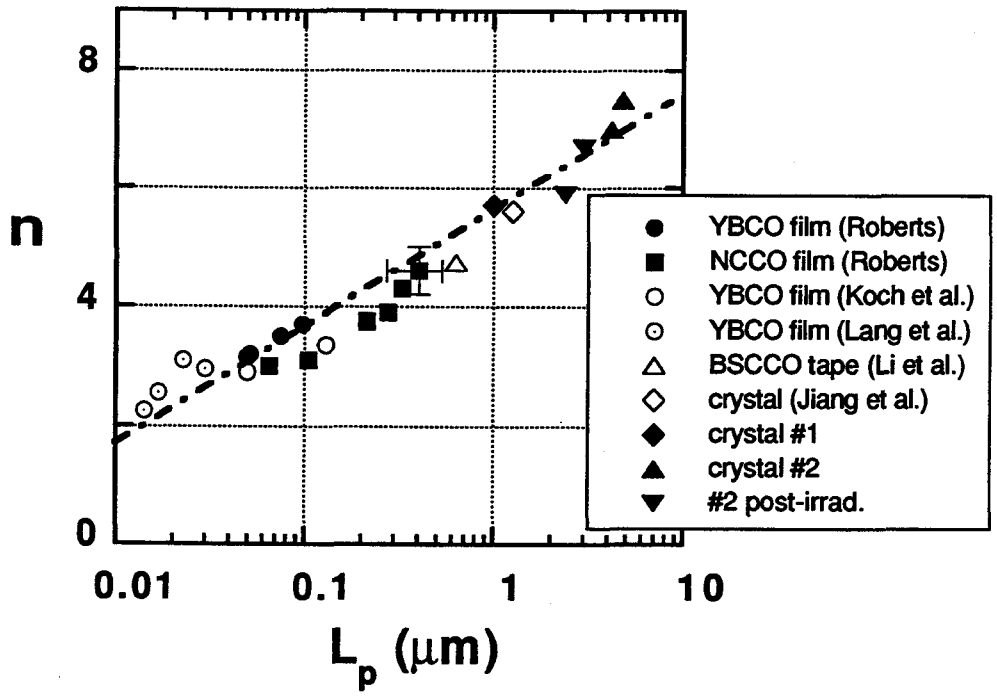

Fig. 4.2: n-L_p results for the analysis, extended to cover several results from the literature. Uncertainties shown for the NCCO point are typical for the non-crystal data.

To provide additional angles for viewing these results, the data are replotted as a function of B (Fig. 4.3a) and J_d (Fig. 4.3b). The B-dependence of n shows the overall difference between the results of thin films and single crystals. The dependence of n on the magnitude of the current underscores the importance of J_d in determining L_p and this representation is roughly equivalent to Fig. 4.2. We prefer to emphasize L_p because it incorporates T and the anisotropy factor. Overall, Fig. 4.2 and 4.3 show that both L_p and J_d are quantities which bring together the otherwise different results of films and crystals.

Notable omissions from the analysis are the detailed V-I data taken for the low-T_c material NbZr (Budhani *et al.*, 1992), for a thick YBCO film (Safar *et al.*, 1996), and for the multilayer compound $DyBa_2Cu_3O_{7-\delta}/(Y_{0.45}Pr_{0.55})Ba_2Cu_3O_{7-\delta}$ (Andersson *et al.*, 1996). The NbZr film in a 4T magnetic field showed isotherms qualitatively similar to those of the copper-oxides. With a T_p of 5 K, a J_d of approximately 3 x 10^8 A/m^2, and an assumed anisotropy factor of unity, Eq. 3.4 gives an L_p estimate of 50 nm which places the NbZr film in the range of the copper-oxide films. However, we find an n value of 9 which places NbZr well off the prevalent trend seen in Fig. 4.2. It should be noted that low-T_c materials as a rule give higher values of n -- commonly in the range of 10-50 -- than the high-T_c materials. Given that caveat, it is interesting to note that in a systematic study of NbTi, n values decreased steadily with increasing field (Jenkins *et al.*, 1991).

The data for a thick twinned film of YBCO is published only in a critically scaled format (Safar *et al.*, 1996). That data showed universal scaling parameters of z = 6.2 and ν = 1.3 in fields from 1 to 9 T, consistent with the predictions of the Bose glass theory. Though n can be determined from z (see Eq. 3.3), we cannot find L_p without a plot of the unscaled data.

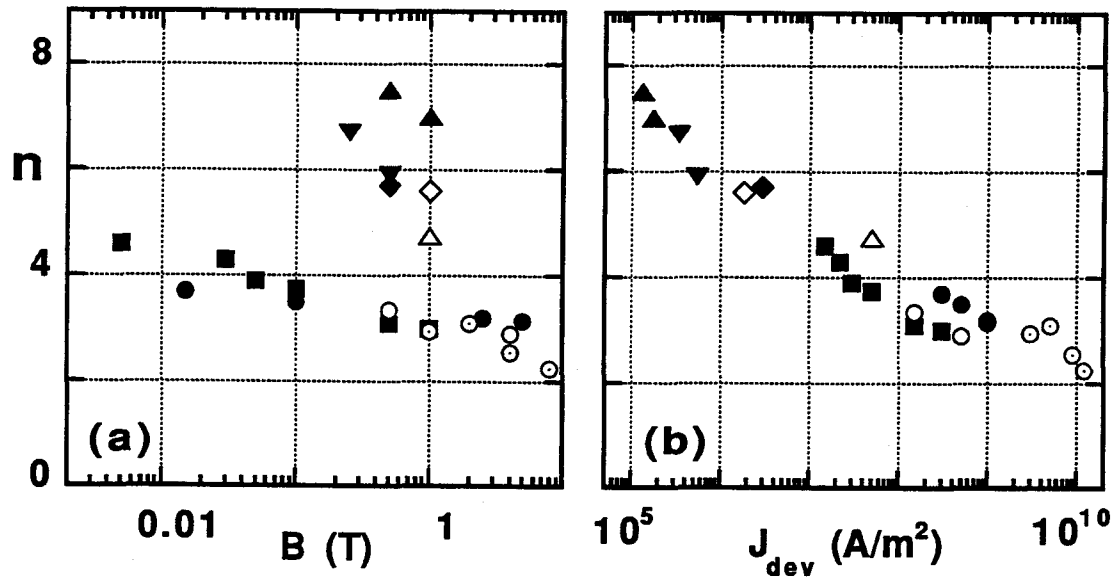

Fig. 4.3: Power law exponent presented against (a) applied field and (b) the deviation current density. Legend here same as for Fig. 4.2.

The multilayer data are more difficult to interpret than the other sets. In an applied field of 1 T, Andersson and coworkers found data that most closely resemble that from our multi-phase sample shown in Fig. 3.19 (Andersson *et al.*, 1996). Nevertheless, the authors defined a temperature T_x and analyzed it as a glass transition temperature. Using their choice for T_p (28 K), a J_d of 3 x 10^8 A/m^2, and their determination of the anisotropy (γ=1/16), we find $L_p \approx$ 25 nm and $n \approx$ 3. This fits nicely into Fig. 4.2 and the multilayer is truly a copper-oxide superconductor. Also worthy of note, Andersson and coworkers mention that their vortex glass z values (related directly to n, see Eq. 3.3) tend to increase for decreasing field; again, this trend is that of the data presented here.

The issue of sensitivity must accompany the analysis above. Due to geometrical factors that contribute to E and J, the floor of sensitivity for data taken on different types of samples can differ

by orders of magnitude. This is most extreme in resistivity plots, like those depicted in Section 3.8. For crystals, the sensitivity is limited to about 10^{-5} Ωcm for high J, while for thin-films, the same voltage sensitivity gives resistivity sensitivity floor of nearly 10^{-8} Ωcm (Roberts *et al.*, 1994). This difference arises from the fact that the J_c values are so much higher for thin films; the sensitivity for E, (from which we extract n), is roughly equivalent for the crystal and film data. Nevertheless, we believe that, as an absolute sensitivity scale for vortex motion, the ratio of the smallest measurable resistivity to the flux flow resistivity is most appropriate. Since the flux flow resistivities of YBCO films and crystals are comparable, the question of whether or not a difference in sensitivity could affect the analysis is an important one.

We cannot drop the resistivity floor for the crystal data, even for hypothetical purposes. However, we can cut thin-film data using a *higher* resistivity floor, back-track to an E-J format and reanalyze the data. We have tried this for the YBCO film data of Roberts (Roberts, 1995; Roberts *et al.*, 1994). In many cases, the extracted parameters are not affected, particularly for the low-field data. For some high-field points, T_p is determined to be slightly higher than before and n is determined to be slightly lower than before. The change in T_p is so slight as to not meaningfully shift L_p, but the change in n can be non-negligible (e.g. a shift from $n = 3.2$ to $n = 2.8$ for the 2.5 T, YBCO thin film data). If n changes, it always decreases, so that having the same sensitivity floor for the crystals and films will, if anything, further separate their n values. This matches the computational findings of Edelman and Larbalestier (1993; see Section 2.2.2) who note that *increasing* sensitivity results in, if anything, a slight increase in n (*ibid.*). Regardless, such a small shift would not disturb the trend observed in Fig. 4.2. While most theories do not mention sensitivity dependence, the experimental work of Charalambous *et al.* claims that pV sensitivity is needed to adequately probe the vortex glass phase (Charalambous *et al.*, 1995). In addition, the reader is referred to Appendix A, where a simulation shows the importance of experimental sensitivity.

4.3 Field Dependence and L_p Interpretation

As noted in the preceding section, both n and L_p vary with field for a given sample and defect density. Specifically, both quantities decrease for an increasing field. A field-dependent n has direct ramifications for second-order phase transitions that predict evidence via critical scaling. Since n varies continuously, universality is violated; this topic is considered in Section 4.4.

Turning to L_p, presumably a quantity of physical significance, one must seek to understand its field dependence. Obviously, the structural defect density of a sample does not change with field. Similarly, the total number of pinning sites should not vary with field. However, as noted in Section 2.3, L_p is susceptible to variations in the strengths of vortex-vortex and vortex-pin interactions. Both of these factors are sensitive to field strength. To put this another way, the *effective* number of pinning sites can depend on the field (Larkin and Ovchinnikov, 1979).

L_p is derived from collective pinning theory (see Section 2.1.1), and the theory's interpretation of L_p assumes the existence of elastic bundles (implicit in this discussion is the equivalence of collective creep and pinning theories for L_p). Unfortunately, the theory provides no straight-forward prediction for the size of elastic bundles with a changing field. In general, a bundle volume is predicted to *grow* with an increasing field (LO, 1979), except near the upper critical field, where the behavior is more complicated (*ibid.*). Since the data we collect is always somewhat close to the superconducting transition, it is possibly too close to $B_{c2}(T)$ to expect a simple field-dependence for L_p. Given that caveat, we take the generic prediction that an elastic bundle should increase in size as the field and vortex interactions strengthen (Blatter *et al.*, 1994).

Without careful examination, the L_p trend observed appears to oppose this prediction. However, the collective pinning prediction

assumes a fixed T, whereas the values of L_p shown for a specific sample in Fig. 4.2 do not represent a fixed T. The value of T_p decreases significantly with increasing field such that an L_p estimate for a 1 T field will always be derived from a lower temperature than an L_p estimate for a 0.1 T field (e.g. for crystal #1, T_p(1T) = 86.3 K, T_p(0.1T) = 89.4 K). Using the same estimate (Eq. 3.4), Worthington *et al.* (1992) extracted L_p estimates for YBCO crystals at various applied fields and also noted a decrease in L_p for an increase in field strength. Those authors credit the decreasing temperature with a decreased effectiveness of the thermal smearing that normally weakens pinning. In addition, they claimed that smaller a_o values (higher fields) make individual vortices less susceptible to thermally induced motion and therefore more responsive to pinning attractions, even though vortex interactions are more important for smaller a_o.

To further examine the meaning of L_p, we calculate the ratio of L_p to the spacing a_o; this provides an approximate measure of bundle population. Assuming a rigid rod model for vortices and cylindrical bundles, a ratio of L_p/a_o = 10 implies Abrikosov-like crystalline order for a bundle of approximately 80 vortices. A plot of this ratio versus field, for YBCO crystal #1 and for an YBCO thin film (Roberts, 1995), shows that the field dependence of L_p/a_o is opposite that of L_p (see Fig. 4.4). (Note that L_p can be extracted with confidence for low-field data which may not yield a reliable n value). The opposite field dependence arises because the spacing a_o simply drops off more severely than L_p with increasing field.

Despite the varying T for the points in Fig. 4.4, the increasing bundle population matches the general predictions of collective pinning mentioned above. Quantitatively, the ratios L_p/a_o for both samples show roughly a $B^{1/3}$ dependence. It is interesting, even surprising, that the B-dependence of L_p/a_o for films and crystals is so similar. The YBCO crystal reports L_p/a_o between 10 and 20, consistent with a picture of small bundle pinning, but the film gives

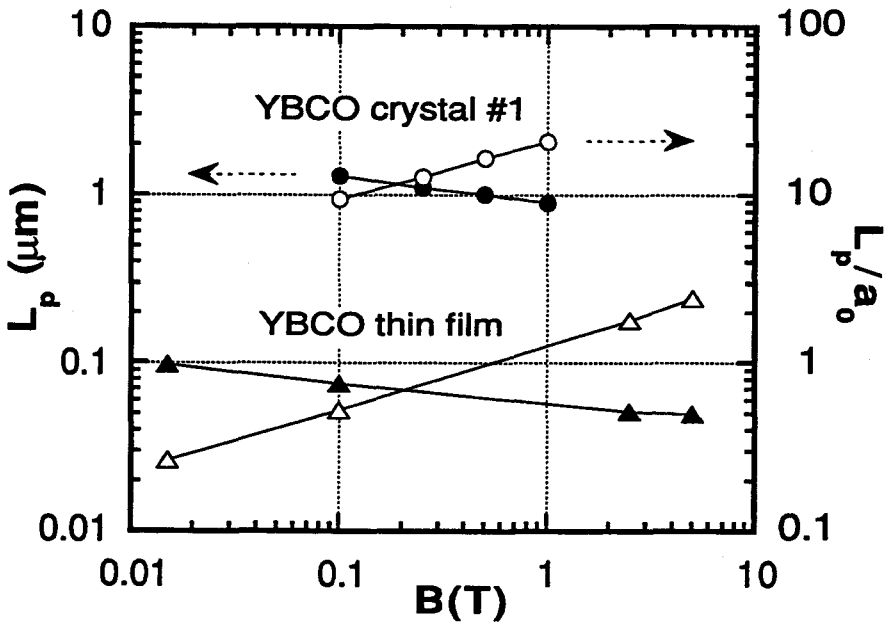

Fig. 4.4: Field-dependence of Larkin-Ovchinnikov length (filled symbols) and bundle-size (open symbols) for YBCO crystal #1 and a thin-film YBCO sample.

L_p/a_o on the order of 1, implying that single-vortex pinning is more appropriate than bundle pinning for the film.

Before leaving the issue of bundle population, we note that the value of n for a specific sample always decreases for an increasing L_p/a_o. Therefore, the central relation shown in Fig. 4.2 does *not* point to a systematic increase of n with increasing bundle population. To the best of our knowledge, no predictions have been made concerning the interplay of these quantities.

Two major misgivings remain for the interpretation of L_p: a technical concern about its magnitude, and a more fundamental question of its relevance in what is quite possibly a *plastic*, rather than elastic, regime. The values of L_p are somewhat puzzling in two cases. First, L_p drops below a_o for the low-field data of the YBCO

thin film (to the extent that $L_p/a_o \approx 0.25$, see Fig. 4.4). This is clearly unphysical in the context of collective pinning theory since a bundle population should be limited to one. Second, L_p reports values on the order of 1 μm for YBCO crystals, even though the twin boundary spacing is believed to be 50-100 nm. Strictly interpreted, this implies that the twin boundaries are extremely weak sources of pinning, in contrast to other results (see Section 5.1).

The more fundamental obstacle to the use of L_p focuses on its inherent assumptions. Historically, L_p is taken from the theory of collective pinning, where weak pinning and the existence of elastic bundles are assumed. Above, we report L_p values for many different types of environments, including low fields (5 mT), high fields (8 T), thin films, and single crystals. With growing evidence of plastic vortex response for a considerable region of H-T-J space, the broad assumption of elastic bundles appears inappropriate (Abulafia *et al.*, 1996). The measurements of Abulafia *et al.* (1996) indicate that plastic vortex response dominates the relatively high T and high J region that we probe in this work (see Section 1.4).

We believe that the quantitative and qualitative misgivings for L_p are related and that a purely collective interpretation should be abandoned. Nevertheless, we do not abandon L_p itself, choosing instead to emphasize that its historical background and the physical meaning of its estimate are not codependent. The L_p estimate presented in Eq. 3.4 is derived from comparing the available thermal energy kT_p with the energy needed to nucleate a flux loop, or vortex kink, in an applied current J_d (see the half-loop in Fig. 2.4, and Charalambous *et al.*, 1995). The estimate includes no assumptions concerning the character of vortex motion. The only access that vortex interactions have to L_p is through J_d, the current at which flux flow begins (see the discussion of flux flow in Chapter 1), and this is in no way restricted to an elastic or plastic picture. In fact, J_d is also the only vehicle through which the character of pinning can affect L_p. Hence, the most sensible interpretation of L_p

assumes that it tracks the competition between vortex-vortex and vortex-pin interactions at T_p. A relatively small L_p underlines the extent to which pinning dominates vortex interactions, and a relatively large L_p points to weaker pinning and the significant influence of vortex interactions. Even in a plastic picture of vortex motion, the latest detailed simulations show that the interactions of vortices are crucial (Faleski *et al.*, 1996; Groth *et al.*, 1996; Reichhardt *et al.*, 1996). In this admittedly qualitative interpretation, L_p values larger than the twin spacing or smaller than a_o are not alarming.

Even if the use of L_p is considered incorrect, the systematic n-J_d relation of Fig. 4.3b remains. The systematic variation of n cannot be dismissed.

4.4 Critical Scaling Results

Much of the data presented in Section 3.8 collapses under the scaling prescription of the proposed second-order phase transitions, namely that of the vortex and Bose glass. Following the methods of Roberts (1995) and the spirit of Eq. 2.12, the scaled resistivity and scaled current density were obtained via

$$\rho_{sc} = \rho \left| 1 - \frac{T}{T_p} \right|^{\nu(d-2-z)} \tag{4.1a}$$

$$J_{sc} = \frac{J}{T} \left| 1 - \frac{T}{T_p} \right|^{-2\nu}, \tag{4.1b}$$

where ν and z are, respectively, the static and dynamic critical exponents. The dimensionality, d, is assumed to be 3. Also mirroring the methods of Roberts, we only scaled data that was both above the noise level and below the high J flux-flow region (Roberts,

1995). Unlike Roberts, we do not "fine-tune" the parameters beyond one or two modifications. The resulting collapses appear in Fig. 4.5 - Fig. 4.10.

If the critical parameters are expected to match the predictions of any theory for twinned crystals, we expect them to match those of the Bose glass. However, as one can see from the scaled data here, the derived exponents do not match the predictions of the Bose glass ($z' \approx 6$-7, $\nu' \approx 1$-1.5). They do not match the vortex glass values ($z \approx 4$-6, $\nu \approx 1$-2) either. More importantly, the derived values of z and ν vary with applied field, from sample to sample, and with fast-neutron irradiation. The continuous variation of the scaling parameters is an obvious outcome when one revisits Fig. 4.2 and recalls that z and z' both depend directly on n (see Eq. 3.3).

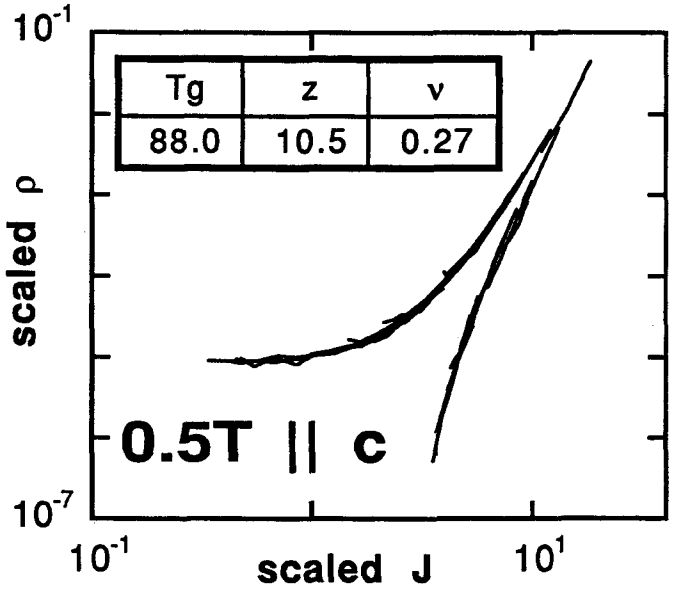

Fig. 4.5: Scaled ρ-J data for crystal #1 in 0.5 T. Scaled data from Fig. 3.13 include 87.57 to 88.59 K.

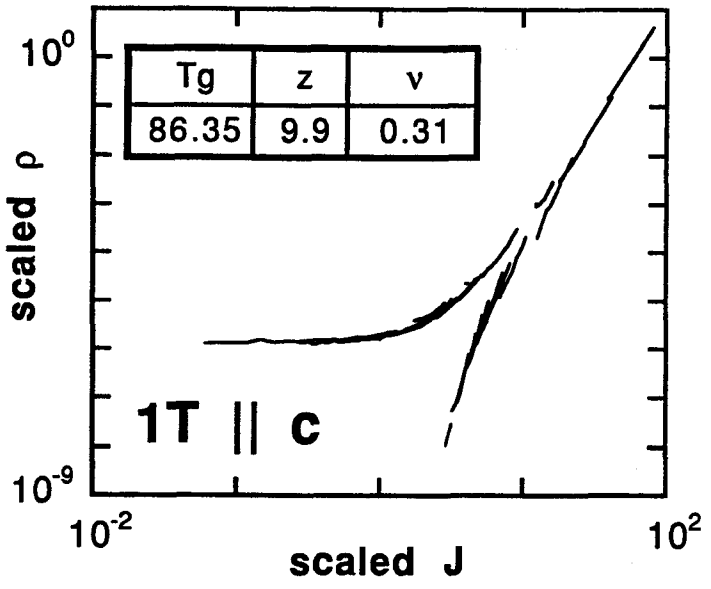

Fig. 4.6: Scaled ρ-J data for crystal #1 in 1.0 T. Scaled data from Fig. 3.14 include 85.35 to 87.11 K.

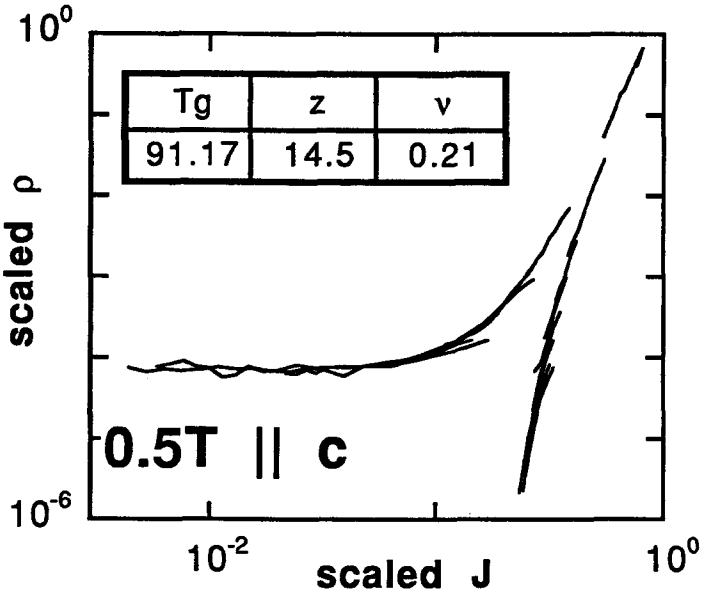

Fig. 4.7: Scaled ρ-J data for crystal #2 in 0.5 T. Scaled data from Fig. 3.15 include 90.60 to 91.65 K.

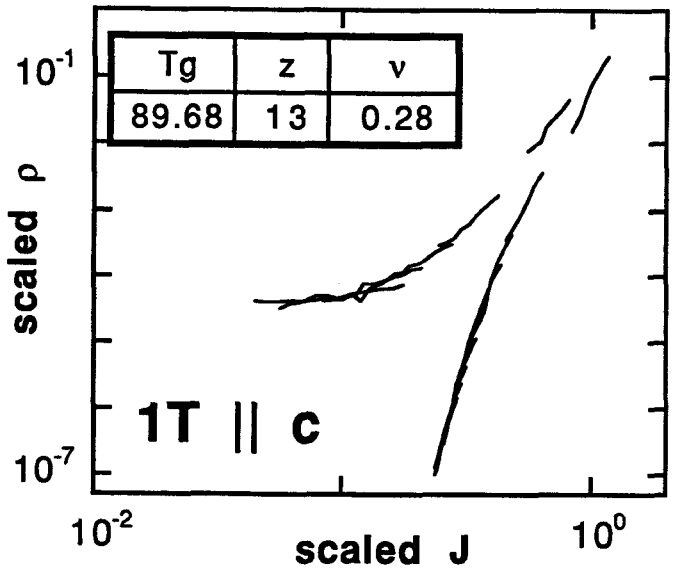

Fig. 4.8: Scaled ρ-J data for crystal #2 in 1.0 T. Scaled data from Fig. 3.16 include 87.78 to 90.30 K.

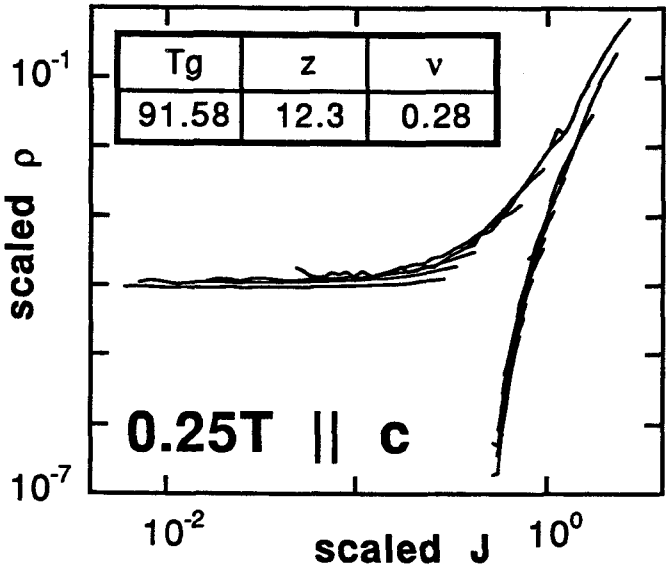

Fig. 4.9: Scaled ρ-J data for crystal #2, irradiated, in 0.25 T. Scaled data from Fig. 3.18 include 90.49 to 92.29 K.

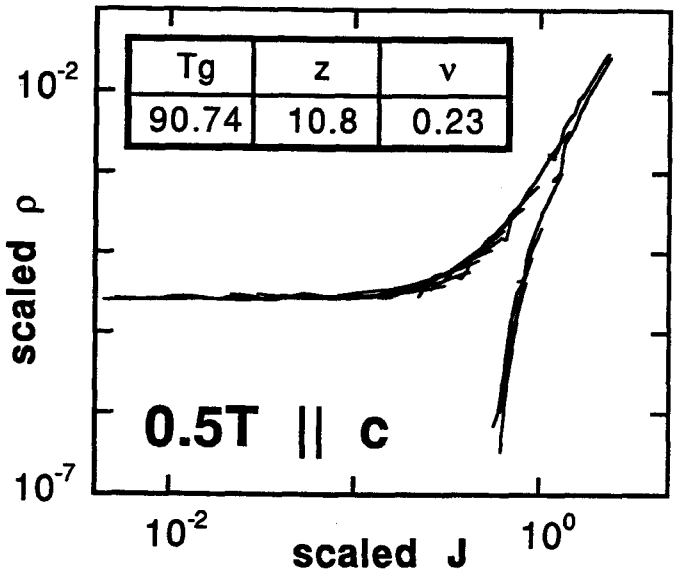

Fig. 4.10: Scaled ρ-J data for crystal #2, irradiated, in 0.5 T. Scaled data from Fig. 3.19 include 89.31 to 91.81 K.

Such deviations violate universality and render the interpretation of scaling debatable. While the striking appearance of two universal functions seen in Fig. 4.5-4.10 is difficult to dismiss, it is possibly little more than a convenient parametrization of ρ-J data. Several possibilities deserve consideration.

Since the quality of the scaling collapse is maintained in a variety of different conditions, it is tempting to include the dependence of the scaling parameters on L_p in hopes of attaining a new truly universal set of parameters. For now, we simply examine the dynamic exponent z. To shed the uncertainties introduced by varying anisotropies, we use the YBCO data in Fig. 4.2 and find that z (via its relation to n, see Eq. 3.3) satisfies

$$z = a_1 + a_2 \log(L_p), \tag{4.2}$$

with $a_1 \approx 10.2$ and $a_2 \approx 3.4$ for L_p expressed in microns. With a similar expression for ν, one could define renormalized parameters z'' and ν'' that would remain constant for any value of L_p. However, the introduction of an extra parameter does not produce a universal set of scaling functions $F_{\pm}$. The shapes of $F_{\pm}$ depend on the original z and ν. Since a major justification for critical scaling is finding universal functions, there is little merit in this modification.

To make a more meaningful effort to modify the scaling analysis, one might incorporate the length scale at a more fundamental level. Renormalization group theory refers to a system parameter that alters the resulting renormalized quantities as a relevant perturbation (Fisher, lecture notes, 1982). In this sense, L_p might be a relevant perturbation because a change in its value forces the flow of the ρ-J data to a new, distinct, fixed point under renormalization. However, it is beyond the scope of the present effort to retool the scaling analysis from here. We emphasize that there is no simple modification in sight. A revamped scaling approach will need to scale quantities other than ρ and J (or E and J) because a constant n value is at the core of the available scaling hypotheses; it is precisely the universal power-law dependence of E on J that guarantees the cancellation of the diverging glass correlation length at T_g (see Eq. 2.12 and Eq. 2.6).

Gingras and Huse have proposed the existence of two distinct superconducting phases, the vortex glass and the pinned lattice (Gingras and Huse, 1996). The authors use a 3D-XY model to calculate the character of vortex systems at various applied fields; in addition to a glassy phase for higher fields, they find a pinned lattice phase for lower fields (*ibid.*). The pinned lattice has long-range spatial order much like the Bragg glass prediction by Giamarchi and Le Doussal (see Section 1.4; Giamarchi and Le Doussal, 1995). Gingras and Huse suggest that the glass-liquid transition could have a different universality class than the pinned lattice-liquid transition. However, the results shown in Fig. 4.2 do

not suggest the existence of two distinct behaviors. No plateaus are observed; instead, the data indicate a continuous change for any so-called universality class.

Other authors have used the 3D-XY model to describe the transition at T_g or T_p as a "multicritical point" (Moloni, *et al.*, 1997). In this view, the glass-liquid vortex phase transition coincides with the critical point of superconducting fluctuations. In fact, the two transitions are not considered to be distinct but rather two interpretations of the same phenomenon (M. Friesen, private communication). This approach treats fluctuations in the phase of the superconducting order parameter, and is consistent with the 3D-XY interpretations of specific heat data (Overend *et al.*, 1994; see Section 1.4). The 3D-XY description is relevant up to a certain field (approximately 50 T or more for optimally-doped single crystals according to Moloni *et al.*, 1997), at which the order parameter begins to suffer fluctuations of phase *and* amplitude (*ibid.*). We note that the 3D-XY scaling approach of Moloni *et al.* (1997) incorporates field dependence in their study of YBCO films.

Some authors studying *V-I* measurements of BSCCO films have chosen to interpret their anomalous exponents (the authors refer to $z \approx 12$, $\nu \approx 0.7$ as unphysical) in terms of a variable designation of d (Yamasaki *et al.*, 1994). They note that by letting $d = 2$ in Eq. 4.1a above, they are able to extract values ($z \approx 5.6$, $\nu \approx 0.7$) that match the vortex glass theory's prediction for $d = 3$. In particular, a choice of $d = 2$ renders Eq. 3.3 as $n = z+1$. A similar approach has been used to explain away anomalous scaling parameters in high-T_c multilayers (Zhao *et al.*, 1997). The justification given for this modification relies on the high anisotropy of materials like BSCCO. In the case of high anisotropy, the vortices lose coherence perpendicular to the Cu-O planes (parallel to B) and the system becomes essentially 2D.

Nevertheless, we believe that such an approach overlooks some important points. Not only does a 2D argument appear less relevant to the case for YBCO crystals in the intermediate fields studied in this work, but the appeal to setting $d = 2$ may not be made on sound theoretical grounds. As we noted in the literature (Roberts *et al.*, 1995), the vortex glass theory predicts that no finite glass transition temperature can be realized in the case of $d = 2$. In addition, to expect $d = 2$ and $d = 3$ cases to share the same universality class is somewhat confusing. One expects different dimensionalities to have distinct universality classes. Therefore, we believe that finding congruence between 2D and 3D scaling exponents does not necessarily make for convincing support of the vortex glass theory, especially when the theory specifically predicts no finite transition temperature in the 2D case.

As described in section 2.5, the vortex percolation model of Yamafuji and Kiss (1996) predicts scaling collapses with pinning-dependent and field-dependent parameters; in this case, the scaling reflects a percolative phase transition. Though their work predicts a change in scaling parameters, they make no quantitative predictions, so we cannot say the work presented here supports their percolative model. This topic will be revisited in Section 5.2 below.

To broadly consider dc *V-I* data in high-Tc materials, one finds a continuing controversy. Some authors, particularly in studies of thin films, have found universal critical behavior for a broad range of applied fields, and they find scaling collapses including up to 17 K worth of *V-I* data (Friesen *et al.*, 1996). On the other hand, theoretical works which include the effect of vortex screening show that a second-order vortex phase transition can exist at a finite temperature for neither 2D nor 3D cases (Wengel and Young, 1996).

In summary, we believe the scaling approach has little merit in the study of dc *V-I* characteristics for crystals of YBCO. However,

it is important to emphasize that we do not extend this conclusion to the theories of second-order transitions themselves. The Bose glass theory, for one, has been experimentally supported in YBCO crystals and thick films using techniques other than critical scaling of V-I characteristics (see Section 2.1.3). Using the scaling approach described here, similar data (Jiang *et al.*, 1993) for single crystal YBCO was analyzed with different criteria for choosing T_g and different parameters were obtained ($z \approx 2$, $\nu \approx 3$). The flexibility of this three-parameter fit should not be underestimated. The quality of the collapse in the work of Jiang *et al.* (1993) was considered by the research community to be good, and the quality of the collapses in this work is at least as strong. Hence, scaling gives conflicting results for YBCO crystals. The approach makes use of the qualitative shape change of the V-I isotherms at some temperature T_g, but without a demonstrable universality, it is just as likely a fortuitous ansatz as it is a signature of vortex phase transitions.

4.5 Other Fitting Attempts

This section includes fitting attempts from the theoretical approaches outlined in Chapters 1 and 2 which either do not successfully describe the data or do not readily lend themselves to interpretation. The popular but controversial phase line is mapped. Also, selected $T < T_p$ data are compared to the predictions of collective creep, half-loop excitation and variable-range hopping (VRH).

As described in Section 1.4, a line in a H-T (in this case we display B-T) diagram separating two distinct regions of mixed state behavior is commonly fit to $B(T) = B(0)(1\text{-}T/T_c)^{\beta}$ (Eq. 1.16). For YBCO crystal #1, we report a T_p for all fields, including those for which an n value or J_d value could not be reliably determined and a value for 1.5 T, an incomplete set of data for other purposes. The

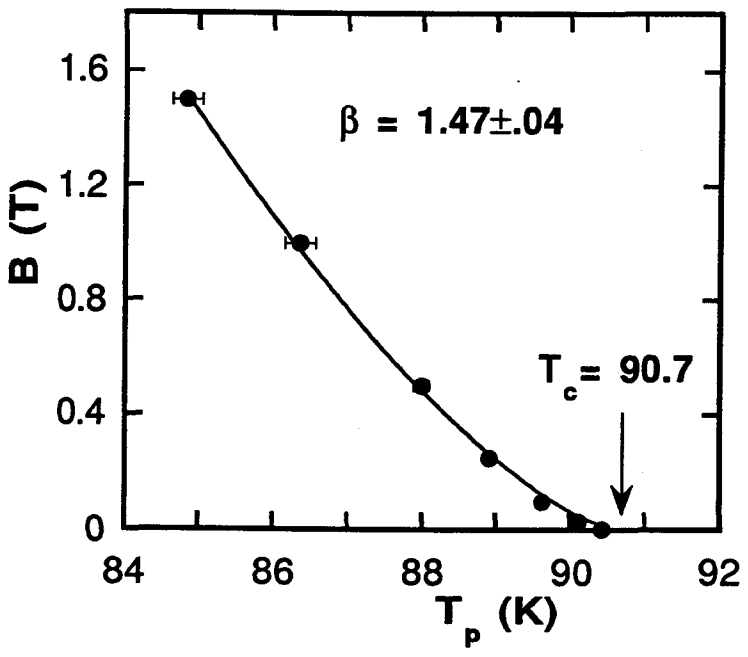

Fig. 4.11: Phase diagram for YBCO crystal #1, with a fit to Eq. 1.16.

results appear in Fig. 4.11, and β = 1.47±.08 joins the results presented in Table 1.2. The uncertainty in our β comes from adjusting the choice of T_c ±15 mK around 90.7 K. Of all the theoretical predictions, this best fits the $\beta = 3/2$ prediction from the model of Blatter and Ivlev (1993). In addition to β, $B(0)$ is allowed to vary and the best fit presented in Fig. 4.11 gives $B(0)$ = 85±10 T, a reasonable value for YBCO (Safar *et al.*, 1992).

For both collective creep theory and the vortex glass theory, the experimental determination of μ, describing the activation barrier's dependence on current density, can provide an important point of comparison (see Sections 2.1.1 and 2.2.2, Eq. 2.4). In this work, μ was derived from the method of Leghissa *et al.*, where one starts from Eq. 2.5 and eliminates the need to fit both a prefactor

for the voltage and also the energy scale U_c (Leghissa *et al.*, 1993). Leghissa *et al.* derive a J-dependent μ from E-J curves using

$$\mu(J) \equiv \frac{\partial}{\partial \log J} \log\left(\frac{\partial \log E}{\partial \log J}\right). \tag{4.3}$$

For the non-linear regions ($T < T_p$) of our YBCO crystal data, this method gives $1 \leq \mu \leq 3$, with B and T dependence. In addition, we find that μ is extremely sensitive to J, even over an individual isotherm, matching the results of Leghissa *et al.* (1993) and Roberts (1995). Loosely speaking, one can say that μ values are higher for the unirradiated crystal #2 than for either crystal #1 or the irradiated crystal #2.

The only theoretical prediction of $\mu > 1$ is for small-bundle pinning ($\mu = 3/2$) in collective creep theory (Blatter *et al.*, 1994), but we are not aware of any theory that accounts for μ values in the range of 2 to 3. In agreement with the misgivings expressed in Section 2.1.1, and in agreement with Roberts (Roberts, 1995), we find that $\mu(J,T,B)$ is of limited use in interpreting our data.

With the specific aim of addressing twinned crystals, the work of Marchetti and Vinokur, as described in Section 2.3, predicts different forms for ρ-J data corresponding to half-loop excitations and VRH (Eq. 2.17 and 2.16, respectively). Though it is derived for the case of low temperatures and a parallel set of twin boundaries normal to the applied Lorentz force, we attempt a fit to our data since this theoretical approach is the most comprehensive to date for twinned YBCO crystals. In Fig. 4.12, a pre-irradiation $T < T_p$ data set for crystal #2 is shown with fits from both Eq. 2.16 and 2.17.

The fit in Fig. 4.12 holds ρ_0, the flux-flow resistivity, constant at its experimental value in Eq. 2.16 and Eq. 2.17. Better fits are obtained by letting ρ_0 vary, but temperature-dependent and unphysical (overly large by an order of magnitude or more) ρ_0

values result. Furthermore, respectively letting $E_k J_0^{1/2}$ and $E_k J_1$ vary in Eq. 2.16 and 2.17 as fitting parameters shows these supposed constants varying considerably for very small changes in temperature. We conclude that the mechanisms of VRH and half-loop excitations do not describe the YBCO crystal *V-I* data in the high-temperature regime.

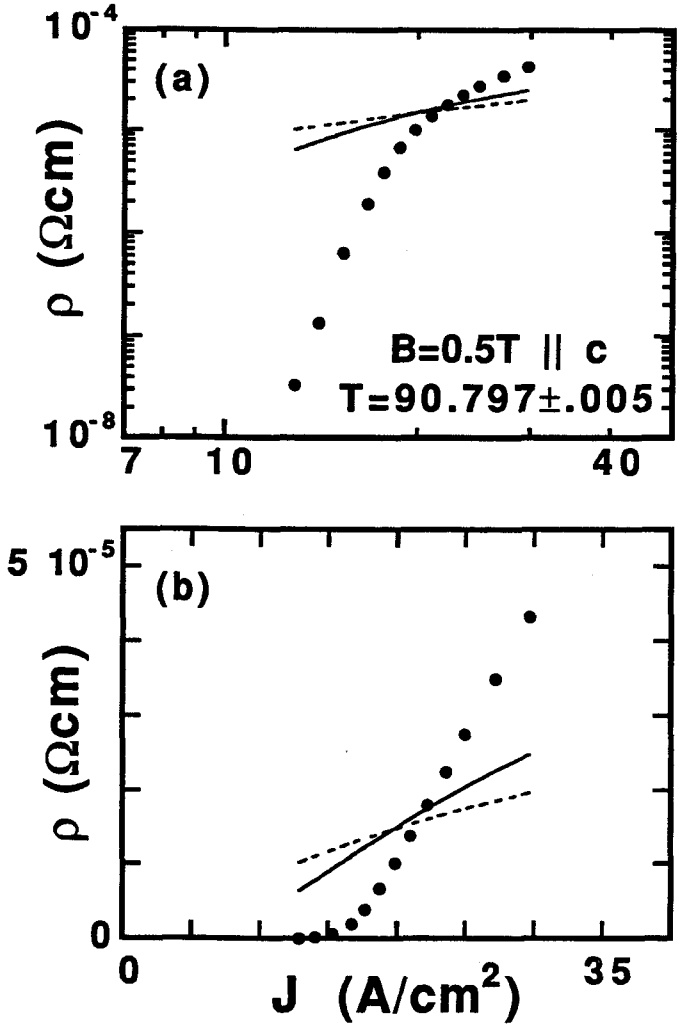

Fig. 4.12: Data fits for VRH (dotted line) and half-loop excitations (solid line) in (a) double-log format and (b) linear format. Data is for crystal #2 before fast-neutron irradiation.

4.6 Experimental Pinning Distributions

Based on the framework of Warnes and Larbalestier described in Section 2.2, second derivatives of sufficiently clean E-J data were taken in hopes of obtaining depinning current distributions. To the best of our knowledge of YBCO studies, this type of analysis has been used only for ceramic powders, where the distributions helped the authors explore intergrain coupling (Babic *et al.*, 1990). Temperature stability and closely-spaced current-density intervals on an isotherm are crucial for derivative analyses; for YBCO crystals the E-J data presented are of the highest quality in those two regards. However, they suffer from the fact that they are collected for a geometrically ramping current. This type of current ramp assures even spacing on the log-log plots of E-J and ρ-J, but it leaves an asymmetric density of points for the derivatives.

The resulting derivatives d^2E/dJ^2 depict reasonable distributions for all three samples, and they will be referred to as effective pinning distributions, f_{eff}. The f_{eff} show remarkable sensitivity to temperature, applied field, and the effects of fast-neutron irradiation. At face value, one concludes this is obvious: since the E-J data show sensitivity to the aforementioned factors, the second derivatives of the same data will likely display sensitivity also. However, where we have seen above that the interpretation of changing E-J data *per se* is debatable, we believe the sensitivity of the f_{eff} leads more readily to physically significant interpretations.

Fig. 4.13 shows a series of f_{eff} traces for the most simple case, an unirradiated crystal, crystal #1, in a relatively low magnetic field of 30 mT. As the temperature rises, the f_{eff} decrease in height and spread out until they apparently have non-zero values at zero applied Lorentz force. Data is sparse on the high-J side of these traces because the data collection for crystal #1 was consistently stopped at the detection of flux flow. For the f_{eff}, the onset of flux

flow coincides with the position of the central peak. Remarkably, the f_{eff} are described in a convincing manner using a Gaussian fit. Specifically, the data were fit to

$$f = C exp\left[\frac{-(J_0 - J)^2}{2\sigma^2}\right], \tag{4.4}$$

where C is the height of the Gaussian, J_0 the midpoint, and σ the width. This is roughly equivalent to, but less rigorous than, the fitting approach of Edelman and Larbalestier (1993) given by Eq. 2.15. We do not intend to report that effective pinning force distributions are actually Gaussian, but the use of Gaussian fitting provides a convenient and informative analytical framework. Gaussian fitting was applied for multiple temperatures for crystal #1 at 30 mT (see Fig. 4.13) and 0.1 T. Fig. 4.14 shows the resulting fitting parameters for both fields at a variety of temperatures, but in this case J_0 and σ are both multiplied by the relevant field values, giving a measure of force densities F_0 and σ_F (JB measures the applied Lorentz force; see Eq. 1.6). This provides a direct window into the pinning forces and allows for easy comparison between different field values.

The information available in Fig. 4.14 is plentiful. Not only do the Gaussian fits report values for the bulk pinning force density, they map out the strength and character of the pinning with changing temperature and field. As temperature increases, the average pinning force decreases and the distribution broadens (this is sometimes called "thermal smearing"), in keeping with most theoretical predictions (Blatter *et al.*, 1994). When the field is increased, pinning is strengthened and the distributions also broaden. Increasing pinning strength with increasing field is predicted for low B regions, where vortex interactions are weak (Blatter *et al.*, 1994). In the cases of both fields, the fits imply that the distributions are more stable for changing T for lower T values and more sensitive to changing T for higher T values.

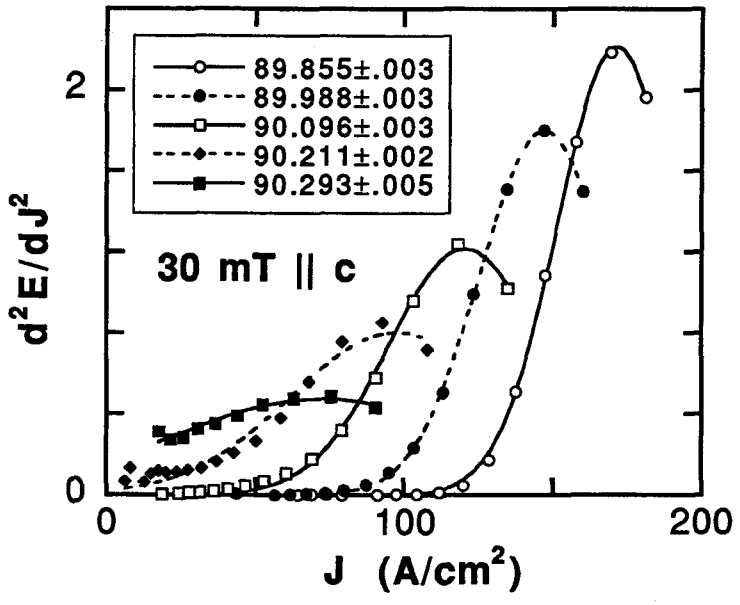

Fig. 4.13: Second derivative data in arbitrary units for YBCO crystal #1 in a 30 mT field. Dashed and solid lines represent Gaussian fits.

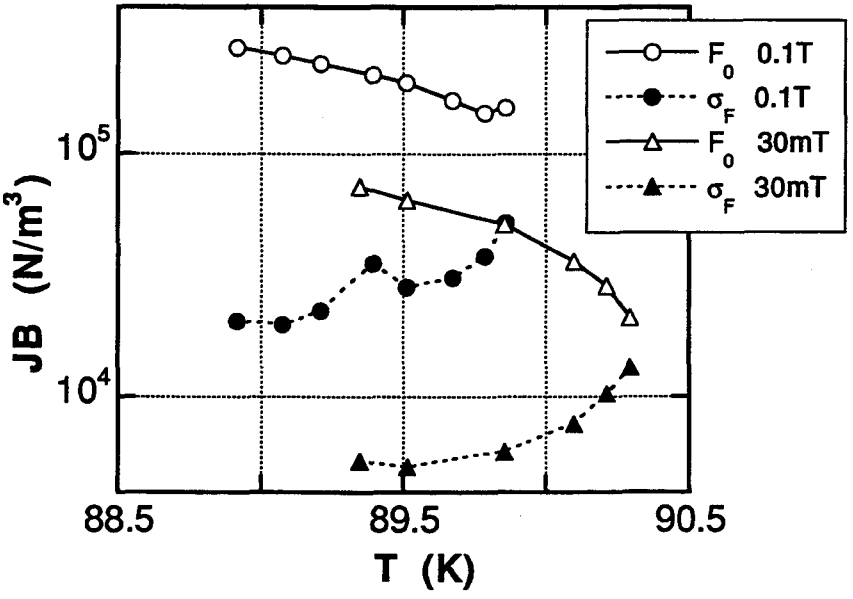

Fig. 4.14: Semi-log plot of fitting parameters expressed as force density versus temperature for crystal #1 at two different fields. Error bars from the fit are less than the point size in each case.

This type of Gaussian fitting to *V-I* data has been used in one other case for high-T_c materials. As described in Section 2.2.2, Edelman and Larbalestier (1993) assume Gaussian distributions of critical currents. Using the analytical result presented in Eq. 2.15, they fit *V-I* data for a BSCCO tape and report Gaussian fitting parameters in terms of *I* for fields between 5 mT and 0.2 T (*ibid.*). Using the dimensions reported for their tape, calculating *J* values, and multiplying their fitting results by the appropriate *B* values, we translate their data into distributions of force density. In this way, we can compare their results directly to those of YBCO crystal #1 (see Fig. 4.15). While the magnitude of force density in the two samples is quite different, the field dependence in this low-field regime is strikingly similar. We attribute the difference in magnitudes to two factors: our data is taken much closer to T_c than is the data of Edelman and Larbalestier (89 K and 77 K respectively); and pinning in BSCCO tapes is known to be much stronger than in YBCO crystals (Li *et al.*, 1994).

To describe the broadening of the distributions with increasing *B*, Fig. 4.15b shows the ratio σ_F/F_o plotted versus *B* for both crystal #1 and the BSCCO tape of Edelman and Larbalestier (1993). The distributions broaden in a remarkably similar manner for increasing *B* in this low-field regime. This broadening of the force-density or critical-current distributions has been related to a decrease in the measured *n* values in dc *V-I* data by Goodrich *et al.* (1990), and also by Edelman and Larbalestier (1993). The logic of these authors can be summarized as follows. As *B* increases, the width of the critical-current distribution increases, the experimental *V-I* trace is less steep, and the measured *n* value is necessarily lower. This matches the observations in Chapter 4, and provides a reasonable explanation for the *B*-dependence of *n* for a given sample noted in Section 4.1.

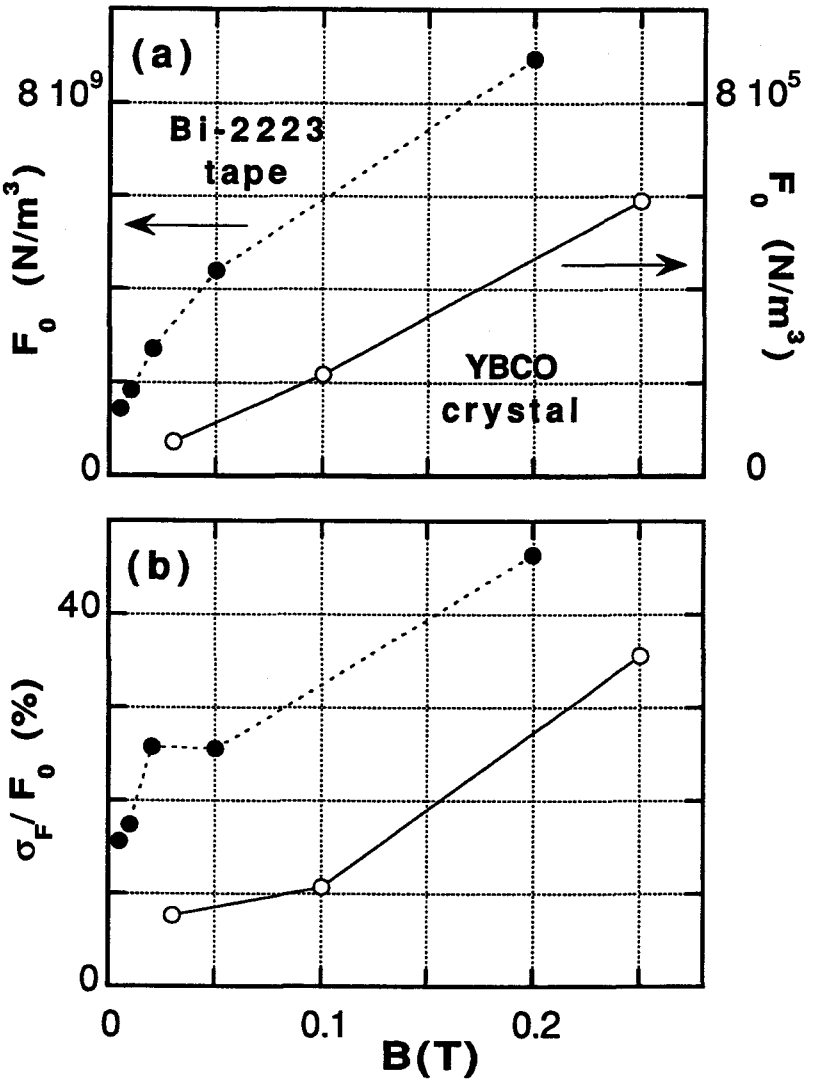

Fig. 4.15: Comparison of Gaussian fitting parameters for an YBCO crystal at 89.3 K and a BSCCO tape at 77 K. Displayed are (a) the central force of the Gaussian force density and (b) the ratio of the width to the central force. The BSCCO data is taken from Edelman and Larbalestier (1993).

In Fig. 4.15, we find $F_0 \alpha B$ for YBCO crystal #1. Interestingly, this matches the findings of recent torque magnetometry measurements on YBCO crystals which show the same linear dependence for $B \leq B_\varphi$ (the matching field) at 77 K (Hiergiest and

Hergst, 1997). The authors in that work note that $F_0 \alpha B$ fit the predictions of Larkin and Ovchinnikov (1979) for single-vortex pinning, where vortex interactions are weak. Since the YBCO crystal data points in Fig. 4.15 should be below B_φ (we estimate 0.25 T $\leq B_\varphi \leq$ 0.75 T), we believe that a single-vortex picture is appropriate in the low-field data for crystal #1. However, we would need a greater number of points before claiming that the YBCO crystal data support Larkin and Ovchinnikov. The average force densities found by Hiergiest and Hergst are some fifty times larger than those plotted for the YBCO crystals in Fig. 4.15. As with the larger magnitudes shown for BSCCO, this can be attributed to the fact that the experiment here was conducted at higher temperatures (89 K versus 77 K).

Fitting the data of higher fields is complicated by two issues: fewer high-J data were collected due to contact heating, as described in Section 3.8, leaving many f_{eff} curves too incomplete to fit; and higher fields cannot often be described by a single Gaussian fit. Especially for fields of 0.5 T and above, for both crystals, before and after fast-neutron irradiation, a more complicated structure emerges in the f_{eff}. Data taken for crystal #2 include more flux flow data than that taken for crystal #1, so the resulting f_{eff} are more complete. Fig. 4.16 shows data taken after for crystal #2 after irradiation.

Note in Fig. 4.16 that the f_{eff} can no longer be described adequately by single Gaussian fits. The apparent two-peak structure is not as clearly out of the noise of the second derivative process as one would like before making bold claims about it. To further probe this feature, an experiment that collected data with linear current ramping would be essential. We make only the following comments about the multiple-peak structure of f_{eff}: it appears in all data (except the low-T region for 0.1 T) for crystal #2 after irradiation; it appears to a lesser extent for 0.25 T and 0.5 T data in crystal #2 before irradiation.

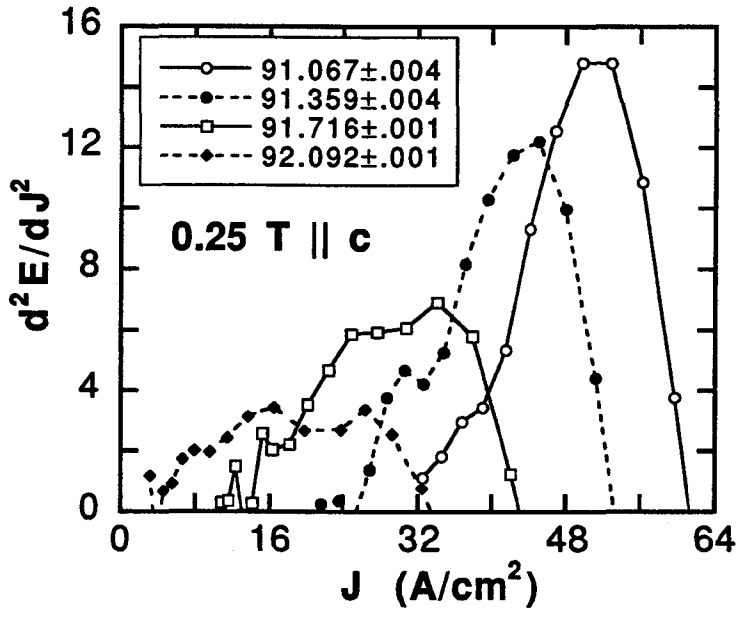

Fig. 4.16: Second derivative data for YBCO crystal in 0.25 T after irradiation.

If there are indeed two separate peaks in an f_{eff}, the most obvious interpretation is that two distinct sources of pinning are manifest in the sample at that temperature and field. In the case of an irradiated sample, this could be attributed to the different pinning characteristics of twin-boundaries and the neutron-damage sites. For an unirradiated crystal, however, the interpretation of a double-peak in f_{eff} is less intuitive. Two possibilities present themselves. The first appears in Radzihovsky's separation of a strong Bose glass and a weak Bose glass for $B > B_{\varphi}$ (see Section 2.4 and Fig. 2.5; Radzihovsky, 1995). For our unirradiated YBCO crystals, this could possibly apply to $B \geq 0.5$ T. The weak Bose glass would necessarily give distributions with two distinct features. The second possibility is set out by the modeling efforts of Faleski *et al.* where the authors show two distinct distributions of vortex velocities for systems with strong pinning (Faleski *et al.*, 1996). In this view, a

double-peak in a velocity distribution is a signature of plastic vortex behavior, where some vortices are strongly pinned and others are relatively free to flow between pinned islands. This is not directly comparable to our f_{eff} since Faleski *et al.* examine instantaneous vortex distributions, while our f_{eff} examine a time-averaged vortex behavior.

Overall, we observe that the effects of increasing magnetic field and irradiation are similar; both tend to increase the overall strength of pinning and broaden the f_{eff}. Fig. 4.17 underlines this point; like Fig. 4.16, the data are all near the same T and plotted versus force density. The effect of irradiation at a constant B and T can be observed, in addition to the pure effect of increasing B for the unirradiated crystal. It is interesting to note that while the minima of the f_{eff} stay relatively fixed for different applied B, the minimum force density is substantially increased after irradiation.

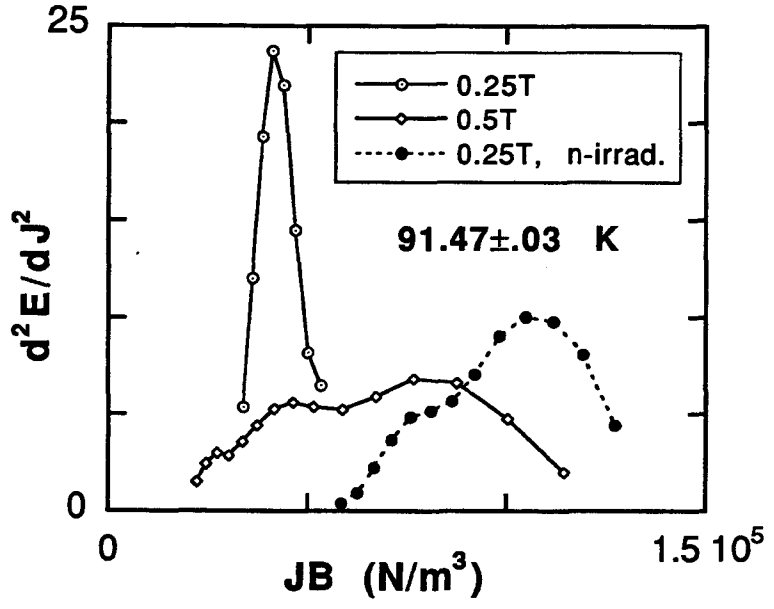

Fig. 4.17: Second derivative data as a function of force density for crystal #2 at 91.47K, including field and irradiation effects.

We have tried to apply the second-derivative approach to the thin-film YBCO data of Roberts, but find that lack of flux-flow data in that work renders the f_{eff} too incomplete for a fruitful analysis (Roberts, 1995). For instance, the vast majority of f_{eff} calculated for the thin-film data did not reach a clear maximum.

We wish to point out the natural relation between the analytical approach of second-derivatives and theories of vortex percolation. No theories of which we are aware describe the experimental f_{eff} more adequately than those of percolative thermal depinning (Ziese, 1996a; Jagla and Balseiro, 1996; Yamafuji and Kiss, 1996). The model of Yamafuji and Kiss (1996) assumes that a percolative transition can be described by critical-current distributions (see Section 2.5). Though the experimental f_{eff} shown here do not exactly match the forms the authors assume (see Eq. 2.25; *ibid.*), the f_{eff} are sensitive to the pinning properties of the crystal in keeping with the predictions percolative models (*ibid.*; Zeise 1996a,b). Furthermore, it should be noted that the calculation and analysis of f_{eff} are naturally compatible with a picture of plastic vortex response (see Section 2.1.1) since the f_{eff} implicitly assume that each vortex has its own depinning current and that a depinned vortex can flow away from its neighbors.

In summary, the second-derivatives present very reasonable forms for effective depinning-current distributions and effective pinning-force-density distributions. Though the data of this thesis is not optimally suited to the analysis, the derived f_{eff} are informative, and the technique shows great promise for future dc V-I experiments on high-T_c materials. They suggest that pinning forces increase via decreasing T, increasing B, or irradiation-induced damage and that the distribution of pinning forces is smeared by increasing T, increasing B, or irradiation-induced damage. Though none of these conclusions is specifically surprising, they have never been so clearly demonstrated using dc V-I data. The results also suggest that the observed variation of n (see Chapter 4) could be

linked to a systematic variation of critical-current (or force density) distribution widths. Of particular interest is the derivation of average pinning-force densities and the subsequent opportunity to compare dc *V-I* data directly to the results of other techniques (e.g. torque magnetometry) and other materials (e.g. BSCCO tapes).

CHAPTER 5

DISCUSSION

The systematic variation of n shown in Section 4.1 together with the derived force distributions in Section 4.6 make a convincing argument for thermal depinning as opposed to a second-order vortex phase transition in twinned crystals of YBCO. The results can be loosely reconciled with the simulations of Yamafuji and Kiss (1996). Nevertheless, several issues are worthy of further investigation. First, knowing that second-order phase transition models (specifically, the Bose glass theory) have found experimental support in twinned YBCO, the question as to where they fail in their predictions for dc V-I characteristics is an open one. Moreover, the qualitative similarity of the data and the continuity exhibited in Section 4.2 across samples (i.e. thin films, tapes and crystals) with different pinning structures question the meaning of dc V-I measurements on a more general level. Second, if a thermal depinning description is apt, one must attempt to explain the demonstrable viability of critical scaling.

5.1 Utility of Voltage-Current Characteristics

As shown in Chapter 4, the dc measurement of V-I characteristics is, at best, an inconclusive method for probing vortex phase transitions in high-T_c materials. Considering that most of the dc V-I characteristics collected for the copper-oxides have been analyzed in the context of phase transitions, questions arise concerning their utility in general. What information can be reliably extracted from this technique?

One can attempt to fit the V-I data to the models of VRH or half-loop excitations. However, these techniques failed to fit the data in Section 4.5. The theories of collective pinning and collective creep have provided mixed results. For $B \leq 0.25$ T, the experimental distributions in crystal #1 at fixed T can be reconciled with single vortex pinning (though an unfortunate semantic choice, this is a subset of collective pinning; see Section 2.1.1). While this matches the predictions of traditional collective pinning theory for low fields and weak vortex interactions (LO, 1979), many of the f_{eff} observations are left unexplained. Namely, collective pinning does not, to the best of our understanding, account for the T-dependence of the distribution widths and midpoints. To address collective creep, an attempt was made to fit the data using the exponent μ (see Section 4.5), but this was clearly not successful. The investigation of other analyses is warranted.

We believe that the analysis of effective pinning-force distributions provides a ready and promising alternative, largely unexplored for HTS. An experiment geared for the mapping of these distributions (as opposed to the mapping of a critical scaling region) could yield a wealth of microstructural information about flux pinning in YBCO crystals as a function of field and temperature. That is to say it would be desirable to collect data well into the flux flow region and to take data at a specific temperature for a greater number of applied fields than are presented here. In this sense we believe that the efforts in Section 4.6 have only scratched the surface for this analytical technique.

To provide insightful context for the physics of a dc resistivity measurement, we note the recent work of Gordeev *et al.* (1996) who studied vortex dynamics in an untwinned YBCO crystal using both dc and ac measurements. The authors find that (for the same B, J amplitude, and T) an ac current of 100 Hz induces a resistive signal in the vortex liquid state ($T_p \leq T < T_c$) approximately four times larger than the resistive signal resulting from a dc current. In

addition, the dc signal is much noisier than the ac signal. The authors attribute the high noise levels to non-uniform flux flow (see Appendix B). They conclude for untwinned crystals that the two types of measurements are measuring very different properties of the vortex assembly, and they paint the following sensible picture. In a dc applied current, pinned vortices are pushed by the Lorentz force to the steepest areas of their local pinning potentials. Those vortices in sufficiently deep wells are stationary, barring a high enough temperature to promote thermal activation over the local pinning barrier. However, for an ac applied current, pinned vortices are free to move locally about a pinning site. In a simple 1D picture, they are free to move from one side of their potential well and back under the influence of the alternating Lorentz force. In this way, pinned vortices that would give zero signal in the dc current contribute to the signal in an ac current.

Since their samples lack twin boundaries, Gordeev *et al.* (1996) propose that the major barrier to thermal activation is provided by the surface of the crystal where vortices must nucleate at one side and exit the other in the presence of a dc current. The authors suggest that the vortices pile up, waiting for those closest to the surface of the crystal to overcome the imposing energy barrier.

In the case of twinned crystals, barriers are not as difficult to find, but we believe that the results of the untwinned case apply. The Bose glass model assumes randomly distributed columnar pins (Nelson and Vinokur, 1993). In the case of twin boundaries, a theoretical treatment has only been applied to the special case of *parallel* twins and an applied Lorentz force *normal* to the plane of the twins (Marchetti and Vinokur, 1995). In our experiment, neither theoretical treatment is especially appropriate. As with most YBCO crystals, ours are twinned in a mosaic pattern (see Fig. 5.1). The twins are, at all times, parallel to the applied field B, but they form a 45° angle to both the applied current J and the resulting Lorentz force F.

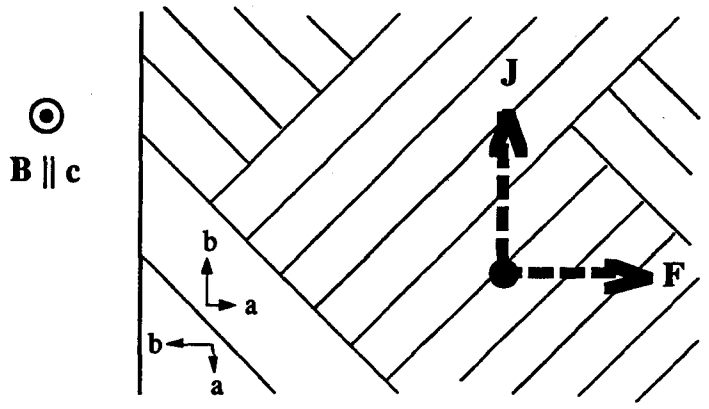

Fig. 5.1: Sketch of *ab* plane and transport geometry in a twinned YBCO crystal. Light lines are twinning planes and the heavy dot represents a lone vortex. The size of the vortex core is greatly exaggerated in relation to the twin boundary separation distance.

For a number of years, the question of whether or not a twin boundary parallel to a Lorentz component *impeded* vortex flow or *assisted* vortex flow was an open one (G. Deutscher and Müeller, 1987; Abrikosov, 1989; Vlasko-Vlasov *et al.*, 1994). Thanks to a series of precise measurements for mosaic-twinned crystals and parallel-twinned crystals, the problem is now better understood (Oussena *et al.*, 1995; Kwok *et al.*, 1996). Unfortunately, as with so many properties of high-T_c materials, the pinning function of twins is T-dependent. For lower temperatures ($T < 80$ K at 6 T according to Kwok *et al.*, 1996), the twins aid the motion vortices in a parallel direction. For higher temperatures, the twins impede vortex motion, regardless of the vortex velocity with respect to the twin planes.

Oussena *et al.* (1996) took measurements of YBCO crystals with mosaic twins, like the crystals in this thesis, but also for a crystal containing only a parallel set of twins. The latter crystal had been cut from the same parent crystal as one of the mosaic crystals, so that their properties could otherwise be considered identical. In

both cases, the twins were oriented along the c-axis and met the sides of the crystals at 45° angles. The widths of the measured magnetization loops were much greater for the crystals with a mosaic twin pattern, which means they pinned vortices much more strongly than the parallel-twins crystal. All data in their experiment were collected at T = 60 K. The authors interpret their data to mean that vortices move rather easily along twin boundaries given a parallel Lorentz force component, but that the intersection of one twinning domain with another perpendicular domain exhibits strong vortex pinning (see Fig. 5.1 above). We note that detailed TEM measurements have shown that a complex accommodation region exists in the crystalline structure at a domain intersection, with microtwins forming on a scale approximately an order of magnitude smaller than the average twin spacing away from the intersection (Drake *et al.*, 1993).

However, as stated above, the function of the twins is temperature dependent. Kwok *et al.* (1996) studied an YBCO crystal with a set of parallel twins and found that, above a field-dependent T_i, twins impeded vortex motion in all directions. They found T_i = 83.1 K for 4 T applied $\parallel c$ and T_i = 79.6 K for 6 T. Assuming that their crystal is similar to ours and extrapolating roughly from those two points, we find that $T_i \approx$ 89 K for 0.5 T, a characteristic field for our measurements. For crystal #1, $T_i > T_p$ (see Fig. 3.13), while for crystal #2, $T_i < T_p$ (see Fig. 3.15). To the best of our knowledge, T_i is in the thick of the fray, and the role of the twins cannot be clearly defined for our measurements.

Nevertheless, we can envision the effect of our dc applied current as follows. For $B < B_\varphi$ -- where every vortex can presumably find a position on a twin -- and the current applied as in Fig. 5.1, vortices far from a twin domain intersection are weakly pinned and, depending on T, may even find motion along the twins relatively easy. However, those sitting on or near one of the domain intersections are very strongly pinned, (we speculate that they face

a thermal activation barrier not unlike that posed by the surfaces of the ultra-clean untwinned crystals mentioned above). This is quite unlike any scenario assumed by the Bose glass theory, where for $B < B_\varphi$, each vortex interacts with a columnar pin. In this light, it is no particular surprise that the Bose glass theory fails to describe the dc data of crystals with mosaic twins. Whereas an ac current of sufficiently high frequency might test the local pinning of vortices, the dc current will primarily test the barriers located at the domain intersections and vortices which might move are impeded by vortices at the intersections.

The recent measurements of Safar *et al.* (1996) provide a counterpoint to the argument above. The authors examine *V-I* data from high-quality, thick films of YBCO. This system is argued to be somewhat like heavily-twinned YBCO crystals but with much more densely-spaced twins. Their data from the thick film shows strong evidence for a Bose glass transition for twins oriented at 45° to the applied Lorentz force (Fig. 5.1) *and* for twins oriented at 0 and 90° to the applied Lorentz force (*ibid.*). However, the dc V-I measurements presented in this thesis clearly disagree with Bose glass predictions for the critical exponents z' and ν'. This could be attributed to the fact that while we are examining $B < 1$ T, Safar *et al.* are examining $B > 1$ T. In addition, the microstructure of thick films is quite different from that of single crystals (Safar *et al.*, 1996), especially for the unirradiated crystals.

One can further dissect dc measurements by first noticing that ac and dc results have rarely shown congruence for YBCO (Yeh *et al.*, 1993), and then determining why the measurements provide different results. Even though the ac literature is somewhat closer to a consensus, it is no less controversial. Specifically, we note the results of ac measurements for twinned YBCO crystals. Most authors in this area interpret their data in terms of second-order phase transitions since the models of second-order transitions have made

concrete predictions regarding the frequency dependence of ac measurements (Fisher *et al.*, 1991; Nelson and Vinokur, 1992).

In 1993, Reed *et al.* and Yeh *et al.* reported four-terminal ac resistivity data which exhibited a scaling collapse consistent with a vortex glass phase transition. The critical exponents ($z \approx 3$ and $\nu \approx 2/3$) did not match vortex glass or Bose glass predictions, but were interpreted as clear evidence for "second-order vortex lattice melting" in twinned YBCO crystals (Reed *et al.*, 1993). The authors reported field-independent behavior for 0.1 to 9 T fields applied parallel to *c*. In 1994, the complex conductivity experiments of Kötzler *et al.* (derived from an ac susceptibility technique) also concluded that they saw evidence for a second-order phase transition, in this case described by critical exponents $z \approx 3.1$ and $\nu \approx 3.1$, universal for fields ranging from 0.4 to 12 T. These values were confirmed later in the same year by Ando *et al.* (1994) who measured the frequency dependence of the ac penetration depth using a two-coil, mutual-inductance technique.

In each case, the authors claim that their results are inconsistent with a standard flux creep or flux flow approach. However, Ziese has recently pointed out that the numerical discrepancy between experiment and theory in these cases, when coupled with the persistent lack of thermodynamic phase-transition evidence, renders the conclusions of the ac experiments highly questionable (Ziese, 1996b).

We wish to underline the field-independence of these results. This includes recent zero-field complex conductivity measurements of YBCO crystals that were consistent with second-order criticality (Anlage *et al.*, 1996). In addition, ac complex conductivity in YBCO thin films has now been shown to exhibit the critical scaling signature and universality class of the vortex glass theory for zero field (Nakielski *et al.*, 1997). Hence, the model of a second-order vortex phase transition describes ac data admirably, even in the

absence of externally induced vortices. At the very least, this emphasizes that ac and dc techniques probe different properties of vortex arrays in YBCO twinned crystals.

We believe that some of the arguments presented in Section 4.4 concerning the viability of critical scaling in these systems apply to ac measurements as well. When the disquieting zero-field results (Nakielski *et al.*, 1997) are coupled with recent theoretical work suggesting that second-order vortex phase transitions cannot be realized for finite temperatures (Wengel and Young, 1996), one is encouraged to explore interpretations of ac data that deviate from a phase transition picture. As with dc data, preliminary efforts have been made to explain ac experiments in terms of percolative depinning (Ziese, 1996a, 1996b).

5.2 Reconciling Percolation and Critical Scaling

The results plotted as n-L_p in Fig. 4.2 suggest that the initial acceptance of critical scaling of dc V-I data as evidence of a universal second-order phase transition (Koch *et al.*, 1989) was premature. The statement is especially strong since the scaling parameters deviate outside of the predicted values in both directions; for example, mediocre quality films in very high fields give abnormally low z values (Lang *et al.*, 1996), while the low-field film data (Roberts *et al.*, 1994, 1995) and the crystal data presented in Section 4.4 give abnormally high z values.

After Koch *et al.* (1989) published their scaled thin-film data, others immediately showed that standard flux creep arguments, given liberal parameter manipulation, could also account for resistivity data which scaled according to the vortex glass prescription (Coppersmith *et al.*, 1990). At the time, the primary defense of the vortex glass theory was the universality of the thin-

film results which flux creep calculations failed to reproduce (reply to Coppersmith *et al.*, 1990). As was shown in thin-film YBCO (Roberts *et al.*, 1994) and as shown now for YBCO crystals (Brown *et al.*, 1997), a true universality does not exist.

Since scaling persists around a power-law isotherm "T_g" for a variety of copper-oxide materials, it is not easily brushed away as a lucky parametrization. Especially if we are to accept the picture of thermal depinning, we must ask how this picture addresses the scaling behavior of resistivity data.

In 1990, in response to the initial reports of critical scaling collapses, Esquinazi presented a viable alternative to the vortex-glass explanation (Esquinazi, 1990); regrettably, this work is seldom cited in the literature. Esquinazi showed that he could recreate the isotherms of Koch *et al.* (1989) using two simple flux flow effects -- normal flux flow of liquid-like vortices, and thermally activated flux flow of vortices depinned in the applied Lorentz force. In the view of Esquinazi, the two different types of isotherms on either side of T_g were just two slightly different regimes of flux flow. However, he did not offer a simulation of critical scaling.

As described in Section 2.5, Yamafuji and Kiss (1996) have shown that scaling collapses can be simulated starting from the assumption of very specific (one might even say contrived) pinning force distributions. Since they must assume five-parameter distributions which are not readily interpreted physically, we find their efforts provoking yet inconclusive.

With the aim of testing the utility and meaning of critical scaling, we have carried out a modest simulation that starts from an extremely basic picture of Gaussian pinning force distributions. The details and results of the simulation are presented in Appendix A.

The resulting scaling collapse of the simulation (see Fig. A.4) might at first be a welcome sight to those who advocate a percolative depinning transition. In percolative models, T_p corresponds to the temperature at which the current distribution first becomes finite at $J = 0$ (Jagla and Balseiro, 1996; Yamafuji & Kiss, 1996). The vortex glass analysis of the simulated data gives a T_p value very close to 90.7, the temperature at which the distribution is nonzero at $J = 0$. However, the simulation also shows that the choice of sensitivity influences the analysis (see Fig. A.2).

We reach two conclusions from the simulation. First, even a very simple model of pinning force distributions can give realistic V-I data for copper-oxide superconductors. We do not believe Gaussians are essential, and more physically meaningful assumptions for the T-dependence would presumably yield more realistic simulated data. This area is worthy of further investigation, particularly for the inclusion of B variations and pinning-density variations. Second, we conclude that critical scaling cannot be reliably linked to a phase transition for four-terminal dc measurements. We find that the choice of T_p is demonstrably dependent on the experimental resolution, reiterating the original misgivings of Esquinazi (1990).

5.3 Summary

This work makes a number of original contributions to the study of YBCO crystals and dc V-I data for high-T_c superconductors. To the best of our knowledge, the following items appear first in this thesis. We have presented ρ-J data for heavily twinned YBCO crystals before and after fast-neutron irradiation. We have demonstrated that the logarithmic derivative of the isotherm at T_p depends systematically on the Larkin-Ovchinnikov length L_p, not just for the YBCO crystals before and after fast-neutron irradiation,

but also for other works in the literature, including thin films of YBCO, thin films of NCCO, and BSCCO tapes. These results encompass data from a wide range of applied magnetic fields. We have shown that the data submit to a critical scaling analysis and give non-universal critical parameters which do not match any of the available theories of second-order vortex phase transitions. We have applied the method of second-derivatives to *V-I* data for YBCO crystals and shown that it provides valuable information about vortex pinning. Finally, we have successfully simulated data assuming *T*-dependent Gaussian distributions of depinning currents and demonstrated that, if the assumptions are appropriate to dc *V-I* data in high-T_c materials, that critical scaling follows, albeit with parameters which depend on experimental sensitivity.

Given these points, we conclude that models of thermal depinning, or percolative depinning, are able to explain dc *V-I* measurements in the copper-oxide superconductors more completely than are the models of vortex phase transitions. Since the results of other techniques have provided a variety of verdicts for vortex phase transitions in twinned YBCO, it is not yet clear if the theories of second-order transitions suffer from relatively minor mistakes in their descriptions of specific techniques (e.g. dc *V-I* data), or from more fundamental problems. In addition, elastic bundle pinning, as described by collective pinning and collective creep theories, does not account for the data. Given the inadequacy of an elastic model and the apparent relevance of thermal depinning, the regime we have explored in twinned YBCO crystals is better described by plastic vortex response, in agreement with other recent experimental and theoretical works.

BIBLIOGRAPHY

Abrikosov, A. A., (1957). Zh. Eksp. Teor. Fiz. 32, 1442 [Sov. Phys. JETP 5, 1174 (1957)].

Abrikosov, A. A., A. I. Buzdin, M. L. Kulic, and D. A. Kuptsov, (1989). Supercond. Sci. Technol. 1, 260.

Abulafia, Y., A. Shaulov, Y. Wolfus, R. Prozorov, L. Burlachkov, Y. Yeshurun, D. Majer, E. Zeldov, H. Wühl, V. B. Geshkenbein, and V. M. Vinokur, (1996). Phys. Rev. Lett. 77, 1596.

Acerbi, E., G. Ambrosio, L. Rossi, and G.Volpini, (1994). IEEE Trans. Mag. 30, 2296.

Anderson, P. W., (1962). Phys. Rev. Lett. 9, 309.

Anderson, P. W., and Y. B. Kim, (1964). Rev. Mod. Phys. 36, 39.

Ando, Yoichi, Hiroshi Kubota, Yoshibumi Sato, and Ichiro Terasaki, (1994). Phys. Rev. B 50, 9680.

Anlage, Steven M., J. Mao, J. C. Booth, Dong Ho Wu, and J. L. Peng, (1996). Phys. Rev. B 53, 2792.

Babic, E., M. Prester, N. Biskup, Z. Marohnic, and S. A. Siddiqi, (1990). Phys. Rev. B 41, 6278.

Baixeras, J., and G. Fournet, (1967). J. Phys. Chem. Solids 28, 1541.

Bardeen, J., L. N. Cooper, and J. R. Schrieffer, (1957). Phys. Rev. 108, 1175.

Bardeen, J., and M. J. Stephen, (1965). Phys. Rev. 140, A1197.

Blatter, G., M. V. Feigel'man, V. B. Geshkenbein, A. I. Larkin, and V. M. Vinokur, (1994). Rev. Mod. Phys. 66, 1124.

Blatter, G., and B. Ivlev, (1993). Phys. Rev. Lett. 70, 2621.

Brandt, E. H., (1995). Rep. Prog. Phys. 58, 1465.

Brandt, E. H., P. Esquinazi, G. Weiss, R. N. Kleiman, P. L. Gammel, L. F. Schneemeyer, J. V. Waszczak, and D. J. Bishop, (1989). Phys. Rev. Lett. 62, 2330.

Brown, B., J. M. Roberts, J. Tate, and J. Farmer, (1997). Phys. Rev. B 55, 8713R.

Caton, R., R. Selim, A. M. Buoncristiani, and C. E. Byvik, (1990). J. Appl. Phys. 67, 7478.

Celasco, M., G. Cone, A. Masoero, V. Popescu, and A. Stepanescu, (1995). Phys. Lett. A 201, 429.

Charalambous, M., R. H. Koch, T. Masselink, T. Doany, C. Field, and F. Holtzberg, (1995). Phys. Rev. Lett. 75, 2578.

Chu, C. W., (1996). Preprint No. 96:109, Texas Center for Superconductivity at the University of Houston.

Chu, C. W., P. H. Hor, R. L. Meng, L. Gao, and Z. J. Huang, (1987). Science 235, 567.

Claus, H., S. Yang, H. K. Viswanathan, G. W. Crabtree, J. W. Downey, and B. W. Veal, (1993). Physica C 213, 185.

Clem, J. R., (1981). Phys. Rep. 75, 2.

Coppersmith, S. N., M. Inui, P. B. Littlewood, R. H. Koch, V. Foglietti, and M. P. A. Fisher, (1990). Phys. Rev. Lett. 64, 2586.

Crabtree, G. W., W. K. Kwok, U. Welp, J. A. Fendrich, and B. W. Veal, (1996). J. Low Temp. Phys. 105, 1073.

Crusellas, M. A., J. Fontcuberta, and S. Piñol, (1992). Phys. Rev. B 46, 14089.

D'Anna, G., P. L. Gammel, H. Safar, G. J. Alers, D. J. Bishop, J. Giapintzakis, and D. M. Ginsberg, (1995). Phys. Rev. Lett. 75, 3521.

Dekker, C., W. Eidelloth, and R. H. Koch, (1992). Phys. Rev. Lett. 68, 3347.

Deutcher, G., and K. A. Müeller, (1987). Phys. Rev. Lett. 59, 1745.

Dolan, G. J., F. Holtzberg, C. Feild, and T. R. Dinger, (1989). Phys. Rev. Lett. 62, 2184.

Doniach, S., S. Ryu, and A. Kapitulnik, (1994). J. Low Temp. Phys. 95, 353.

Drake, A., M. Aindow, M. Rand and J. S. Abell, (1993). J. Crys. Growth 128, 762.

Edelman, H. S., and D. C. Larbalestier, (1993). J. Appl. Phys. 74, 3312.

Esquinazi, P., (1990). Sol. St. Comm. 74, 75.

Essmann, U., and H. Träuble, (1967). Phys. Lett. 24 A, 526.

Faleski, M. C., M. C. Marchetti, and A. A. Middleton, (1996). Phys. Rev. B 54, 12427.

Farmer, J. W., University of Missouri, Research Reactor and Physics Department, Columbia MO 65211, USA.

Farmer, J. W., D. L. Cowan, X. Ding, and D. Bradford, (1994). Physica C 235-240, 2893.

Farrell, D. E., W. K. Kwok, U. Welp, J. Fendrich, and G. W. Crabtree (1995). Phys. Rev. B 51, 9148.

Farrell, D. E., J. P. Rice, and D. M. Ginsberg (1991). Phys. Rev. Lett. 67, 1165.

Feigel'man, M. V., V. B. Geshkenbein, A. I. Larkin, and V. M. Vinokur, (1989). Phys. Rev. Lett. 63, 2203.

Feigel'man, M. V., and V. M. Vinokur, (1990). Phys. Rev. B 41, 8986.

Fendrich, J. A., W. K. Kwok, J. Giapintzakis, C. J. van der Beek, V. M. Vinokur, S. Fleshler, U. Welp, H. K. Viswanathan, and G. W. Crabtree, (1995). Phys. Rev. Lett. 74, 1210.

Feynman, R., (1972). *Statistical Mechanics*, (Benjamin, Reading, MA)

Fisher, D. S., M. P. A. Fisher, and D. A. Huse, (1991). Phys. Rev. B 43, 130.

Fisher, M. P. A., (1989). Phys. Rev. Lett. 62, 1415.

Fisher, M. P. A., P. B. Weichman, G. Ginstein, and D. S. Fisher, (1989). Phys. Rev. B 40, 546.

Friesen, M., Physics Building, Purdue University, W. Lafayette, IN 47907-1396.

Friesen, M., J. Deak, L. Hou, and M. McElfresh, (1996). Phys. Rev. B 54, 3525.

Friesen, M., P. Muzikar, (1997). submitted to Phys. Rev. B. Physics Dept., Purdue University, West Lafayette, IN 47907-1396.

Frischherz, M. C., M. A. Kirk, J. Farmer, L. R. Greenwood, and H. W. Weber, (1994). Physica C 232, 309.

Gammel, P. L., L. F. Schneemeyer, and D. J. Bishop, (1991). Phys. Rev. Lett. 66, 953.

Gammel, P. L., L. F. Schneemeyer, J. V. Waszczak, and D. J. Bishop, (1988). Phys. Rev. Lett. 61, 1666.

Giamarchi, T., and P. Le Doussal, (1995). Phys. Rev. B 52, 1242.

Giamarchi, T., and P. Le Doussal, (1996). Phys. Rev. Lett. 76, 3408.

Gingras, M. J. P., D. A. Huse, (1996). Phys. Rev. B 53, 15193.

Ginzburg, V. L., (1961). Soviet Phys. Solid State 2, 1824.

Ginzburg, V. L., L. D. Landau, (1950). Zh. Eksp. Teor. Fiz. 20, 1064.

Glazman, L. I., and A. E. Koshelev, (1991). Phys. Rev. B 43, 2835.

Glover, R. E., and M. Tinkham, (1957). Phys. Rev. 104, 844.

Goodrich, L. F., A. N. Srivastava, M. Yuyama, and H. Wada, (1993). IEEE Trans. Appl. Sup. 3, 1265.

Gordeev, S. N., P. A. J. de Groot, M. Oussena, A. V. Volkozub, S. Pinfold, R. M. Langan, R. Gagnon, and L. Taillefer, (1996). J. Low Temp. Phys. 105, 1147.

Govorkov, S. A., E. V. Ill'ichev, and V. A. Tulin, (1994). JETP 78, 986.

Groth, J., C. Reichhardt, C. J. Olson, S. Field, and F. Nori, (1996). Phys. Rev. Lett. 77, 3625.

Habbal, F., and W. C. H. Joiner, (1977). Phys. Lett. 60A, 434.

Hiergeist, R., and R. Hergt, (1997). Phys. Rev. B 55, 3258.

Higgins, Mark J., and S. Bhattacharya, (1996). Physica C 257, 232.

Holton, G., H. Chang, and E. Jurkowitz, (1996). Am. Scientist 84, 364.

Houghton, A., R. A. Pelcovits, and A. Subdo, (1989). Phys. Rev. B 40, 6763.

Huberman, B. A, and S. Doniach, (1979). Phys. Rev. Lett. 46, 950.

Huse, D. A., M. P. Fisher, and D. S. Fisher, (1992). Nature 358, 553.

Jagla, E. A., C. A. Balseiro, (1996). Phys. Rev. B 53, 15305.

Jeandupeux, O., A. Schilling, H. R. Ott, and A. van Otterlo, (1996). Phys. Rev. B 53, 12475.

Jenkins, R. G., H. Jones, N. Killoran, and W. Timms, (1991). IEEE Trans. Magn. 27, 1182.

Jensen, H. J., A. Brass, Y. Brechet, and A. J. Berlinsky, (1988). Phys. Rev. B 38, 9235.

Jiang, W., N.-C. Yeh, D. S. Reed, U. Kriplani, D. A. Beam, M. Konczykowski, T. A. Tombrello, and F. Holtzberg, (1994). Phys. Rev. Lett. 72, 550.

Jiang, W., N.-C. Yeh, D. S. Reed, U. Kriplani, T. A. Tombrello, A. P. Rice, and F. Holtzberg, (1993). Phys. Rev. B 47, 8308.

Jones, W., and N. H. March, (1973). *Theoretical Solid State Physics, Volume 1*, (Dover, New York).

Kim, Y. B., (1965). Phys. Rev. 139, A1163.

Koch, R. H., V. Foglietti, W. J. Gallagher, G. Koren, A. Gupta, and M. P. A. Fisher, (1989). Phys. Rev. Lett. 63, 1511.

Konczykowski, M., L. I. Burlachkov, Y. Yeshurun, and F. Holtzberg, (1991). Phys. Rev. B 43, 13707.

Koshelev, A. E., (1992). Physica C 198, 371.

Kötzler, J., M. Kaufmann, G. Nakielski, R. Behr, and W. Assmus, (1994). Phys. Rev. Lett. 72, 2081.

Krusin-Elbaum, L., L. Civale, G. Blatter, A. D. Marwick, F. Holtzberg, and C. Field, (1994). Phys. Rev. Lett. 72, 1914.

Krusin-Elbaum, L., L. Civale, V. M. Vinokur, and F. Holtzberg, (1992). Phys. Rev. Lett. 69, 2280.

Kwok, W. K., J. A. Fendrich, S. Fleshler, U. Welp, J. Downey, and G. W. Crabtree, (1994). Phys. Rev. Lett. 72, 1092.

Kwok, W. K., J. A. Fendrich, C. J. van der Beek, and G. W. Crabtree, (1994). Phys. Rev. Lett. 73, 2614.

Kwok, W. K., J. A. Fendrich, V. M. Vinokur, A. E. Koshelev, and G. W. Crabtree, (1996). Phys. Rev. Lett. 76, 4596.

Kwok, W. K., S. Fleshler, U. Welp, V. M. Vinokur, J. Downey, and G. W. Crabtree, (1992). Phys. Rev. Lett. 69, 3370.

Lang, W., C. Fussenegger, S. Proyer, E. Stangl, and D. Bäuerle, (1996). Zeitschrift Für Physik B 100, 13.

Larkin, A. I., and Y. N. Ovhcinnikov, (1973). Zh. Eksp. Teor. Fiz. 65, 1704 [Sov. Phys. JETP 38, 854 (1974)].

Larkin, A. I., and Y. N. Ovchinnikov, (1979). J. Low Temp. Phys. 34, 409.

Leghissa, M., A. Koniger, M. Lippert, W. Dorsch, M. Kraus, and G. Saemann-Ischenko, (1993). Z. Phys. B 92, 163.

Legris, A., F. Rullier-Abenque, and P. Lejay, (1993). Phys. Rev. B 48, 10634.

Li, Qiang, H. J. Wiesmann, M. Suenaga, L. Motowidlow, and P. Haldar, (1994). Phys. Rev. B 50, 4256.

Maggio-Aprile, I., Ch. Renner, A. Erb, E. Walker, and Ø. Fischer, (1995). Phys. Rev. Lett. 75, 2754.

Mao, J., D. H. Wu, J. L. Peng, R. L. Greene, and S. M. Anlage (1995). Phys. Rev. B 51, 3316.

Marchetti, M. C., and V. M. Vinokur, (1995). Phys. Rev. B 51, 16276.

Marley, A. C., M. J. Higgins, and S. Bhattacharya, (1995). Phys. Rev. Lett. 74, 3029.

Marley, A. C., and M. B. Weissman, (1995). Phys. Rev. B 52, 7965.

Matsui, Y., K. Yanagisawa, and N. Fujiwara, (1991). Jap. J. of Appl. Phys. 30, 1375.

Meissner, W., and R. Ochsenfeld, (1933). Naturwissenschaften 21, 787.

Merithew, R. D., M. W. Rabin, M. B. Weissman, M. J. Higgins, and S. Bhattacharya, (1996). Phys. Rev. Lett. 77, 3197.

Moloni, K., M. Friesen, S. Li, V. Souw, P. Metcalf, L. Hou, and M. McElfresh, (1997). Phys. Rev. Lett. 78, 3173.

Nakielski, G., D. Görlitz, Chr. Stodte, and M. Welters, (1997). Phys. Rev. B 55, 6077.

Natterman, T., (1990). Phys. Rev. Lett. 64, 2454.

Nelson, D. R., and V. M. Vinokur, (1992). Phys. Rev. Lett. 68, 2398.

Nelson, D. R., and V. M. Vinokur, (1993). Phys. Rev. B 48, 13060.

Oussena, M., P. A. J. de Groot, K. Deligiannis, A. V. Volkozub, R. Gagnon, and L. Taillefer, (1996). Phys. Rev. Lett. 76, 2559.

Oussena, M., P. A. J. de Groot, S. J. Porter, R. Gagnon, and L. Taillefer, (1995). Phys. Rev. B 51, 1389.

Overend, N., M. A. Howson, and I. D. Lawrie, (1994). Phys. Rev. Lett. 73, 3238.

Palstra, T. T. M., B. Batlogg, R. B. van Dover, L. F. Schneemeyer, and J. V. Waszcsak, (1989). Appl. Phys. Lett. 54, 763.

Placais, B., P. Mathieu, and Y. Simon, (1993). Phys. Rev. Lett. 70, 1521.

Radzihovsky, L., (1995). Phys. Rev. Lett. 74, 4923.

Reed, D. S., N.-C. Yeh, W. Jiang, U. Kriplani, and F. Holtzberg, (1993). Phys. Rev. B 47, 6150.

Reed, D. S., N.-C. Yeh, M. Konczykowski, A. V. Samoilov, and F. Holtzberg, (1995). Phys. Rev. B 51, 16448.

Reichhardt, C., C. J. Olson, J. Groth, S. Field, and F. Nori, (1996). Phys. Rev. B 53, R8898.

Roberts, J. M., (1995). *Critical Scaling of Thin-film YBaCuO and NdCeCuO Resistivity-Current Isotherms*, Ph.D. thesis, Oregon State University.

Roberts, J. M., B. Brown, B. A. Hermann, and J. Tate, (1994). Phys. Rev. B 49, 6890.

Roberts, J. M., B. Brown, and J. Tate (1995). Phys. Rev. B 51, 15281.

Safar, H., S. R. Foltyn, Q. X. Jia, and M. P. Maley, (1996). Phil. Mag. B, 74, 647.

Safar, H., P. L. Gammel, D. A. Huse, D. J. Bishop, W. C. Lee, J. Giapintzakis, and D. M. Ginsberg, (1993). Phys. Rev. Lett. 70, 3800.

Safar, H., P. L. Gammel, D. A. Huse, D. J. Bishop, J. P. Rice, and D. M. Ginsberg, (1992). Phys. Rev. Lett. 69, 824.

Salamon, M. B., J. Shi, N. Overend, and M. A. Howson, (1993). Phys. Rev. B 47, 5520.

Sásik, R., and D. Stroud, (1995). Phys. Rev. Lett. 75, 2582.

Sauerzopf, F. M., H. P. Wiesinger, H. W. Weber, and G. W. Crabtree, (1995). Phys. Rev. B 51, 6002.

Thouless, D. J., P. Ao, and Q. Niu, (1996). Phys. Rev. Lett. 76, 3758.

Tinkham, M., (1975). *Introduction to Superconductivity*, (McGraw-Hill, New York).

Ullmaier, H., (1975). *Irreversible Properties of Type II Superconductors*, (Springer-Verlag, New York).

van der Beek, C. J., and P. H. Kes, (1991). Phys. Rev. B 43, 13032.

Veal, B. W., Division of Material Science, Argonne National Laboratory, Argonne, IL, 60439 USA.

Vlasko-vlasov, V. K., L. A. Dorosinskii, A. A. Polyanskii, V. I. Nikitenko, U. Welp, B. W. Veal, and G. W. Crabtree, (1994). Phys. Rev. Lett. 72, 3246.

Wahl, A., V. Hardy, A. Maignon, C. Martin, Ch. Simon, and J. Provost, (1994). Physica C 235-240, 2827.

Warnes, W. H., Rogers Hall 308, Dept. of Mech. Engr., Oregon State University, Corvallis, OR, 97331.

Warnes, W. H., (1988). J. Appl. Phys. 63, 1651.

Warnes, W. H., and D. C. Larbalestier, (1986). Appl. Phys. Lett. 48, 1403.

Welp, U., J. A. Fendrich, W. K. Kwok, G. W. Crabtree, and B. W. Veal, (1996). Phys. Rev. Lett. 76, 4809.

Welp, U., W. K. Kwok, G. W. Crabtree, K. G. Vandervoort, and J. Z. Liu, (1989). Phys. Rev. Lett. 62, 1908.

Wengel, C., and A. P. Young, (1996). Phys. Rev. B 54, R6869

Wöltgens, P. J. M., C. Dekker, J. Swuste, and H. W. de Wijn (1993). Phys. Rev. B 48, 16826.

Wörderweber, R., (1992). Phys. Rev. B 46, 3076.

Worthington, T. K., M. P. A. Fisher, D. A. Huse, John Toner, A. D. Marwick, T. Zabel, C. A. Field, and F. Holtzberg, (1992). Phys. Rev. B 46, 11854.

Worthington, T. K., F. H. Holtzberg, and C. A. Field, (1990). Cryogenics 30, 417.

Wu, H., N. P. Ong, R. Gagnon, and L. Taillefer, (1997). Phys. Rev. Lett. 78, 334.

Wu, M. K., J. R. Ashburn, C. J. Torng, P. H. Hor, R. L. Meng, L. Gao, Z. J. Huang, Y. Wang, and C. W. Chu, (1987). Phys. Rev. Lett. 58, 908.

Yamafuji, K., and T. Kiss, (1996). Physica C 258, 197.

Yamasaki, H., K. Endo, S. Kosaka, M. Umeda, S. Yoshida, and K. Kajimura, (1994). Phys. Rev. B 50, 12959.

Yeh, N.-C., W. Jiang, D. S. Reed, U. Kriplani, and F. Holtzberg, (1993). Phys. Rev. B 47, 6146.

Yeh, N.-C., D. S. Reed, W. Jiang, U. Kriplani, F. Holtzberg, A. Gupta, B. D. Hunt, R. P. Vasquez, M. C. Foote, and L. Bajuk, (1992). Phys. Rev. B 45, 5654.

Zeldov, E., N. M. Amer, G. Koren, A. Gupta, R. J. Gambino, and M. W. McElfresh, (1989). Phys. Rev. Lett. 62, 3093.

Zeldov, E., D. Majer, M. Konczykowski, V. B. Geshkenbein, V. M. Vinokur, and H. Shtrikman, (1995). Nature 375, 373.

Zhao, B., F. Ichikawa, T. Fukami, T. Aomine, J.-J. Sun, B. Xu, and L. Li, (1997). Phys. Rev. B 55, 1247.

Ziese, M., (1996a). Physica C 269, 35.

Ziese, M., (1996b). Phys. Rev. B 53, 12422.

Ziese, M., P. Esquinazi, A. Gupta, and H. F. Braun, (1994). Phys. Rev. B 50, 9491.

APPENDICES

APPENDIX A

DATA SIMULATION

Analogous to the distributions derived in Section 4.6, we start with depinning-current distributions. However, unlike the complicated behavior of the experimental distributions, we assume Gaussians with centers J_0 and widths σ varying linearly with temperature. We emphasize that this overly simple temperature dependence is best interpreted as a zeroth-order thermal depinning model and that it does not include the sort of cross-over in temperature that one might expect for a phase transition.

In all, fifteen temperatures are simulated, spaced at 0.1 K, between 90.0 and 91.4 K. This roughly corresponds to a low-field (e.g. 0.1 or 0.25 T) V-I window in crystals, and the parameters of the first (90.0 K) distribution are chosen to approximate those taken from a Gaussian fit to the experimental data. The distributions are normalized to represent a constant number of vortices for all temperatures (each f, integrated from $J = 0$ to ∞, gives the same constant). The form of the first distribution is given by

$$f_{sim} = C\,exp\left[\frac{-(J_{sim} - J_0)^2}{2\sigma^2}\right] \qquad \text{(A.1)}$$

where σ and J_0 were given temperature dependence. Specifically, they depend linearly on temperature via

$$\sigma(T) = 5 + 10 \cdot \Delta T \qquad \text{(A.2a)}$$

$$J_0(T) = 220 - 150 \cdot \Delta T \qquad \text{(A.2b)}$$

where $\Delta T = T$ - 90.0 K. The prefactor C in Eq. A.1 is adjusted by normalization for each temperature. Selected distributions appear

in Fig. A.1. All distributions are calculated in a spreadsheet format, with data points spaced in a logarithmic fashion between J_{sim} = 0.01 A/cm^2 to J_{sim} = 300 A/cm^2; this produces data that is most easily comparable to the experimental data.

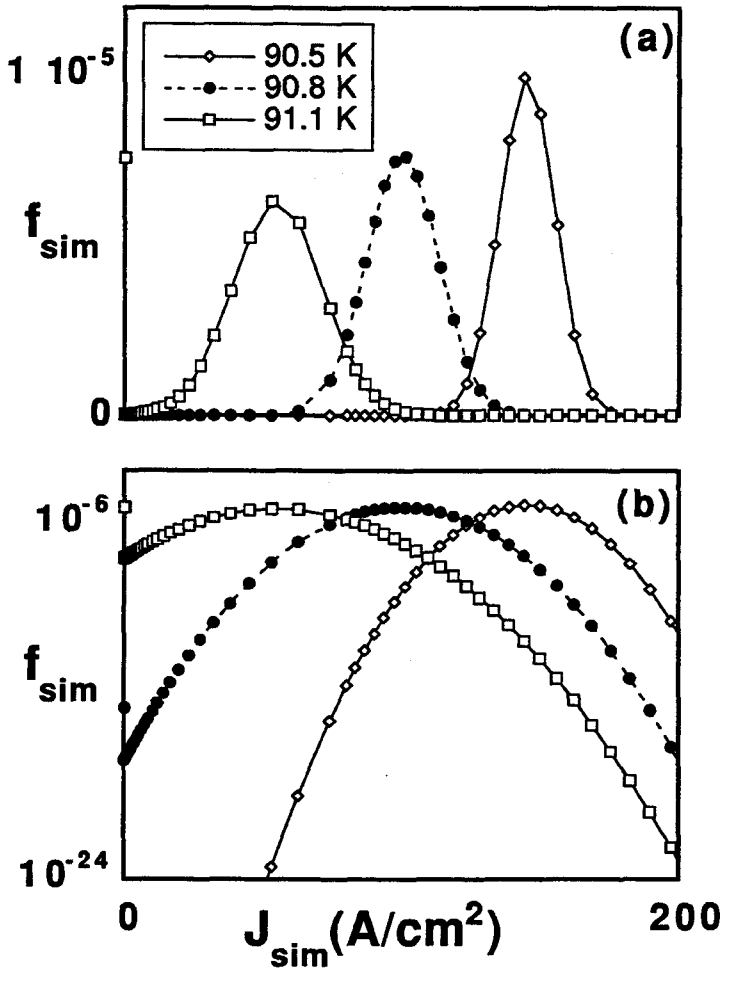

Fig. A.1: Simulated pinning distributions in (a) linear and (b) semi-log representations.

This approach to modeling V-I data has been used by Edelman and Larbalestier (1993) as noted in Section 2.2.2. The authors simulated data using an analytic expression for V (see Eq. 2.15), and in this way their results are more precise than the discreet method we present here. However, they do not treat the case of varying temperature. Similar to the work of Edelman and Larbalestier (1993), we do not let the distributions exist for $J < 0$. When a Gaussian intersects the Y-axis ($T \geq 90.7$ in this case), the area under the $J < 0$ tail of the Gaussian is "piled" in a distribution bin adjacent to $J = 0$. This is physically sensible since if a pinning distribution is nonzero at $J = 0$, a number of vortices will be depinned at zero current. For example, a distribution centered at $J = 0$, will have half of its total population depinned at $J = 0$. The $J = 0$ peaks can be observed on the y axis in Fig. A.1; the points at $J = 0$ correspond to a liquid-like vortex population.

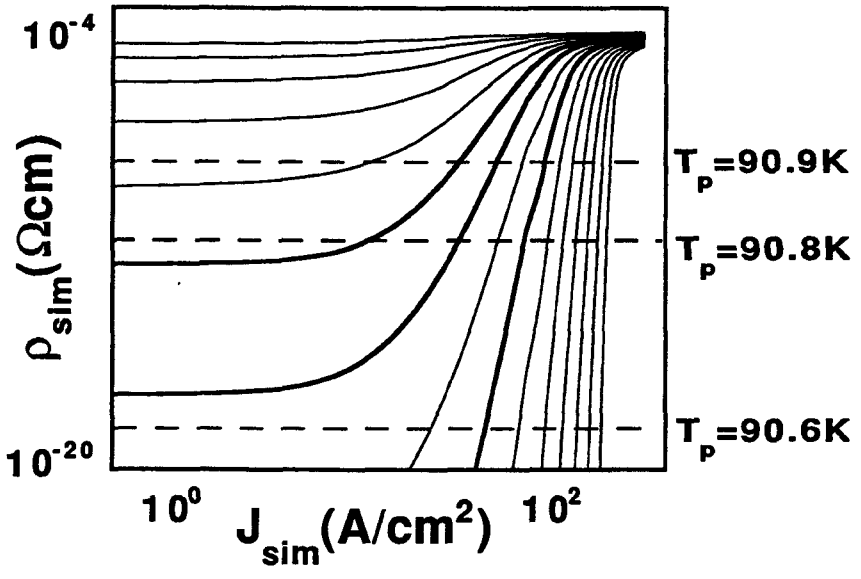

Fig. A.2: ρ-J data simulated from Gaussian distributions of depinning currents for 90.0-91.4 K. Dashed lines denote the effect of assumed sensitivity on the derivation of T_p. Darker curves highlight the T_p candidates.

By simply integrating the distributions twice -- reversing the relation given by Eq. 2.14 -- we simulate E-J data, assuming unity for geometrical factors, and ρ-J data where $\rho = E/J$. The resulting isotherms, shown in Fig. A.2, provide a strong qualitative match of transport data for copper-oxide superconductors, including the YBCO crystals presented in Chapter 3.

Before comparing the simulation to experimental data in more detail, one must choose a sensitivity, or a resistivity floor, at which to cut the data. Ideally, an analysis of the simulated data would give the same results independent of the sensitivity, but Fig. A.2 clearly shows that the sensitivity choice is crucial. The three different sensitivities depicted in Fig. A.2 each give a different value of T_p, using the same criteria that was described in Section 3.9 -- the same criteria that is used for analysis of the experimental data. It follows that the derived n values vary as well, generally increasing for increasing sensitivity.

For presentation we arbitrarily select a pV/cm sensitivity for the simulated E values. Having chosen a sensitivity, the simulated traces compare nicely to experimental data. The isotherms between 90.0 and 90.5 are closely spaced and show an exponentially down-turning character. At 90.8 K, a roughly power-law isotherm is simulated, and for 90.7-91.4 K the isotherms spread out and show finite linear resistivities. In addition, all isotherms show the flattening out signature of flux flow for high values of J. Using a critical scaling analysis, we derive $z = 29$ from the power-law slope ($n = 15$) at 90.8 K and ν=0.45 by extracting an $S = \nu(z\text{-}1) = 13$ value from the temperature dependence of the linear resistivities (Roberts, 1995; see Eq. 2.7). It is interesting to note that the linear resistivities extracted from this simulation give a power-law fit which has been interpreted in the literature as a signature of a second-order phase transition (see Section 2.1.2). As shown in Fig. A.3, the data even bend away from the power-law at higher temperatures, just like the experimental data (Roberts *et al.*, 1994).

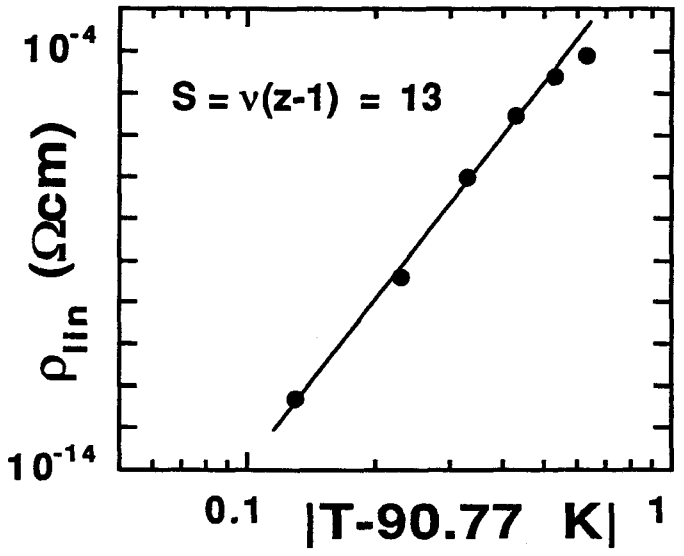

Fig. A.3: Linear resistivities plotted versus $|T\text{-}T_p|$ for simulated data. According to the vortex glass theory, the slope gives S, and data that deviates from the power-law at high T falls outside the critical scaling regime (Roberts *et al.*, 1994).

After conservatively cutting some of the flux flow data, the isotherms are scaled according to a vortex glass analysis. Fig. A.4 shows the collapsed data and the results of optimizing the collapse by changing the parameters in a manner consistent with $S = \nu(z\text{-}1)$ as per the vortex glass theory. This collapse is striking; the deviations from the two branches occur for the remnant flux flow data and for the 91.4 K data. The deviation of 91.4 K is quite similar to data that is considered to be outside of the scaling regime in a vortex glass analysis, matching the deviation of the linear resistivity point for 91.4 K in Fig. A.3 (Roberts *et al.*, 1994; Friesen *et al.*, 1996); a strikingly similar deviation can be seen in Fig. 4.9, the critical scaling for an YBCO crystal in 0.25 T. The resulting critical exponents (z = 33; ν = 0.4) match neither the experimental results for YBCO crystals nor the predictions of any second-order

vortex phase transition. Given that we do not fine-tune the Gaussian parameters or their temperature dependence, the extreme exponents are not surprising. We believe the demonstration of a scaling collapse -- qualitatively consistent with a second-order transition in many if not all aspects -- is the crucial result.

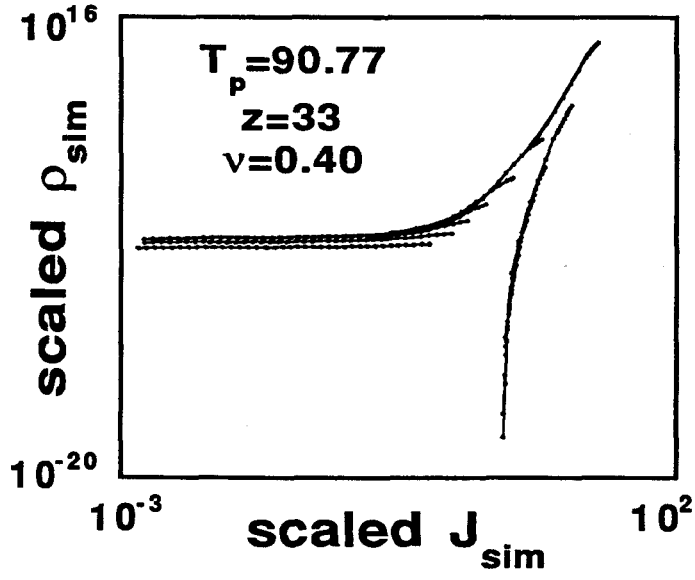

Fig. A.4: Scaled data from the simulation with derived critical parameters.

APPENDIX B

VOLTAGE FLUCTUATION INVESTIGATION

At times, the dc four-terminal measurements were visited by some rather rowdy voltage fluctuations. In most cases, the observed noise was both field and current-dependent, but independent of whether or not the magnet was operated in persistent mode. For the combination of high fields ($B > 1$ T) and high currents ($I > 10$ mA), this made I-V data collection impractical. In general, the higher fields necessitated higher probing currents which magnified the noise effect. Luckily, these regimes are usually outside of the practical range of the experiment since catastrophic contact heating and sample heating arise in the high-field, high-current environment.

The voltage noise was most severe in the irradiated crystal; for unirradiated samples, the voltage noise was not a limiting factor. However, since such fluctuations were never observed for thin film superconductors using a similar experimental configuration (Roberts, 1995), careful examinations of the noise were carried out for crystal #2 after its first irradiation and for crystal #3. Though much data has been accumulated in a variety of conditions for these samples, the results are largely inconclusive; this is primarily due to the fact that the fluctuations have been absent in measurements of crystal #3 after Jan. 20, 1997. (Recall that we cannot repeat measurements on crystal #2 since it was destroyed after the second irradiation). Given the date-dependence of the measurements, the position of the experiment on the fourth floor of a building, the busy schedule of repairs in the building this year, and the replacement of several large pieces of equipment on the sixth floor, we must conclude that mechanical vibrations are a viable candidate for *all* of the fluctuations we observed.

Each set of noise data was taken at a stabilized temperature, a constant applied field, and a constant current with the same dc four-terminal technique described in Chapter 3. Sets of up to 120 voltage measurements were taken and the standard deviation of the voltage signal is reported as the noise level. For any twenty points of a large set the standard deviation is roughly equivalent, so all sets consist of at least thirty voltage measurements. For both samples, these types of noise sets were collected for various currents (1 μA to 40 mA) and various applied fields (ambient to 5 T). Most of the these measurements were made below T_c, such that the average signal was approximately zero. Fig. B.1 depicts the current dependence of the voltage fluctuations, σ_V, for a 1 T applied field. Fig. A.2 depicts the field dependence of σ_V for low current values.

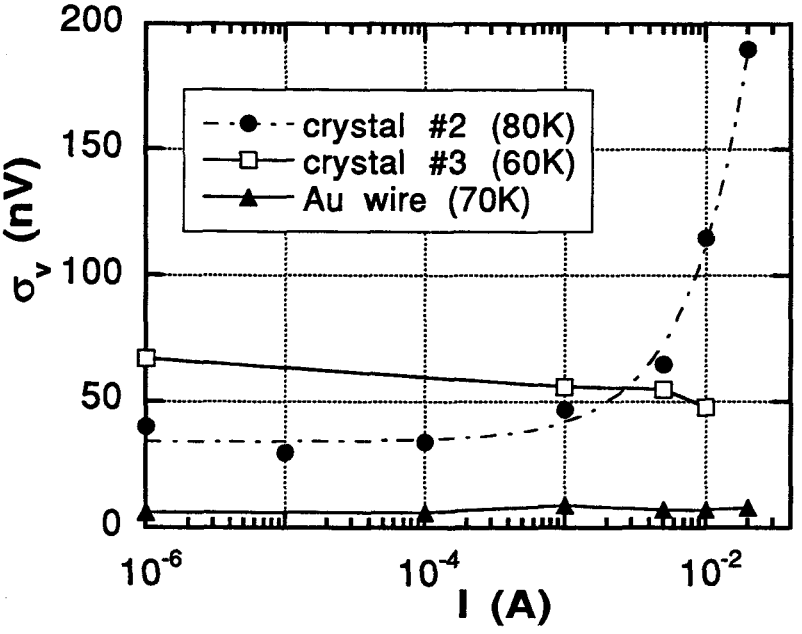

Fig. B.1: Semi-log depiction of voltage fluctuations versus applied current in 1 T. Data for crystal #2 are post-irradiation and the dashed line is a linear fit.

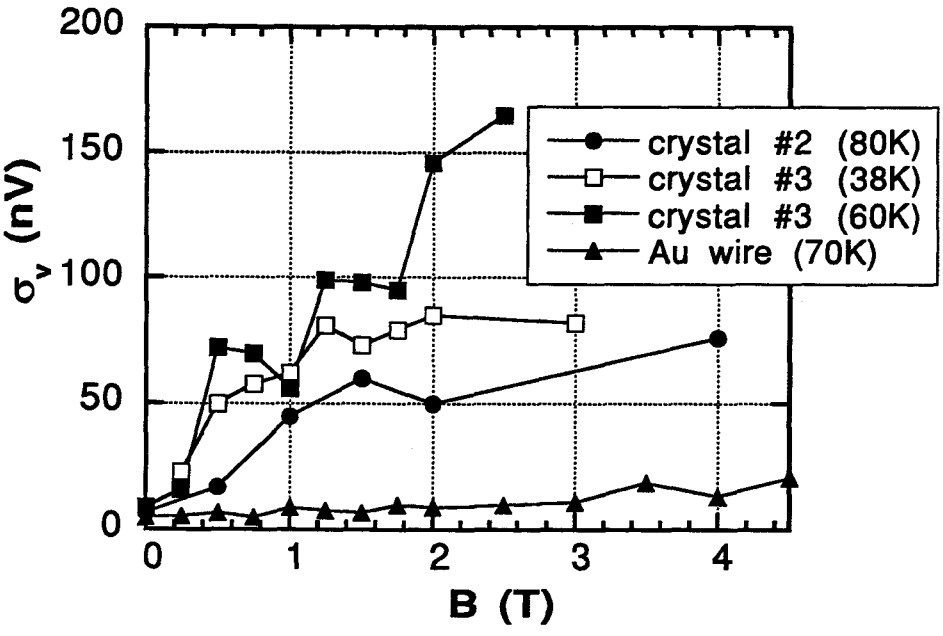

Fig. B.2: Voltage fluctuations as a function of field for 1 mA. Data for crystal #2 are post-irradiation.

It is interesting to note the non-negligible temperature dependence of the fluctuations in Fig. B.2 for crystal #3 for $B \geq 2$ T. A sample-temperature-dependence speaks against mechanical vibrations as the source of the fluctuations and speaks for vortex motion. In addition, the fluctuation levels measured for an Au wire in the same geometrical configuration and the same sample holder are much lower in both Fig. B.1 and Fig. B.2.

The most striking fluctuations occurred for higher currents in crystal #2 after fast-neutron irradiation. In Fig. B.3, we show the fluctuations as a function of applied field for currents of 10 and 40 mA. These fluctuation levels were repeatable to within 5%, even for the large hump seen for 40 mA around 1 T.

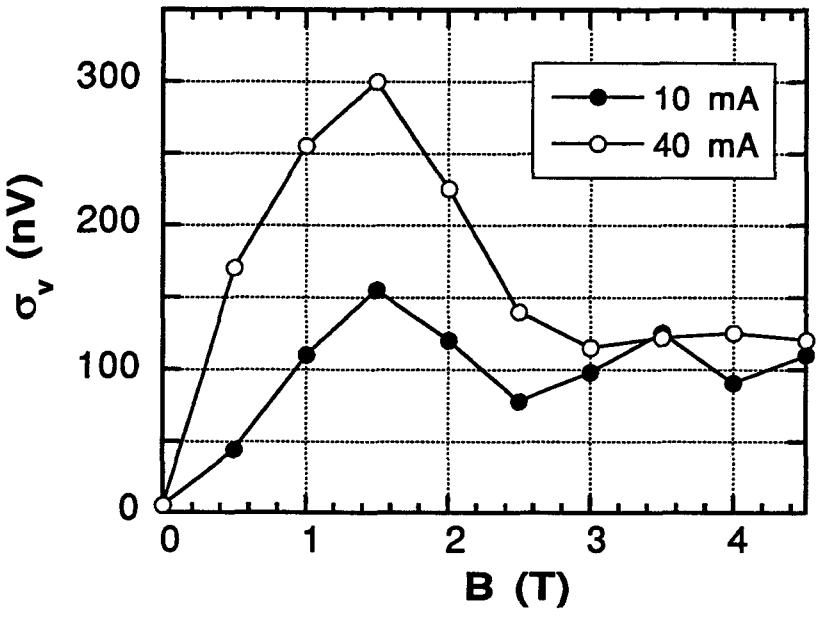

Fig. B.3: Voltage fluctuations versus field for crystal #2 after irradiation. Data collected at 72 K with the $B \parallel c$.

To test the effects of sample-holder geometry on the measured noise, a new optimized holder was produced (see Fig. B.4). The noise levels for an Au wire were reduced by 50% for $B \geq 4$ T using the optimized holder. However, as one can see from Fig. B.2, the fluctuations measured for an Au wire in the standard holder were negligible in comparison to the fluctuations in the crystals.

We are confident that the fluctuations are not caused by the experimental set-up outside of the cryogenic dewar. Voltage fluctuations showed no dependence on the rate of data collection, filtering techniques, or the current configuration of the superconducting magnet (it can be run in persistent mode with no external current applied). The dramatic field-dependence of the

results shows that the fluctuations are localized to the sample and the sample-holder's electric leads. We are fairly sure that the fluctuations do not originate in the sample holder wires, which leaves three possibilities: fluctuations of some sort in the superconducting state of the crystals; low-frequency mechanical vibrations in the building; and fluctuations resulting from the electrical contacts to the crystals. The last case is unlikely since we can think of no mechanism by which contact-related noise would be field-dependent.

Below, we cite several possible vortex-related causes for the noise fluctuations observed in the irradiated crystal, but must first present this caveat: since no fluctuations have been observed after a certain date (1/20/97), we must admit that the entire effect could be caused by mechanical vibrations in the building. In fact, since the Au-wire data trials were run *after* the trials for crystal #2 and #3 (and after 1/20/97), it is possible that the quiet Au-wire data shown in Fig. B.1 and Fig. B.2 are not pointing to voltage fluctuations in the crystals, but rather to calendar-dependent vibration effects. The date-dependence of fluctuations in crystal #3 are depicted in Fig. B.5.

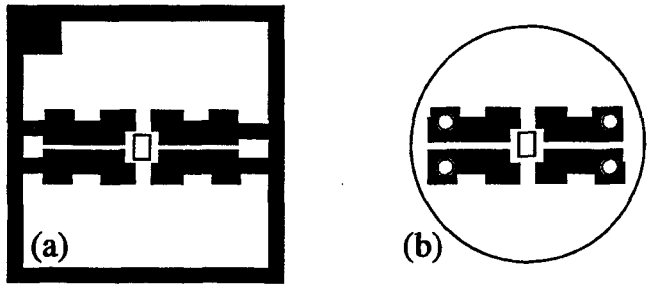

Fig. B.4: Optimized sample holder, shown to scale in its (a) production phase and (b) experiment phase. This is to be compared to Fig. 3.5. The new holder presents smaller pick-up loops for the possibility of magnetic flux oscillations.

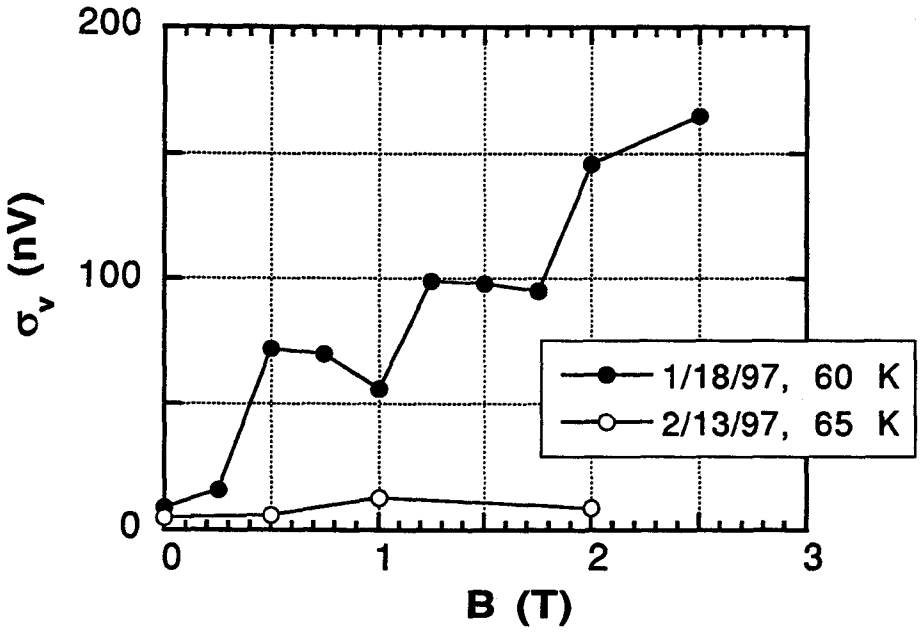

Fig. B.5: Voltage fluctuations versus field for crystal #3 on two different dates.

The study of vortex-related noise already comprises a rich sub-field of superconductivity research. Interested parties are referred to several works. Habbal and Joiner (1977) linked changes in pinning strength in $Pb_{80}In_{20}$ foils to observed changes in the flux flow voltage noise. The voltage noise associated with the process of flux flow was thoroughly discussed by Clem (1981). More recently, authors have suggested that voltage noise in the mixed state is linked to plastic (as opposed to elastic, see Section 2.1.1) vortex motion (Faleski *et al.*, 1996).

A theoretical refinement of the flux-flow work of Clem is provided for type-II superconductors by Placais *et al.* (1993). The authors emphasize the role of inhomogeneous critical currents in the creation of dc voltage fluctuations; in particular, they point to

the difference that can arise between surface currents and bulk transport currents in a superconducting sample of finite size. The sharp difference in current creates turbulent flow patterns which account for flux flow noise in dc measurements.

High levels of dc voltage noise have recently been reported for $T < T_c$ in untwinned YBCO crystals (Gordeev, *et al.*, 1996). The authors found fluctuations on the order of 100 nV (at 87 K and a field of 2 T applied parallel to the c-axis) in a four-terminal measurement similar to the ones in this thesis. The authors attribute this noise in the mixed state to non-uniform motion of vortices. In particular, since their crystalline sample is very clean and twin-free, they submit that the noise is caused by activation barriers on the surfaces of the crystal. The process of vortices nucleating at one edge of the crystal and dissipating as they leave the other edge is very inhomogeneous since, in a real crystal, the surfaces are highly nonuniform on the microscopic scale relevant to vortices. Though our crystals are twinned, it is possible that the explanation presented by Gordeev *et al.* is applicable to the noise we observe.

Studies of the low-T_c superconductor $2H$-$NbSe_2$ have recently shown current and field-dependent voltage noise (Marley *et al.*, 1995). The authors claim that low-frequency broad-band noise in voltage measurements is a signature of plastic vortex motion. They measure the ac noise-power spectra for $2H$-$NbSe_2$ for a variety of fields, current amplitudes and frequencies. They find sharp peaks in the field-dependence of the noise-power spectra just under the upper critical field and describe the data with an onset of vortex-lattice plasticity. The peak they observe as a function of field is not unlike the results presented in Fig. B.3.